AN EXPERIMENTAL STUDY OF TAYLOR-GOERTLER VORTICES IN A CURVED RECTANGULAR CHANNEL

Robert Joe McKee

uate School
fornia 93940

NAVAL POSTGRADUATE SCHOOL
Monterey, California

THESIS

AN EXPERIMENTAL STUDY OF TAYLOR-GOERTLER VORTICES IN A CURVED RECTANGULAR CHANNEL

by

Robert Joe McKee

Thesis Advisor: M. D. Kelleher

June 1973

Approved for public release; distribution unlimited.

T155138

An Experimental Study of Taylor-Goertler Vortices in a Curved Rectangular Channel

by

Robert Joe McKee
Lieutenant, United States Naval Reserve
B.S., University of California, Santa Barbara, 1968

Submitted in partial fulfillment of the
requirements of the degrees of

MASTER OF SCIENCE IN MECHANICAL ENGINEERING
and
MECHANICAL ENGINEER
from the

NAVAL POSTGRADUATE SCHOOL
June 1973

Thesis
M2154
c.1

Library
Naval Postgraduate School
Monterey, California

ABSTRACT

A rectangular cross section channel, with both a straight and a curved portion, was designed and built to create the laminar secondary Taylor-Goertler vortex flow. An aerosol was used to visualize these flow patterns, and photographs of the results are presented. A hot wire anemometer investigation of one location in the curved section was conducted to obtain the mean velocity profiles and turbulence levels. The pressure drop along both the straight and the curved sections was measured and compared. A constant temperature wall heater was also designed and installed in the straight section of the channel. Approximate values of the heating losses were obtained and the overall and local heat transfer coefficients were calculated for the straight portion of the channel. It was concluded that the vortices develop with both velocity increases and distance along the channel, and that the increase in pressure drop due to the vortices varied from near zero to approximately 20% with increasing Reynolds numbers.

TABLE OF CONTENTS

I. INTRODUCTION ---------- 11

A. DESCRIPTION OF VORTICES ---------- 11

B. BRIEF HISTORY ---------- 13

II. NATURE OF THE PROBLEM ---------- 17

A. INTENT OF THIS STUDY ---------- 17

B. DESIGN REQUIREMENTS ---------- 18

C. DESCRIPTION OF APPARATUS ---------- 24

III. FLOW VISUALIZATION ---------- 39

A. EXPERIMENTAL CONSIDERATIONS ---------- 39

B. PATTERNS AND PICTURES OF THE FLOW ---------- 41

IV. VELOCITY AND TURBULENCE MEASUREMENTS ---------- 51

A. EXPERIMENTAL PROCEDURES ---------- 51

B. VELOCITY PROFILES ---------- 53

C. TURBULENCE LEVELS ---------- 62

V. PRESSURE DROP MEASUREMENTS ---------- 72

A. EXPERIMENTAL PROCEDURES ---------- 72

B. PRESSURE DROP ---------- 74

VI. HEAT TRANSFER MEASUREMENTS ---------- 85

A. EXPERIMENTAL PROCEDURES ---------- 85

B. RESULTS ---------- 89

VII. CONCLUSIONS ---------- 102

VIII. RECOMMENDATIONS ---------- 104

APPENDIX A: ERROR ANALYSIS ---------- 106

APPENDIX B: COMPUTER RESULTS FOR VELOCITY AND TURBULENCE ---------- 108

APPENDIX C: CALCULATIONS AND COMPUTER RESULTS FOR PRESSURE DROP ---------- 119

APPENDIX D: COMPUTER RESULTS FOR HEAT TRANSFER ------- 129

LIST OF REFERENCES ---------- 158

INITIAL DISTRIBUTION LIST ---------- 161

FORM DD 1473 ---------- 162

LIST OF TABLES

Table

I. PRESSURE DROP PER FOOT FOR TWO FOOT INTERVALS CALCULATED BY LEAST SQUARES --------- 78

II. PRESSURE DROP PER FOOT FOR ONE FOOT INTERVALS CALCULATED BY LEAST SQUARES --------- 80

III. PRESSURE DROP PER FOOT FOR TWO FOOT INTERVALS MEASURED VALUES ---------- 81

LIST OF FIGURES

Figure

1. Sketch of Taylor-Goertler Vortices ---------- 12
2. Reynolds Number vs. Dean Number ---------- 21
3. Cross Section of Channel ---------- 25
4. Arrangement of Apparatus ---------- 27
5. Aerosol Generating Equipment ---------- 29
6. Lighting and Camera Arrangement ---------- 31
7. Hot Wire Anemometer Arrangement ---------- 32
8. Pressure Drop Measuring Equipment ---------- 34
9. Heating Apparatus ---------- 37
10. Photographs of Vortices Re = 609 ---------- 45
11. Photographs of Vortices Re = 875 ---------- 46
12. Photographs of Vortices Re = various --------- 47
13. Photographs of Vortices Re = 1033 ---------- 48
14. Photographs of Vortices Re = 1166 ---------- 49
15. Photographs of Vortices Re = 1457 ---------- 50
16. Velocity Profiles Re = 609 ---------- 55
17. Velocity Profiles Re = 875 ---------- 56
18. Velocity Profiles Re = 1166 ---------- 57
19. Velocity Profiles Re = 1298 ---------- 58
20. Velocity Profiles Re = 1457 ---------- 59
21. Velocity Profiles Re = 1722 ---------- 60
22. Velocity Profiles Re = 1934 ---------- 61
23. Typical Position of Hot Wire ---------- 63

24. Turbulence Intensity Re = 609 ---------- 64

25. Turbulence Intensity Re = 875 ---------- 65

26. Turbulence Intensity Re = 1166 ---------- 66

27. Turbulence Intensity Re = 1298 ---------- 67

28. Turbulence Intensity Re = 1457 ---------- 69

29. Turbulence Intensity Re = 1722 ---------- 70

30. Turbulence Intensity Re = 1934 ---------- 71

31. Pressure Below Atmospheric vs. Pressure Taps ---------- 75

32. Percentage Increase in Pressure Drop vs. Reynolds Number ---------- 82

33. Pressure Drop Coefficient vs. Pressure Taps ---------- 84

34. Heat Transfer Coefficient Tw = 125 ---------- 95

35. Heat Transfer Coefficient Tw = 133 ---------- 96

36. Heat Transfer Coefficient Tw = 143 ---------- 97

37. Heat Transfer Coefficient Tw = 139 ---------- 98

38. Heat Transfer Coefficient Tw = 131 ---------- 99

TABLE OF SYMBOLS

A	area
Ac	cross sectional area
Aw	area of the wall heater
As	area of a single heater strip
a	half the height of the channel
b	half the width of the channel
Cp	pressure drop coefficient
cp	specific heat
De	Dean number
Dh	hydraulic diameter
d	spacing of channel wall
Go	Goertler number
Gr	Grashoff number
H	local heat transfer coefficient
Hm	mean heat transfer coefficient
Ho	overall heat transfer coefficient
k	thermal conductivity
L	a distance along the channel in the flow direction
Nu	Nusselt number
Pr	Prandtl number
p	pressure, a relative measured value
Qc	heat energy transferred by conduction and convection
Qr	heat energy transferred by radiation
Re	Reynolds number based on hydraulic diameter

Ri	radius of inner wall or cylinder
Ro	radius of concave wall
T	temperature
Ta	Taylor number
Tb	bulk temperature of a fluid
$T\ell m$	log mean temperature difference
Tw	average temperature of the wall heater
U	mean velocity of flow
$\dot{V}$	volumetric flow rate
δ	boundary layer thickness
ε	emissivity
ρ	mass density
σ	Stefan-Boltzmann Constant
μ	viscosity
ν	kinematic viscosity

ACKNOWLEDGEMENT

The author wishes to express his appreciation to all those who made this work possible. It is impossible to give a complete list of people to whom the author is indebted but it is hoped that by naming those who deserve a special note of thanks, all will know that their efforts were appreciated.

The guidance and advice of the author's thesis advisor, Professor M. Kelleher, and his efforts made this undertaking possible. The personnel of the Mechanical Engineering Shop and particularly Messrs. K. Mothersell, G. Bixler, and T. Christian deserve a special thanks for their timely and careful assistance in preparation of the experimental apparatus. The author is very grateful for the assistance of Mrs. V. Culley of the Mechanical Engineering Office in obtaining material and completing administrative requirements. Finally, to my wife Catherine, for her patience through repeated manuscript typings and for her support throughout the study, a heartfelt thank you.

I. INTRODUCTION

A. DESCRIPTION OF VORTICES

The phenomenon best known as Taylor-Goertler vortices is caused by a body force instability in fluid flows. Specifically, Taylor-Goertler vortices are a secondary flow induced by centrifugal forces. In a channel, such as used in this investigation, the fluid near the center of the channel is subjected to larger centrifugal forces than the slower moving fluid near the concave wall. Thus, the tendency is for the fluid in the center of the channel to move outward toward the wall. The fluid near the wall is unable to resist this action and must move in the spanwise direction and then radially inward replacing the central fluid. Once in the center of the channel, this fluid obtains the higher flow velocity, and the tendency to move toward the concave wall. This cyclic motion forms the rotating Taylor-Goertler vortices.

Such vortices, caused by centrifugal forces, occur in many cases of curved flow. Taylor-Goertler vortices are laminar vortices with their axes in the direction of the main flow, and with secondary velocities in both perpendicular directions. Such spiral vortices occur in counter rotating pairs. There is frequently a regularly spaced cellular structure associated with these vortices. A sketch of this type of flow pattern is shown in Figure 1.

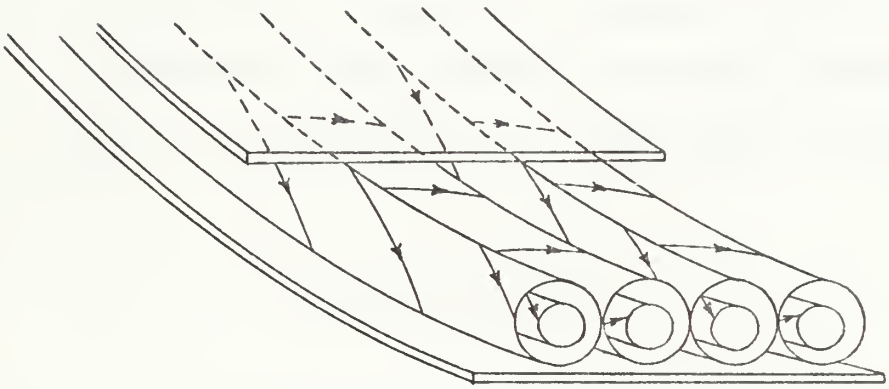

Figure 1. Sketch of Taylor-Goertler Vortices.

B. BRIEF HISTORY

The first person to consider the instability of curved flows was Lord Rayleigh who found a stability criterion for inviscid fluid rotating symmetrically about an axis [Ref. 1]. His criterion for a stable flow required that the product of the local circumferential velocity and the local radius of curvature either increase or at least remain constant as the radius increases. An example of an unstable flow described by Lord Rayleigh is the flow between a fixed outer cylinder and a concentrically rotating inner cylinder. In 1923, G. I. Taylor published an extensive analytic and experimental study of such unstable Couette flows of viscous fluids between rotating cylinders [Ref. 2]. The Taylor number, defined as

$$Ta = \frac{U^{*}d}{\nu}\sqrt{\frac{d}{Ri}}$$

was shown to be a characteristic parameter of such flows with a critical value for the onset of the instability. The secondary flow observed between the cylinders when the outer was fixed and the inner rotated has been shown to be vortices whose axes were in the circumferential direction. These vortices were named as Taylor vortices. In recent years, there have been a large number of investigations of cylindrical Couette flow. The torque required to rotate a cylinder in the presence of Taylor vortices was measured by P. Castle, et al. [Ref. 3]. The same type of instability in the boundary layer along concave walls was first investigated by

H. Goertler in 1940 [Ref. 4]. The Goertler number, which is similar to the Taylor number, is a parameter characteristic of curved boundary layer flows and is defined as

$$Go = \frac{U^*\delta}{\nu}\sqrt{\frac{\delta}{R}}$$

where δ is the boundary layer thickness. When the Goertler number exceeds a critical value, the presence of Goertler vortices is observed. H. W. Liepmann [Ref. 5] was among the investigators to continue and verify Goertler's experimental work. The approximate analytic results obtained by Goertler have been verified with an exact solution by the German investigator G. Hammerlin as reported by H. Schlichting [Ref. 6]. These results were also verified with an extensive numerical solution completed by A. M. O. Smith [Ref. 7].

The problem of instability of viscous fluids flowing in a curved channel was first considered by W. R. Dean in 1928 [Ref. 8]. Dean found a parameter, similar to the Taylor and Goertler numbers, which governs the onset of Taylor-Goertler vortices in curved channels. The analytic work done by Dean has been verified by W. H. Reid [Ref. 9] among others. The experimental work on secondary flows in channels seems very limited. Until just recently, the possible effects of Taylor-Goertler vortices on heat transfer had not been studied. In 1965, L. Persen [Ref. 10] considered the effect of Goertler type vortices on the heat transfer from a wall for the special cases of both a very high and a very low Prandtl number. The first experimental work with the effect

of Taylor-Goertler vortices on heat transfer in a boundary layer was reported by P. McCormack et al. [Ref. 11] in their 1970 study. With some limiting assumptions, a numerical solution for the heat transfer in curved rectangular channels was reported by K. Cheng and M. Akiyama in 1969 [Ref. 12]. Analytic and experimental results for a fully developed, constant wall heat flux, square cross section curved channel were obtained in 1970 by Y. Mori, et al. [Ref. 13].

Although Taylor-Goertler vortices are a laminar flow, they have secondary velocity components and are more complex than one would expect. Furthermore, as indicated by H. W. Liepmenn [Ref. 5], these vortex flows are potentially a key to understanding transition to turbulent flow. Taylor-Goertler vortices have similarities to other vortex flows such as wing tip vortices and the vortex rolls in forced convection heating of fluid layers described in the paper by M. Akiyama et al. [Ref. 14]. The striations seen at stagnation points on bluff bodies and the cross hatching on reentry bodies have also been attributed, at least in part, to the presence of Taylor-Goertler vortices, as reported by L. Persen [Ref. 15].

There are many possible applications that could result from investigation and understanding of these vortex phenomenon. Potential application include improved cooling of turbine blades and other external surfaces, reduction of pressure losses in bends, and improved mixing in laminar

flows. Heat exchangers which could utilize the low pressure drop in laminar flow as well as the enhanced heat transfer in the presence of vortices would be a significant advancement in heat transfer.

II. NATURE OF THE PROBLEM

A. INTENT OF THIS STUDY

Because future application of the Taylor-Goertler vortex phenomenon may take place in closed channels, it was intended to study the effect of these secondary flows in a curved channel of rectangular cross sectional area. To investigate Taylor-Goertler vortices in a curved rectangular channel, the presence of the vortices had to be verified. It was intended to visualize the flow in order to confirm the presence of the vortices. How rapidly the vortices would form and to what extent they would fill the channel was not known. It was intended to use the flow visualization technique to study, as far as possible, the size, the form, and the development of the vortices.

Other planned measurements included a hot wire anemometer check of the turbulence level to insure that the flow was laminar. The velocity profiles in the channel were also to be obtained to determine what effect the secondary flow would have on the mean velocity. The additional velocity components in Taylor-Goertler vortices produce Reynolds stress not present in other laminar flows. It was planned to measure the pressure drop along both the straight and curved portions of the channel used in this investigation to determine the effect, if any, of these Reynolds stresses on the pressure drop. An increase in the pressure drop would be anticipated because it is known that additional

energy is required to maintain the secondary flow. This energy is supplied to the Taylor-Goertler vortices by an interaction of the mean and secondary velocity components. The works of G. I. Taylor [Ref. 2] and P. Castle et al. [Ref. 3] have shown the increase in torque required to rotate a cylinder in the presence of Taylor vortices.

The Taylor-Goertler vortices would also be expected to effect the heat transfer from the concave wall. This effect would result from the secondary velocity components transporting heated fluid from the wall towards the center of the channel, and carrying cooler fluid from the center to the wall. It was intended to study the requirements for measuring the effects of this action on the heat transfer from the concave wall.

B. DESIGN REQUIREMENTS

In order to study Taylor-Goertler vortices, an apparatus had to be built which would give the values of the non-dimensional parameters required to produce the secondary flow. The limit of stability of the basic laminar flow in a curved channel against the formation of Taylor-Goertler vortices is well known, and is presented as a critical Dean number by W. Reid [Ref. 9]. If the Dean number, defined as

$$De = \frac{U^{*}d}{\nu}\sqrt{\frac{d}{R_o}} \quad ,$$

exceeds a value of 36, it is presumed that Taylor-Goertler vortices will be present. Furthermore, it is known that the

rate of development of the vortices will be somewhat dependent on how much greater than 36 the Dean number becomes. It is known that the size of the vortices will depend in some manner on the dimensions of the channel. Investigators of Taylor-Goertler vortices on concave walls have reported vortices from the size of the boundary layer to ten times larger, dependent on geometric factors [Ref. 7]. The Dean number had to be greater than the critical value of 36 and be adjusted within a workable range. One hundred fifty was taken as the upper limit of this range, as it was assumed the vortices would be fully developed by at least this value.

The minimum critical Reynolds number, based on hydraulic diameter, at which turbulent flow is observed in a parallel-plate channel is given by G. Beavers, et al. [Ref. 16] as Re = 2200. Several investigators including H. Liepmann [Ref. 5] and R. Nunge [Ref. 17] have reported that the decrease in the critical Reynolds number due to curvature is small, especially for a large radius of curvature. Therefore, the maximum Reynolds number, based on hydraulic diameter, selected for this investigation was Re = 2000. The Reynolds number had to be high enough for the flow velocities to be measured accurately. A minimum of Re = 100 was used for the design of the experimental apparatus.

The design procedure involved checking the effects of several factors on the range of the nondimensional variables. The working fluid, the channel height, and the flow rate selected, each have an effect on both the Reynolds number

and the Dean number. The radius of curvature also effects the Dean number. Trial and error was used to select the height and width of the channel's cross section, and the following inequality in the Reynolds number was checked to give the range of velocities

$$100 \leq Re \leq 2000$$

The inequality in the Dean number given below was then checked to give the range of the radius of curvature.

$$36 \leq De \leq 150$$

When the velocity range was practical to obtain and easy to measure, and when the radius of curvature was reasonable for construction, the design variables were considered feasible. The resulting relationship between the Reynolds number, based on hydraulic diameter, and the Dean number with the ratio of radius of curvature to plate spacing as a parameter is shown in Figure 2. The selected design is represented by the line $R/d = 48$.

The design of the apparatus for this investigation was also constrained by time and cost limitations. The material and equipment to be used had to be workable, available without long delay, and inexpensive. Water and air were the only working fluids considered as practical. The flow velocities at which water satisfied the Reynolds number and the Dean number requirements were too low to measure by ordinary means. Furthermore, water requires more elaborate construction to prevent leakage from the channel. For these

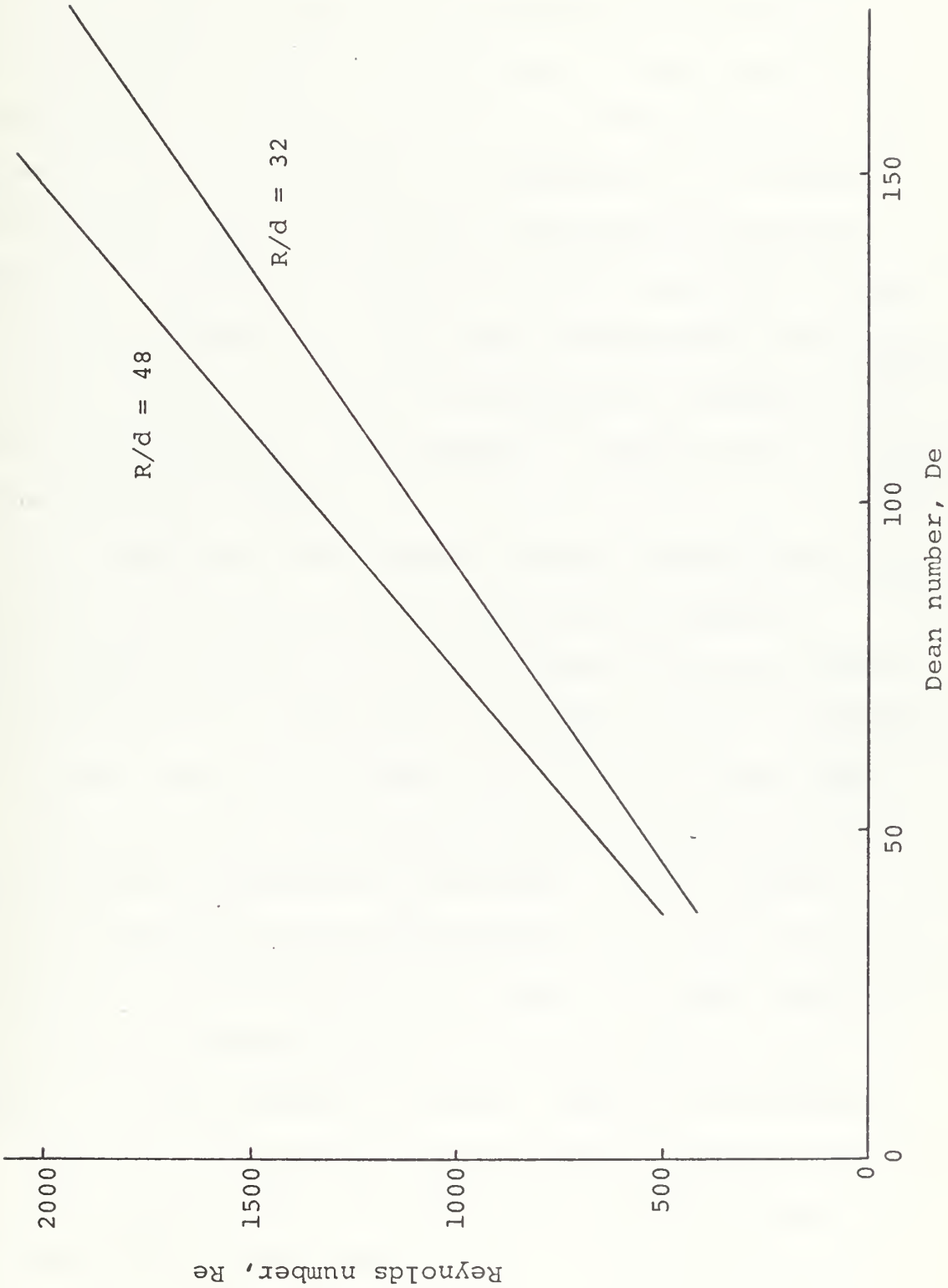
R/d = 48
R/d = 32
Reynolds number, Re
2000
1500
1000
500
0
0
50
100
150
Dean number, De

Figure 2

reasons, air was selected as the working fluid. For design purposes, the value of the fluid properties at estimated operating temperatures were taken from reference tables. The length of the entrance region in the design channel was checked to see that it would not be excessive. To insure smooth entering flow, the entrance contraction section was designed in accordance with considerations given by M. Cohen and N. Ritchie [Ref. 18]. The intent to visualize the flow required the use of a workable, transparent, inexpensive material for the walls of the channel. Plexiglas was selected for this purpose.

It was hoped that the results obtained for both pressure drop and heat transfer would be comparable to infinite parallel plate solutions, so a large aspect ratio was chosen. The pressure drop for flow between parallel plates is known from an exact analytic solution and is not of a large magnitude. This magnitude was compared with the sensitivity of the laboratory micromanometer available. It was decided that the pressure drop could be measured, but only if a sufficiently long test section was built. No exact solution exists for the pressure drop in a curved channel in the presence of Taylor-Goertler vortices. However, the studies by R. Nunge [Ref. 17] and by K. Cheng and M. Akiyama [Ref. 12] indicates a rather small increase in the friction factor in curved channels of large aspect ratio. It was assumed that the curved test section would be sufficiently long to allow measurement of the pressure drop.

To measure the effects of Taylor-Goertler vortices on the heat transfer from a constant temperature concave wall of a curved channel requires comparative data for one wall of a flat plate channel. Heat transfer data for a flat plate channel with one constant temperature wall is very limited. Limiting values of the Nusselt number and other comparative values can be obtained from R. Shah and A. London's report [Ref. 19]. The design of a heater plate to measure this type of heat transfer presented special requirements. As with any flat plate heater, more power would be convected away from the upstream edge than from points farther downstream. Therefore, to obtain an uniform wall temperature, by electrical heating, separate resistance elements with individual voltage controls were required. A multiple channel regulated power controller was not immediately available, but it was determined that such an instrument could be constructed. Grade A nichrome was selected for the heating elements because of this metal's large specific resistance, small temperature coefficient of resistance, and relative low cost. The many power leads and temperature recording leads would have to reach the heating element through the channel wall. For this reason a castable plastic resin was selected for constructing the heater section. Although only a flat heater plate was to be constructed for the first tests, design considerations were given to adapting this construction method to a heater plate for the curved section. Other aspects of the heated section construction will be discussed later. To insure that the heat

transfer data would be for forced convection, and would not contain the effects of free convection, the value of the governing dimensionless group was checked against the requirement

$$Gr * Pr * \frac{Dh}{L} \leq 1000$$

given by J. Holman [Ref. 20]. It was found that this requirement imposed a significant temperature difference limitation for water as the working fluid, but allowed a large temperature range for the selected working fluid, air.

The effects of the many design requirements discussed above was to make the design problem somewhat difficult. However, the working fluid, the geometry, and the flow velocities to be studied are of values frequently encountered in practice.

C. DESCRIPTION OF APPARATUS

The cross section of the channel was 0.250 inches high and 10.0 inches wide. It had an aspect ratio of 40 and a cross sectional area of 0.017361 square feet. The hydraulic diameter of this channel was 0.040650 feet. The channel was made of two one-quarter inch thick sheets of plexiglas separated by rolled metal spacers which also formed the sides of the channel as shown in Figure 3. Steel was used for the spacers in the straight section of the channel and for added flexibility, aluminum was used in the curved portion. A straight portion of this channel, consisting of a

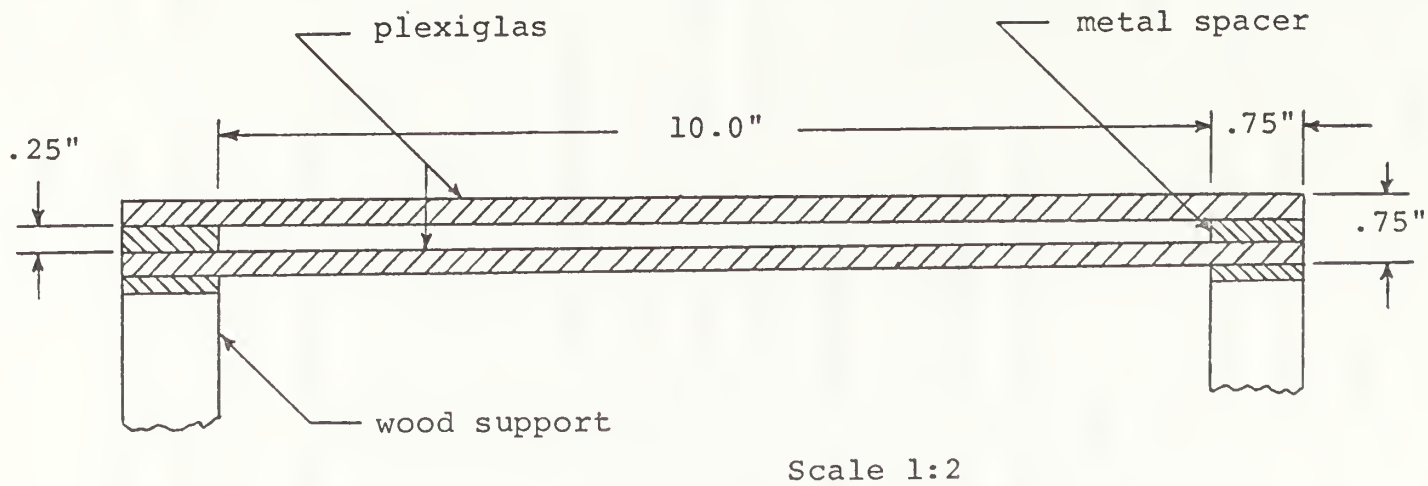

Figure 3. Cross Section of Channel.

two foot long entrance section and a two foot long test section, preceded the curved section. The radius of curvature of the interior concave wall of the curved section was one foot. The curved section was formed by heating the plexiglas and bending it over a carefully constructed wood frame. This wood frame was also used to support the entire channel. The curved portion of the channel completed a 180 degree turn and was followed by a short straight section.

The flow of air entered the channel through a contraction section attached to the beginning of the entrance region and covered by a cheesecloth screen for most of the experimental work. The flow left the channel through an exhaust nozzel which was connected to flexible tubing of one inch inside diameter. The tubing led the flow through a Fischer and Porter Company variable area flow meter, model number 10 A3565. This rotometer had a 100% full scale flow rate of 11.1 standard cubic feet of air per minute and an accuracy of ±0.5% of full scale. The flow was drawn through the flow meter, the flexible tubing, and the channel by an electrically driven Cadillac, model G12, centrifugal blower. The blower speed was controlled by varying motor voltage with a variac. The voltage was supplied by a Sorenson, R 1050, A.C. voltage regulator. The general arrangement of this apparatus is shown in Figure 4.

The idea of using an aerosol for visualizing the flow was taken from a paper by O. Griffin and C. Votaw [Ref. 21]. The advantages and ease of using an aerosol are derived from

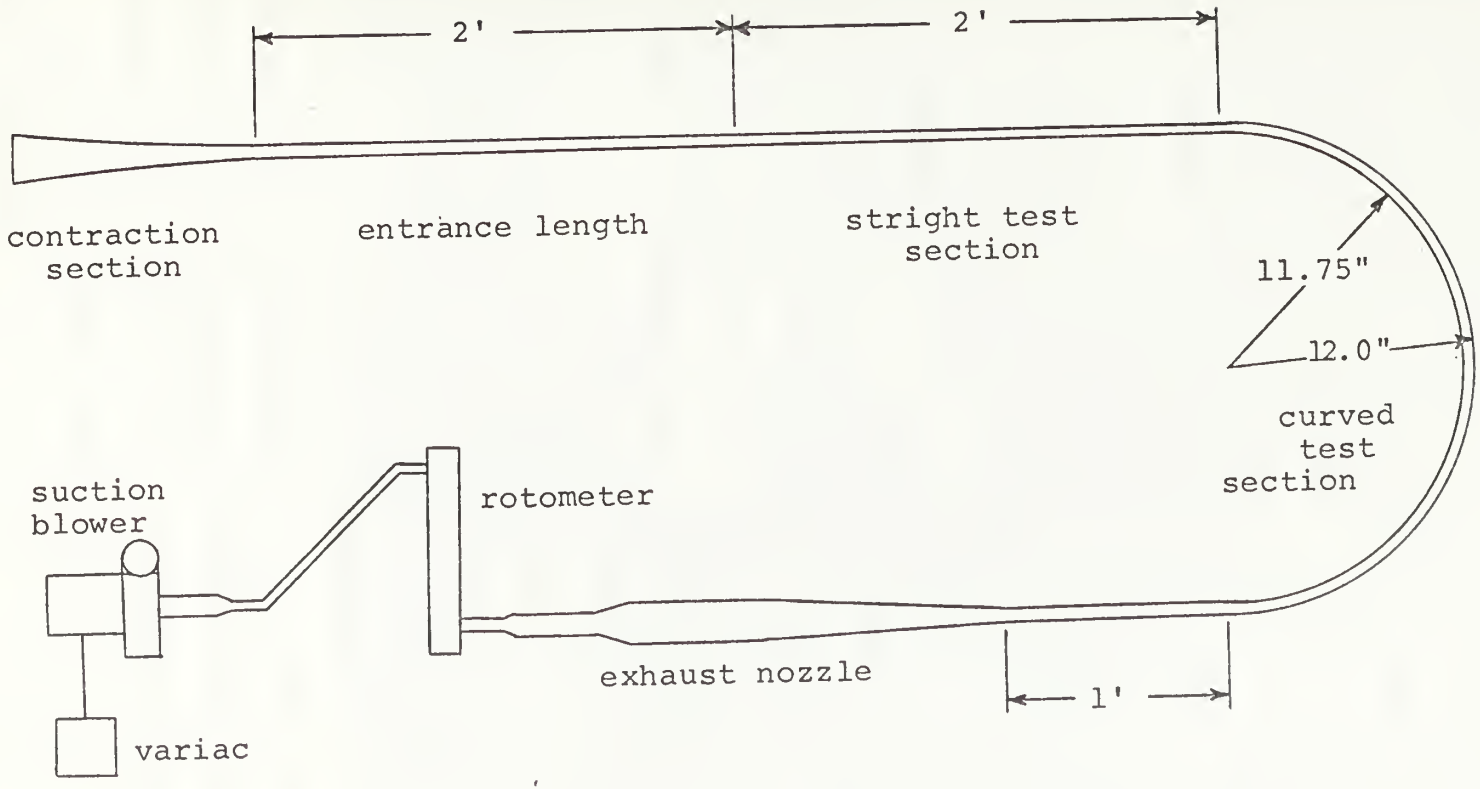

Figure 4. Arrangement of Apparatus.

the non-toxic and non-corrosive properties of the DOP, di (2-ethylhexyl)-phthalate, chemical used. The equipment used to make the aerosol was built in accordance with a United States Naval Research Laboratory report by W. Echols and J. Young [Ref. 22] and personal communications with O. M. Griffin. Air from a regulated and filtered supply was piped to an atomizer nozzle submerged in a jar of DOP. In addition to the pressure regulator, there was a throttling valve on the air line and the depth of submergence of the nozzle could be adjusted. The aerosol from the top of this jar was collected and led to a jet impactor in a second jar. The effect of the jet impactor was to remove excessively large particles and to make a smaller, more uniform aerosol particle size. The aerosol was then led to a settling chamber where the pressure was reduced to nearly atmospheric level by bleeding off the excess aerosol. Flexible injection tubing of 0.250 inch inside diameter connected the settling chamber to the contraction section where the aerosol entered the channel. The aerosol generating equipment is pictured in Figure 5. The character of the aerosol used was such that visualization of the flow was facilitated by illuminating slits along the channel and viewing them at approximately 90° to the light. A single 650 watt Colortran light, model 100-071, was placed on the side of the channel opposite the viewer. The light was collimated with a paper cone lined with aluminum foil. Flat black paper was taped to the outside of the channel walls to make four narrow

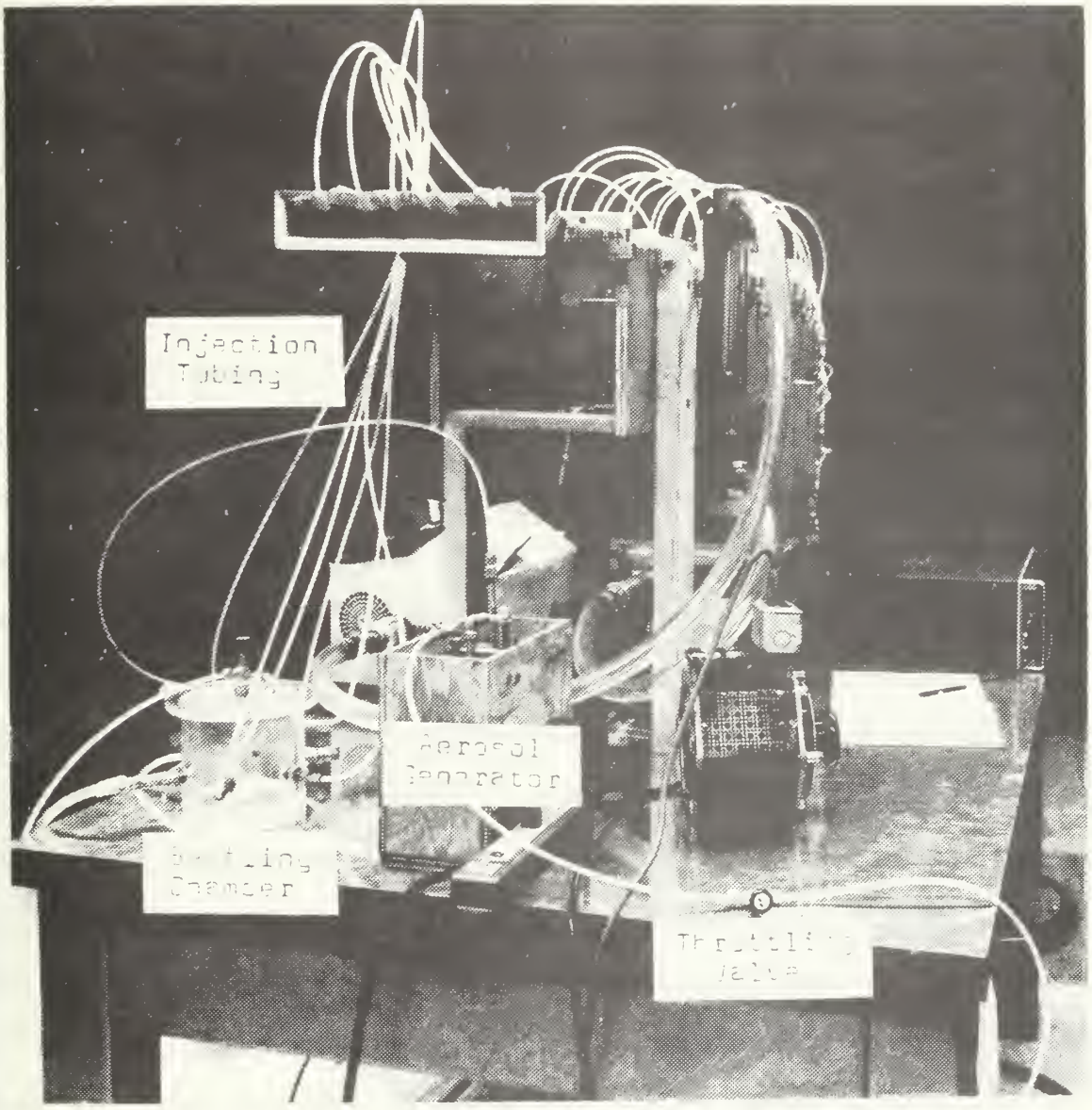

Figure 5. Aerosol Generating Equipment.

slits. The light beam was directed through one of these slits so that a small area of the flow could be visualized. A Nikomat 35 mm camera and a Nikon 55 mm f3.5 Macro-Nikkor lens was used to obtain photographs of the flow patterns. A sketch of the lighting and camera arrangement is shown in Figure 6. The visualization techniques and procedures will be discussed more fully when the photographs are presented.

In addition to visualizing the flow it was planned to measure the velocity profile. Due to the size of the channel, a sub miniature hot wire anemometer probe, Thermo-Systems Inc. model 1279, which had a 90° bend in the supports was used to measure the turbulence levels. This probe was located three inches from the center line of the channel and 20 inches of arc length downstream from the start of the curved portion of the channel. The probe was placed in a plug and inserted through the convex wall of the channel. The inside surface of this plug fit flush with the wall of the channel, and had the same radius of curvature. The 0.035 inch diameter body of the hot wire anemometer protruded from the plug and was fastened to a micrometer barrel which was mounted on a machined block attached to the outside of the channel. In this way, the movement of the wire from very close to the concave wall of the channel to near the convex wall could be controlled and measured. This arrangement is shown in Figure 7. The leads from this probe were connected to a Thermo-System Inc. hot wire anemometer system, model 1050, including a Hewlett-Packard RMS Meter.

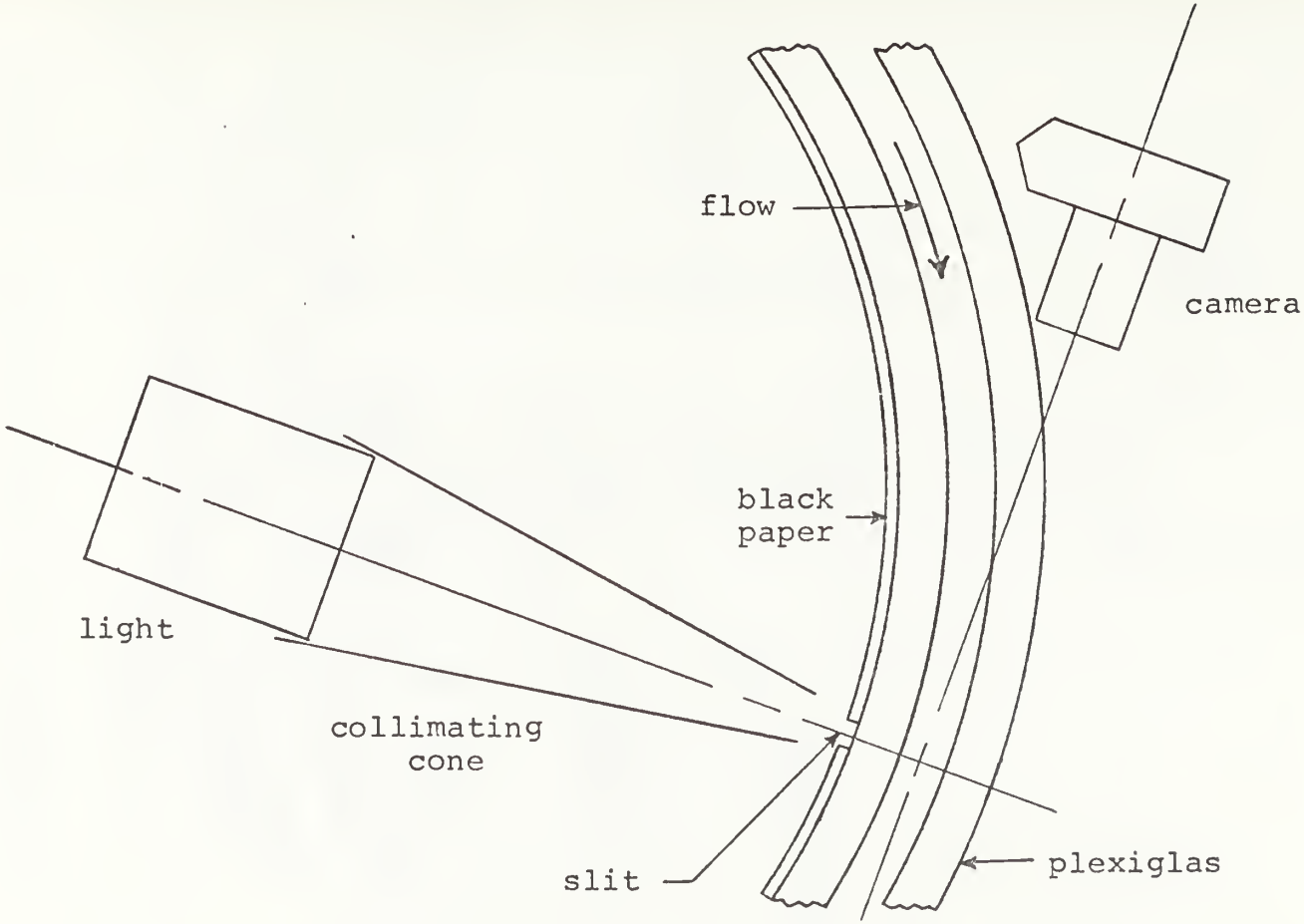

Figure 6. Lighting and Camera Arrangement.

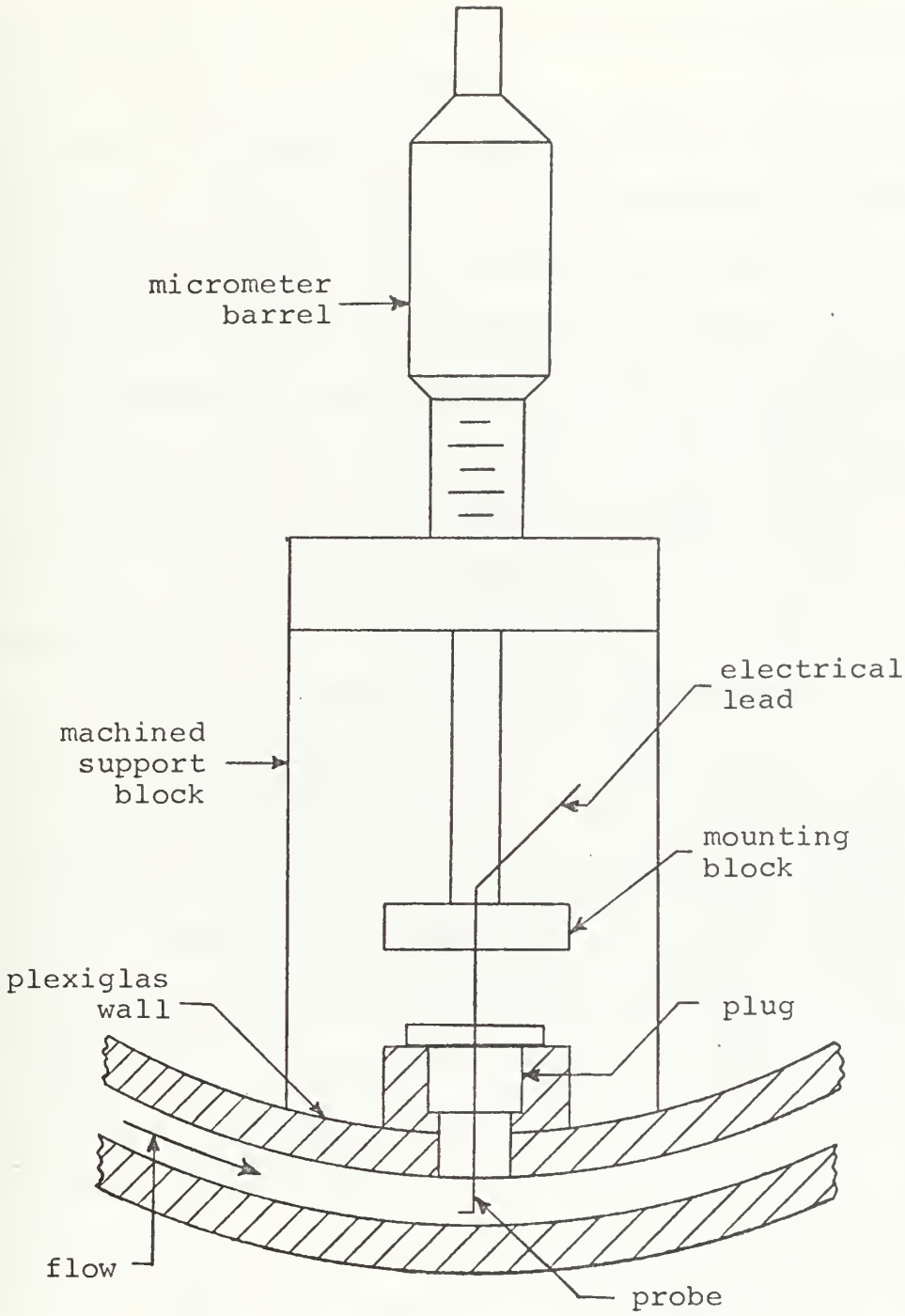

Figure 7. Hot Wire Anemometer Arrangement.

A Thermo-Systems Inc. calibrator, model 1125, was used to calibrate the hot wire anemometer.

In order to measure the pressure drop along the length of the channel, pressure taps and a micromanometer were required. Pressure taps were located every three inches along the entire length of the channel, starting two inches from the beginning of the entrance section and alternately set 0.250 inches to the right or left of the center line. Along the curved section, the three inch spacing was measured on an arc of one foot radius, resulting in a total of 28 pressure taps with number 17 being two inches into the curved section. These pressure taps consisted of a 0.040 inch diameter hole drilled into the channel with a short plexiglas tube glued into a 0.250 inch hole counterbored over the smaller holes. Flexible tubing with pressure fittings was connected to these short tubes to facilitate connecting and disconnecting the micromanometer. The instrument used in this investigation was an E. Vernon Hill and Company Type C micromanometer with a range up to two inches of water and a sensitivity of 0.001 inches of water. This micromanometer is of the re-zeroing type where the reservoir is raised to return the meniscus to the same level it had before the pressure was applied, and the amount the reservoir is raised indicates the pressure. A photograph of the channel and the pressure measuring apparatus is shown in Figure 8.

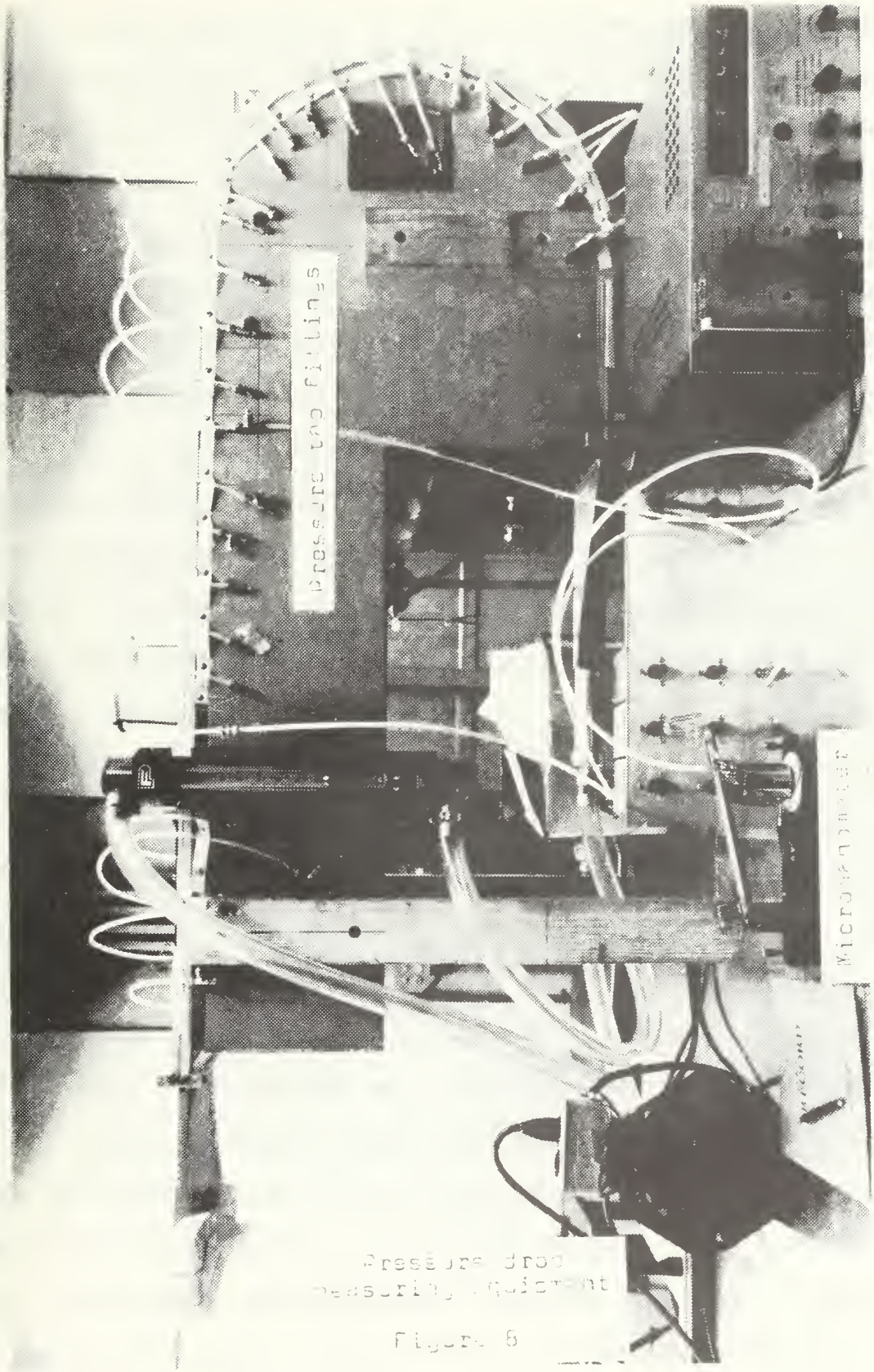

Pressure drop
measuring equipment

Figure 8

The bulk temperature of the air was measured six inches after the entrance of the channel, and three inches after the heating plate, by four thermocouples spaced across the channel at each location. Copper-constantan thremocouples were used. They were located at different heights in the channel and connected in parallel to give the average bulk temperature. An ice bath reference junction was provided, and these thermocouples and the others used in this experiment were connected through a switch to a Dymec digital voltmeter, model 2401B. These thermocouples and a sample of the others used in this study were calibrated in a Rosemont Laboratory Calibration System. In this constant temperature bath, the temperature was determined by a platinum resistance thermometer.

A wall heater was constructed for the straight test section of the channel. This heater was formed of forty 0.004 inch thick, 0.125 inch wide strips of nichrome run across its 11.5 inch width. These metal ribbons were placed in a mold by hand and spaced approximately 0.010 inches apart. The streamwise length of the plate was 5.50 inches. A copper-constantan thermocouple was welded to the center of each of the nichrome strips. Power leads were connected to one side of each strip four inches from the center of the plate. On the other side of the centerline, the strips were connected together in pairs to make 20 electric circuits. The 20 heaters were individually supplied by a specially constructed, regulated

high current D.C. power supply and a 20 channel power controller. The D.C. power supply had a 200 amp capacity and a maximum RMS ripple of one millivolt. The power controller was a 20 channel potentiometer biased series regulated voltage source with a temperature compensated reference voltage. The components of this power controller were mounted on a common heat sink in order to improve the stability of operation. The power supply and controller are shown in operation in Figure 9. When all the power leads and thermocouple leads were in place, APCO 210 epoxy resin with APCO 180 hardener was poured into the mold. This thermal set plastic was cured at room temperature for approximately 24 hours. When the heater plate was removed from the mold, it was found to be warped. A metal frame was constructed, securely attached to the outer edges of the 0.250 inch thick casting and adjusted to produce a completely flat plate. A further problem experienced with the casting involved some of the nichrome strips near the trailing edge of the plate that had pulled away from or sunk into the plastic during drying. This resulted in rough spots on the surface of the plate. The loose strips were cut and removed from the heater, and the low spots, from the 33rd strip to the end of the plate, were filled with epoxy. The plate was then lightly sanded, resulting in a smooth surface. The first 16 heating circuits remained useable, which resulted in a heated area 8.125 inches wide by 4.384 inches in the flow direction.

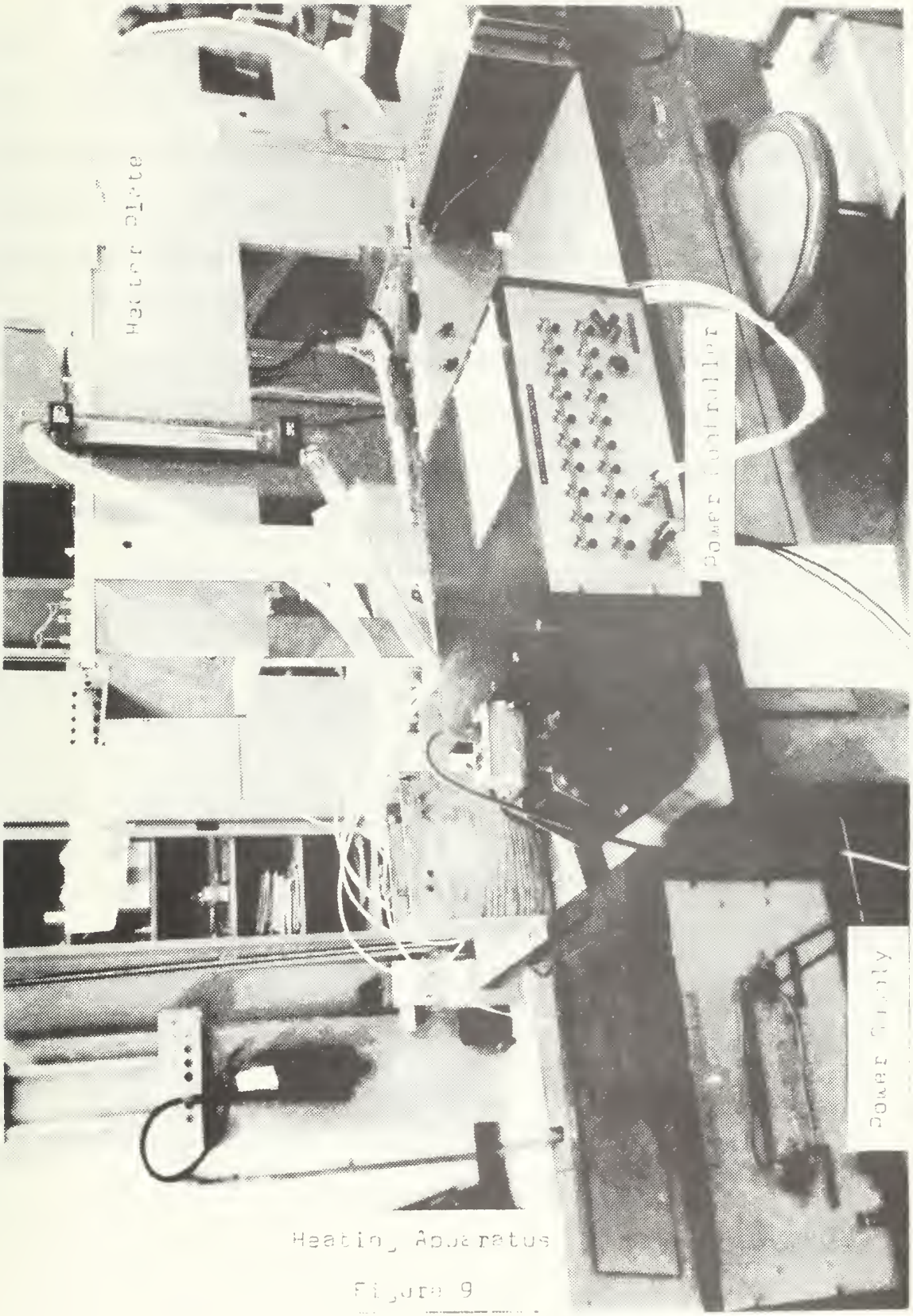

Heating Apparatus

Figure 9

After the other experimental work was completed, a 5.50 inch piece of the upper wall of the channel, between the two foot ten inch station and the three foot 3.50 inch station, was removed. The heater was placed into this cut, becoming part of the straight wall of the channel with the nichrome ribbons exposed to the flow of the air. The top of the heater and the surrounding channel walls were then covered with a 0.125 inch thick layer of Johns-Manville Company Min-K insulation. The Min-K was covered with a one inch layer of glass wool. Each piece of the apparatus was cleaned and carefully prepared before the experimental work began.

III. FLOW VISUALIZATION

A. EXPERIMENTAL CONSIDERATIONS

The aerosol generating equipment was found to be very versatile as to the amount and quality of the aerosol produced. After much trial and error, good quality aerosol was found to be that of relatively small particle size and low exhaust pressure. This aerosol appeared much like cigarette smoke when discharged into the room. A supply air pressure of 30 pounds per square inch, or slightly less, an atomizer nozzle submergence of approximately 0.50 inches, and a low settling chamber pressure were the conditions which produced this aerosol. Producing this quality aerosol and getting the right amount of it into the channel proved to be important in visualizing the flow. Viewing the aerosol at the proper angle relative to the incident light was also important. For lighting, the best arrangement was to place a single, strong light near the center of curvature of the channel and to shine it radially outward. The collimated beam of light was directed through narrow slits formed from black paper taped to the channel. If this small area of the flow was viewed from an angle tangent to the channel, the vortex patterns could be readily seen. This viewing location was the same as the camera location shown in Figure 6. Four such narrow slits were made along the curved section of the channel. The first slit was located 7.50

inches from the beginning of the curved portion of the channel. The second was 12.00 inches downstream from the first, and the third was 11.50 inches farther downstream. The last slit was located at the end of the curved section, 8.0 inches from the third slit. At the location of this fourth slit, the channel enters the final straight section.

To obtain photographs of the flow patterns in each of these slits, the camera with the 55mm macro lens was mounted on a tripod and moved as close to the channel as possible. The camera was aligned with the axes of the vortices by placing the camera on a tangent to the channel. In the case of the first and second slits, the flow was coming toward the camera, and in the case of the third and fourth slits, the flow was away from the camera. Due to the many reflections observed from the surfaces of the plexiglas, the room was darkened while the photographs were taken. A Gossen "Luna-Pro" exposure meter with a variable angle spot meter attachment was used to assist in obtaining the proper exposure settings. Under these difficult conditions, several attempts were required before satisfactory photographs were obtained.

Other arrangements for viewing the flow were also tried. Looking radially inward through the channel toward a less intense light located near the center of curvature showed a different type of pattern. The patterns seen were streaks or lines in the direction of the flow. These patterns were similar to those seen by other investigators including

L. Persen [Ref. 15]. Several methods of injecting the aerosol into the flow were also tried. The methods involving small tubes or fittings did not work because sufficient aerosol would not pass through these passages. The results obtained from the other methods were for the most part the same as for the method chosen. In a few cases, the early development patterns appeared differently, depending on how the aerosol entered the channel. The fully developed vortex pattern, however, always appeared the same.

B. PATTERNS AND PICTURES OF THE FLOW

The pictures of the vortex patterns are presented in Figures ten through 15. Below each picture is a slit number, a Reynolds number and a Dean number indicating the location of the slits, the flow rate and the value of the characteristic parameter for secondary flow respectively. For the channel used in this investigation, the Dean number is related to the Reynolds number by

$$De = 0.073973 * Re.$$

The line below the vortex patterns in these enlarged pictures is the concave wall of the channel. The line of reflected light above the vortices is the inner wall of the channel which is 0.25 inches from the concave wall. The photographs taken at slit four appear slightly different than the others because the lighting angle and therefore the reflections from the plexiglas were slightly different. The pictures in each figure are arranged with slit one at the top of the page

and the downstream slits in order below the first. The Reynolds numbers of the pictures in each figure are intended to be of the same magnitude. There is not complete representation of the same Reynolds numbers or an even sampling of the slit location because of the moderately high failure rate of obtaining pictures. In spite of this difficulty, the photographs presented are indicative of the Taylor-Goertler vortices as observed. The figures are in order of increasing average Reynolds number.

A number of distinct patterns appear repeatedly in these pictures. At the lowest velocities, the aerosol remains near the concave wall in a pattern that is not clearly a fully developed vortex flow. Examination of these patterns in Figures 10a, 10b, 11a, and 12a show that the ends are curled up. This same pattern has been observed farther downstream in slit three at flow rates lower than pictured here. This pattern occurs predominately near the beginning of the curved section. From extended observation of both this pattern and the motion at the curled end, it is felt that they represent the beginning of a developing weak vortex.

The next form considered looks much like a "mushroom." This pattern is exemplified by Figures 12b, 11b and the right side of 10c. The appearance of two different patterns under the same conditions, as in Figure 10c, was observed occasionally. Such occurrances are possibly explained in terms of the actual finite width of the channel which produces a stronger velocity gradient near the side walls than in the

middle. A difference in the placement of the aerosol injection tubes could also contribute to the appearance of different patterns at the same flow rate. Furthermore, as the vortices develop and occupy more space in the channel, some will be distorted to make room for the others. At higher Reynolds numbers, the top of the curl pattern, as in Figures 13a, 14a, and 15a, could be considered a "mushroom" on a small scale. The "mushroom" shape occurs farther downstream or at higher velocities than the first pattern discussed. This shape always proceeds in distance or flow rate, the first clear vortex patterns. The "mushroom" has been observed to lead directly into distinct vortices and therefore should be considered as a developing vortex.

The next pattern is the round form shown in Figures 11c, 13b, 14b, and 15b. These forms represent a counter rotating pair of vortices with flow leaving the concave wall in the center and curling back toward the wall on either side. These round vortex patterns do not appear to occupy all the space in the channel. In Figure 13b there appears to be space above the vortices, and in Figure 15b the space appears below the vortices. However, the aerosol which is what was photographed does not necessarily show the entire vortex pattern. The aerosol shows a streakline line pattern which may be somewhat dependent on how the aerosol enters the developing vortices. As the flow rate and the downstream distance increases, the fully developed vortex patterns appear. These vortices, as shown in Figures 10d, 11d, and

12c are the full height of the channel and occupy a nearly cellular area. Such patterns could be considered as fully developed Taylor-Goertler vortices.

As the velocities continued to increase, the vortices grew in width until they began to crowd one another, as seen in Figures 13c, 14c, 14d and 15d. If the distance or the Reynolds number were increased farther, an unsteady oscillatory motion developed in the spanwise direction. This action which could be observed by eye, was difficult to show in a still photograph. Figure 13d is the result of such an attempt. The observations indicated that the sideways oscillations of the vortices may involve the absorption of one vortex by an adjacent growing one. It was apparent that an increase of oscillatory motion would have led to turbulence.

It was evident from the photographic study that the vortices did require some distance to develop. Several different flow patterns were observed during the development. At high-flow rates, less distance was required for the vortices to become full size. There were several complexities observed in the flow patterns which could lead to further studies.

(a). Slit 1 Re = 609 De = 45.0

(b). Slit 3 Re = 609 De = 45.0

(c). Slit 4 Re = 662 De = 49.0

(d). Slit 4 Re = 742 De = 54.9

Figure 10

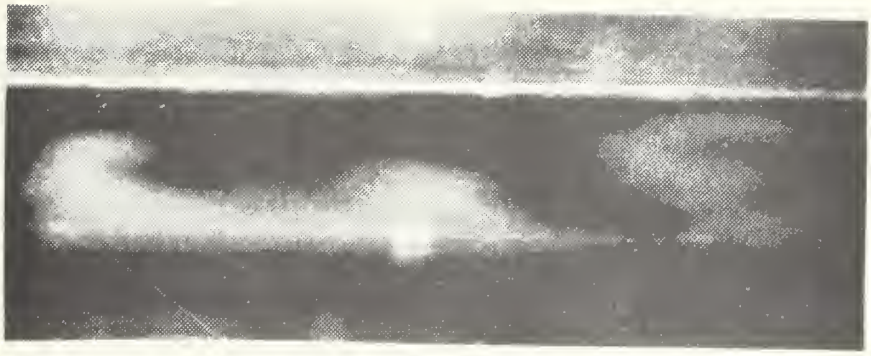

(a). Slit 1 Re = 874 De = 64.7

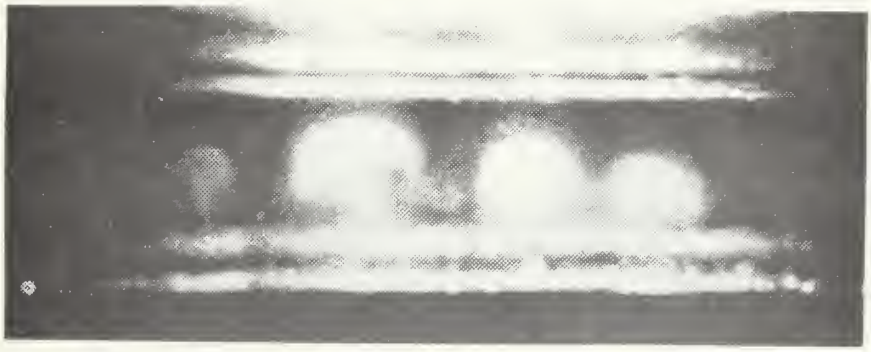

(b). Slit 3 Re = 742 De = 54.9

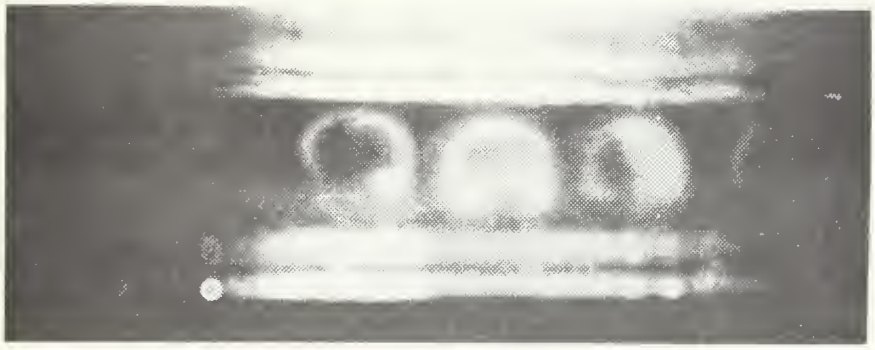

(c). Slit 3 Re = 874 De = 64.7

(d). Slit 4 Re = 874 De = 64.7

Figure 11

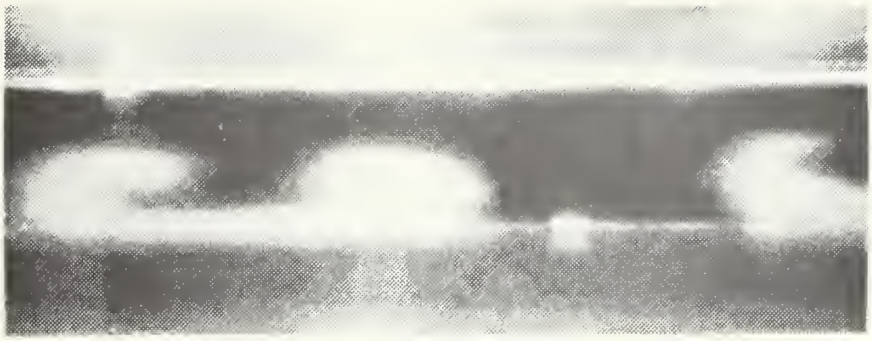

(a). Slit 1 Re = 874 De = 64.7

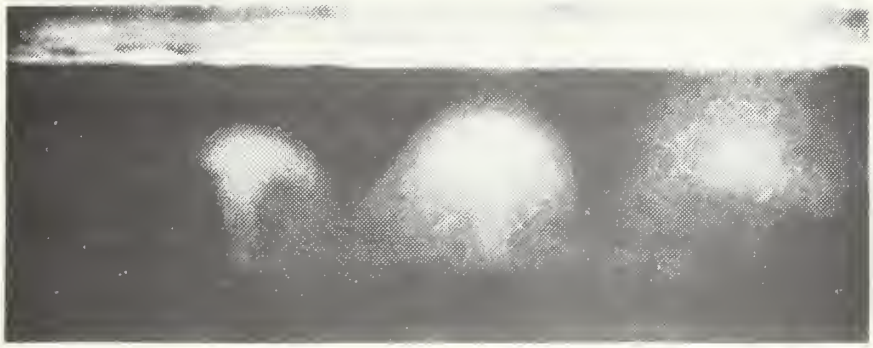

(b) Slit 2 Re = 954 De = 70.6

(c). Slit 3 Re = 927 De = 68.6

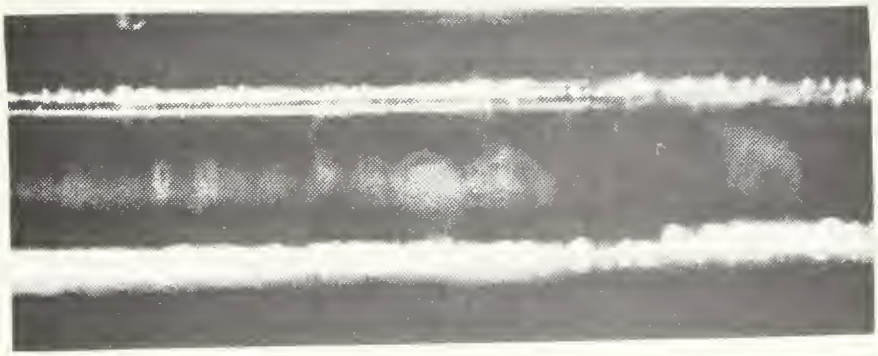

(d). Slit 4 Re = 874 De = 64.7

Figure 12

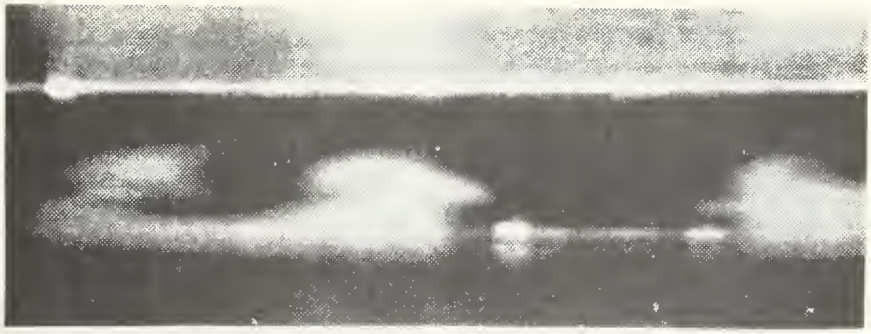

(a). Slit 1 Re = 1033 De = 76.4

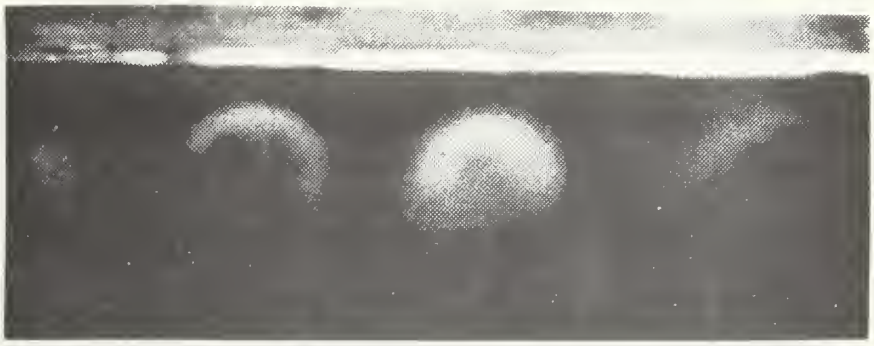

(b) Slit 2 Re = 1033 De = 76.4

(c) Slit 3 Re = 1033 De = 76.4

(d) Slit 4 Re = 1033 De = 76.4

Figure 13

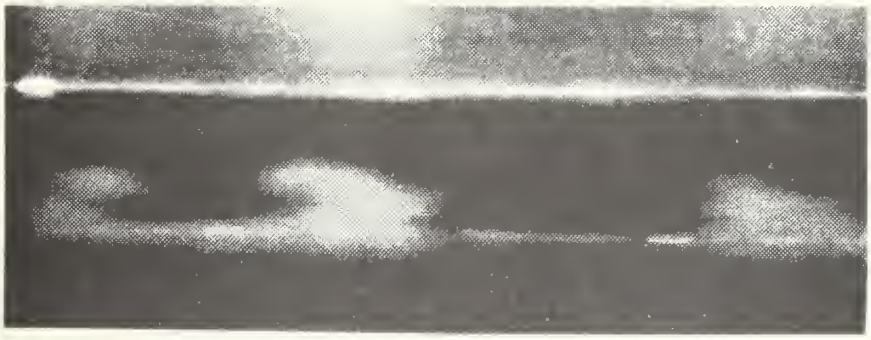

(a) Slit 1 Re = 1166 De = 86.3

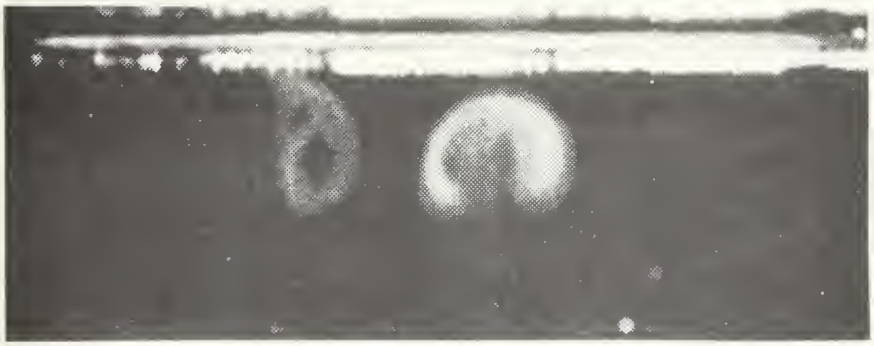

(b) Slit 2 Re = 1166 De = 86.3

(c) Slit 3 Re = 1033 De = 76.4

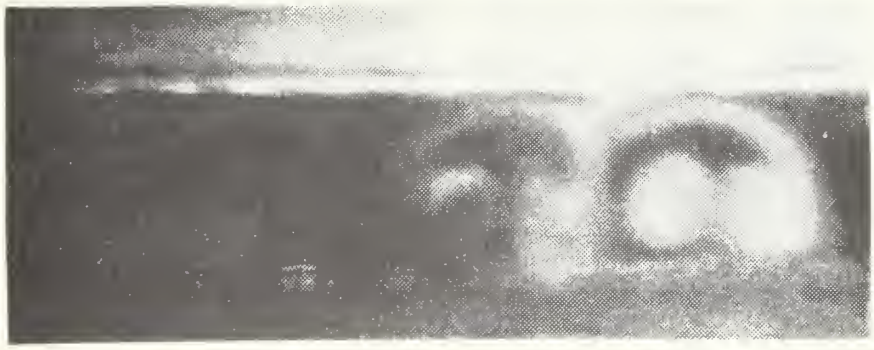

(d) Slit 3 Re = 1166 De = 86.3

Figure 14

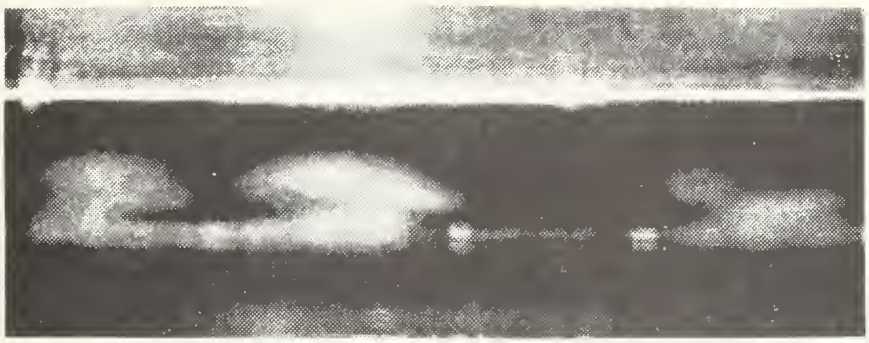

(a) Slit 1 Re = 1457 De = 107.8

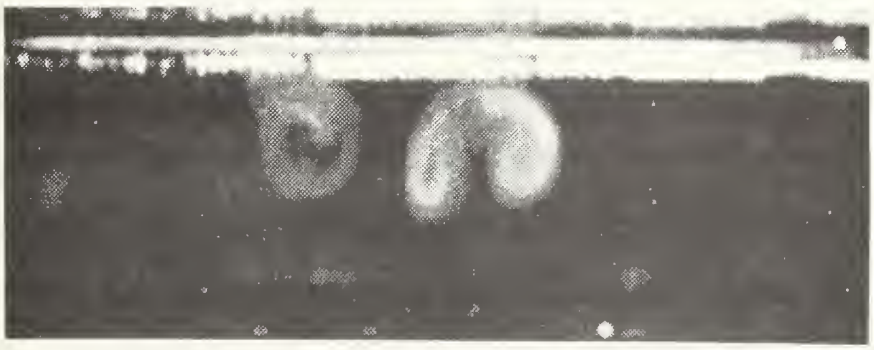

(b) Slit 2 Re = 1245 De = 92.1

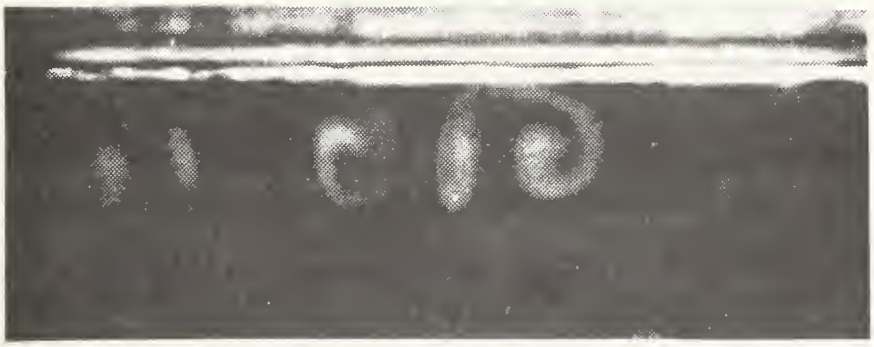

(c) Slit 2 Re = 1457 De = 107.8

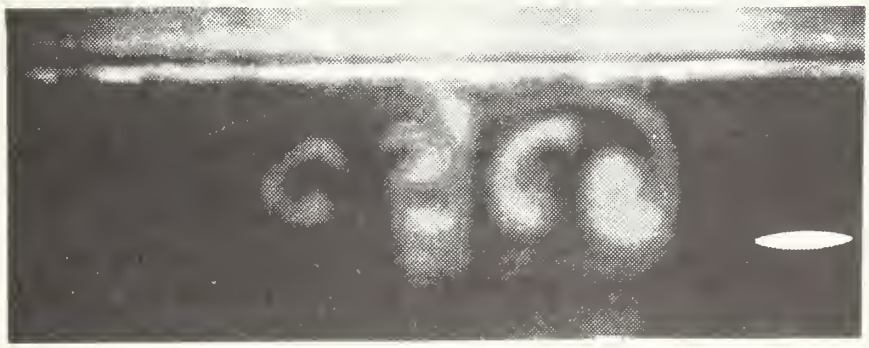

(d) Slit 3 Re = 1298 De = 96.0

Figure 15

IV. VELOCITY AND TURBULENCE MEASUREMENTS

A. EXPERIMENTAL PROCEDURES

The sub miniature hot wire anemometer probe to be used to obtain the mean velocity profiles was connected to the anemometer. The cold resistance of the wire was measured as 7.90 ohms. Based on an overheat ratio of 1.5, the anemometer's operating resistance was set at a value of 11.85 ohms. The anemometer's signal was fed into an oscilliscope so that the patterns could be observed. Stability and trim controls were adjusted for maximum frequency response. The probe was centered in the chamber of the calibrator. A filtered air supply was connected to the calibrator, and the pressure drop across the calibrator's flow nozzle was measured by an incline manometer. With the anemometer switched to run, the flow rate through the calibrator was adjusted to different levels. The pressure drop in inches of water, the bridge output voltage, and the RMS voltage were recorded. This data was reduced by the calibration program shown in Appendix B and the square of the output voltage was plotted as a straight line against the square root of the flow velocity in feet per second. The slope and intercept of that straight line were the values required to reduce further data, and were found to be 0.710 and 2.020 respectively.

The hot wire anemometer was removed from the calibrator and inserted as far into the plexiglas mounting plug as possible. The mounting block for the micrometer barrel was attached to the stem of the probe, and the distance from the base of the block to both the top of the plug and to the hot wire were measured. The difference in these machine vernier readings was 0.050 inches. This was as close as the hot wire anemometer could come to the convex wall of the channel. The micrometer barrel and a straight piece of steel wire had been used to measure the distance across the channel at the location of the plug. This distance was found to be 0.240 inches, indicating that the probe would have a travel of 0.190 inches across the channel. When the plug was inserted into the channel and the micrometer was attached to the mounting block, the micrometer reading was 0.460 inches. The hot wire anemometer was carefully moved until the supports for the wire contacted the concave wall of the channel. The micrometer reading at this point was 0.270 inches, verifying the 0.190 inches of travel. The wire itself was very close to, but not touching, the wall. The data was taken between these micrometer settings of 0.270 inches and 0.460 inches.

Before the data was taken, the channel, the blower, and the electronic instruments were allowed a warm up period of about one hour. After the warm up, the flow rate was adjusted and a minimum of 30 minutes was allowed for steady state to be achieved. At each flow rate, the temperature of

the incoming fluid was measured and the micrometer was moved 0.010 inch between data positions. At each position, the flow rate was checked to see that it was stable, and the micrometer setting, the output voltage, and the RMS voltage were recorded. This data was reduced by a computer program which plotted the mean velocity and the turbulence intensity against the distance from the concave wall. This program and the printed results are contained in Appendix B.

B. VELOCITY PROFILES

The velocity recorded and shown in the figures which follow was not just the mean velocity component down the channel, but the vector sum of the streamwise and the radial velocity components. The portion of the response that was due to the radially inward or outward flow could not be determined by this one set of measurements. However, at the flow rates of this experiment, a nearly parabolic velocity profile would be expected if the secondary flow was not present [Ref. 17]. This has also been shown for curved channels of square cross section [Ref. 13]. The position of the hot wire relative to the vortices was not determined during the tests. Considering the nature of vortex motion, a shift in the position of the vortex relative to the probe could have made a difference in the velocity indicated. The location of the hot wire anemometer was very close to the second slit used in flow visualization. Thus, for each flow rate, the vortices may be considered to have developed to a corresponding level.

Figures 16 through 22 show the mean velocity in feet per second versus the distance from the concave wall in hundredths of an inch. There was a maximum uncertainty of approximately 0.010 inches on the location of the wall. The uncertainty in the velocity measurement using the T.S.I. system was at most 0.05 feet per second. Figure 16 shows a parabolic shape with a small increase in velocity indicated near 0.060 inches. This point may be associated with an active point of a developing vortex. The step in the velocity shown near the wall could be associated with the probe actually contacting the wall, or with the error in positioning. In this case, and in all other graphs, the curve should be extended to zero at the wall. Although a vortex was most probably present, Figure 17 shows no irregularities in the velocity profile. Perhaps the probe was located near the center of a vortex at this time. The same comment could be true of Figure 18. The magnitude of the velocity is increasing as would be expected.

Figure 19 shows a variation from the parabolic profile. As indicated by Figure 15b, the vortices were growing at this Reynolds number and a different portion of the vortex may have been acting on the wire. In Figure 20 the velocity profile appears much different. In this case, the radial velocity component was larger near the wall than in the center of the channel. Figure 21 is much the same as Figure 20. A different profile appears in Figure 22. This last profile could be explained in terms of the hot wire

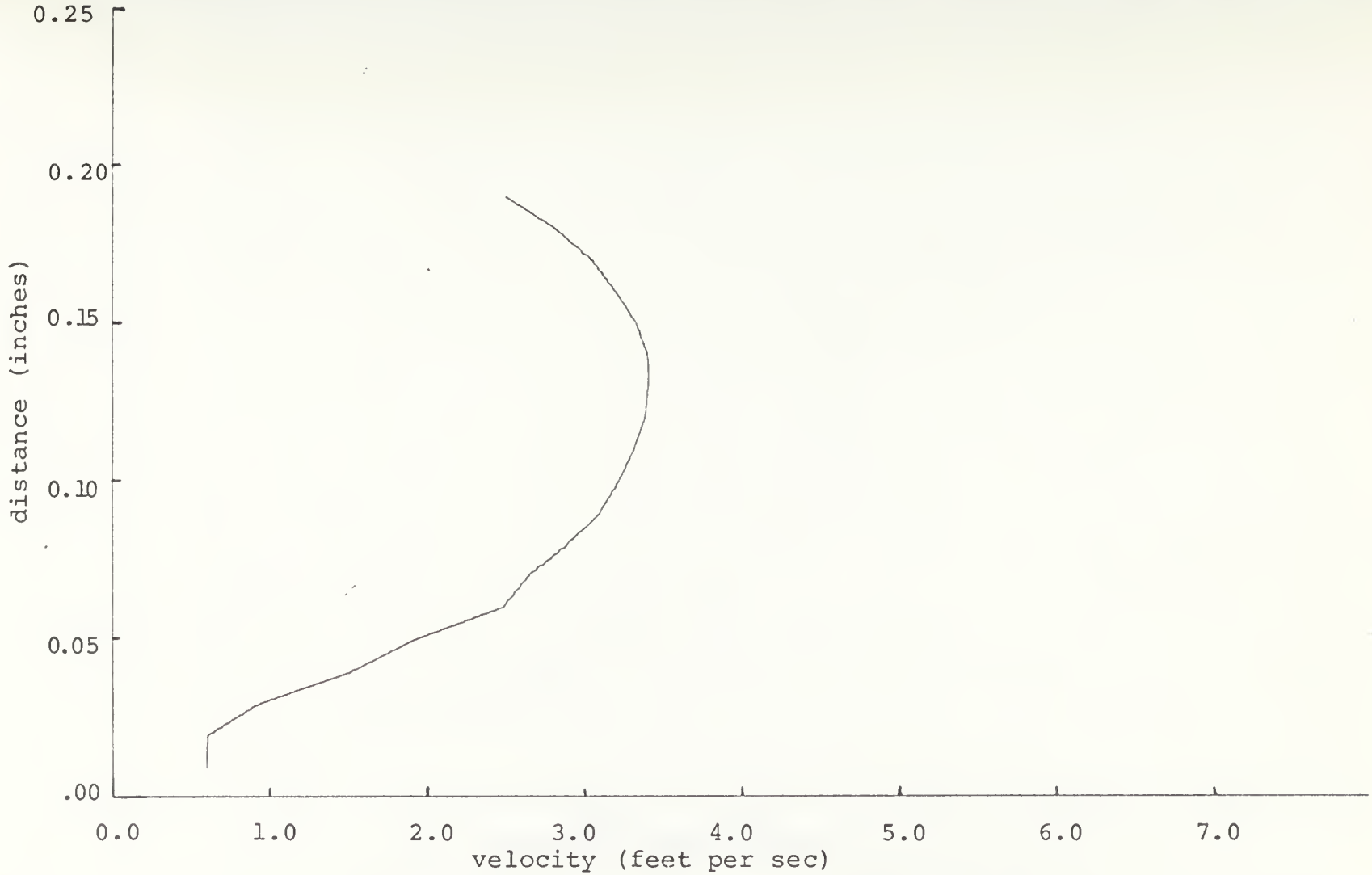

Figure 16. Velocity Profile Re = 609

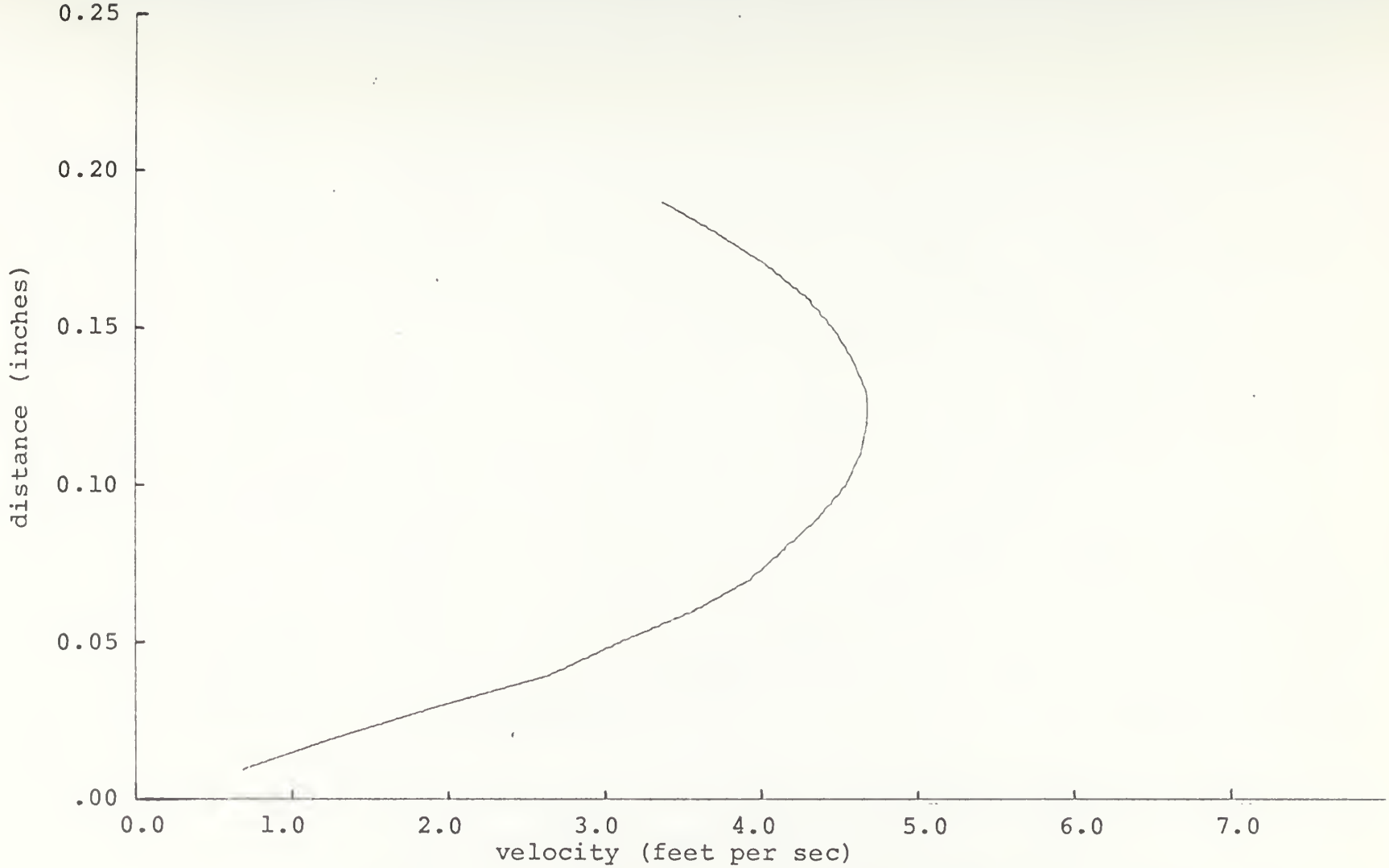

Figure 17. Velocity Profile Re = 875

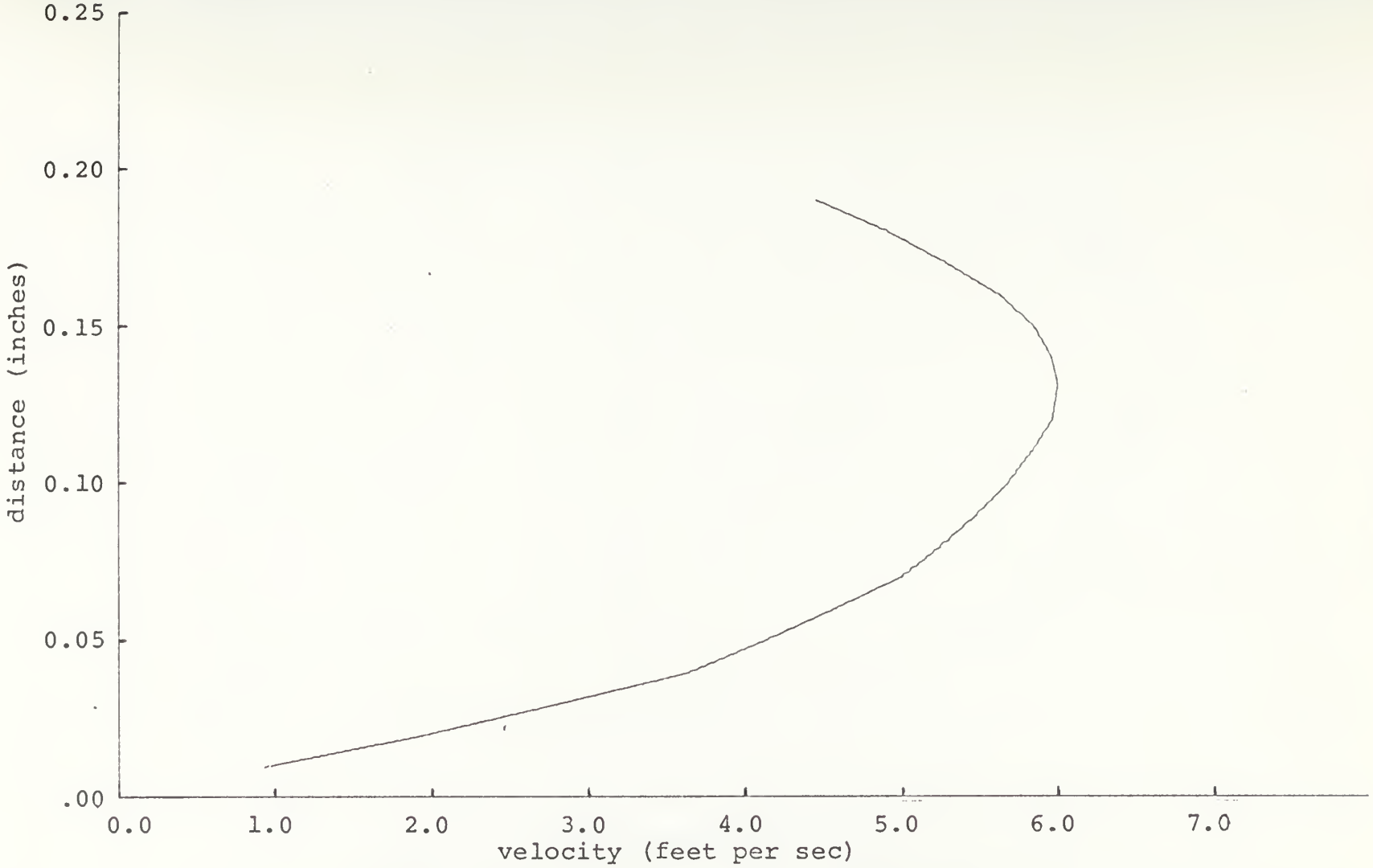

Figure 18. Velocity Profile Re = 1166.

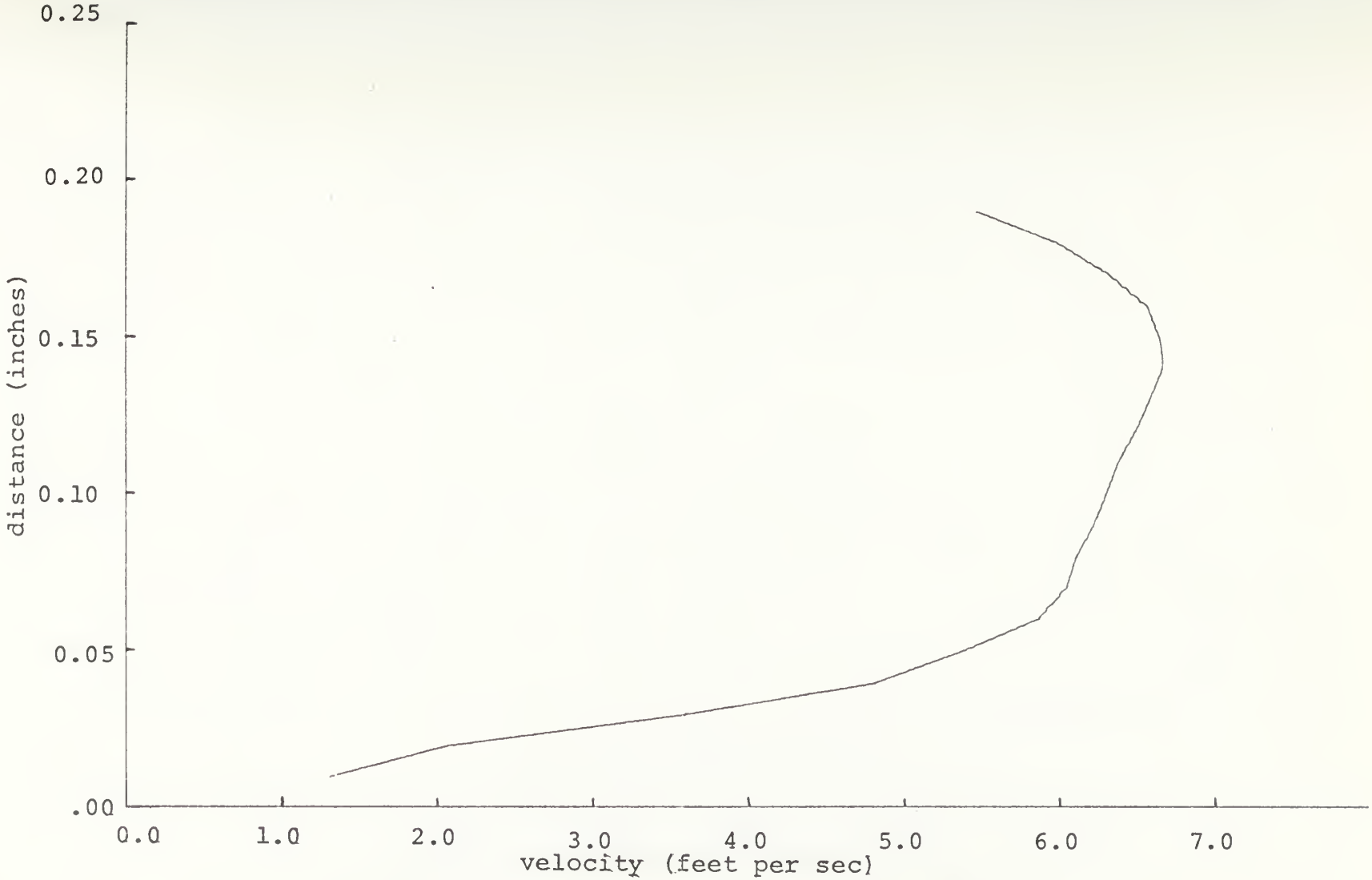

Figure 19. Velocity Profile Re = 1298.

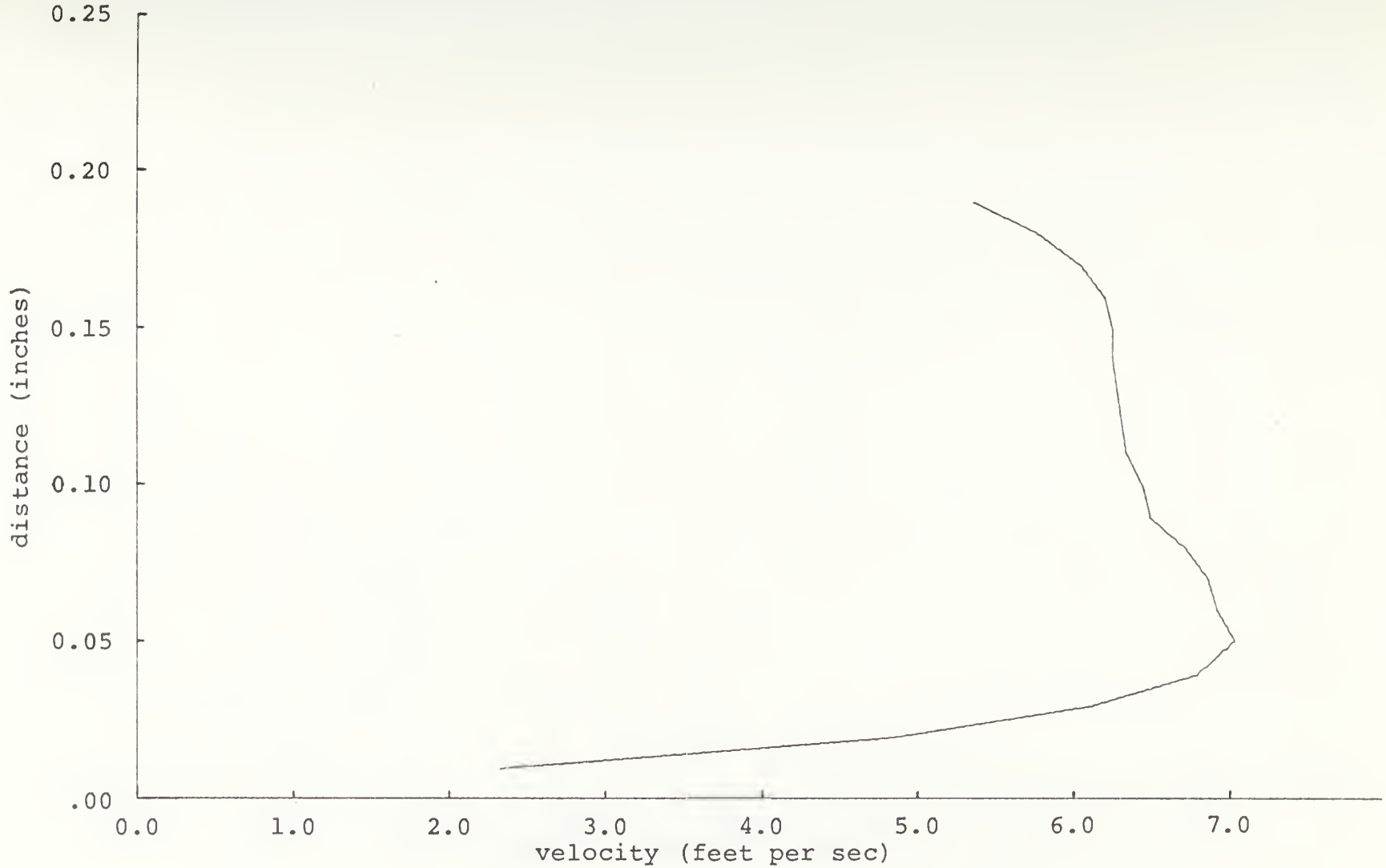

Figure 20. Velocity Profile Re = 1457

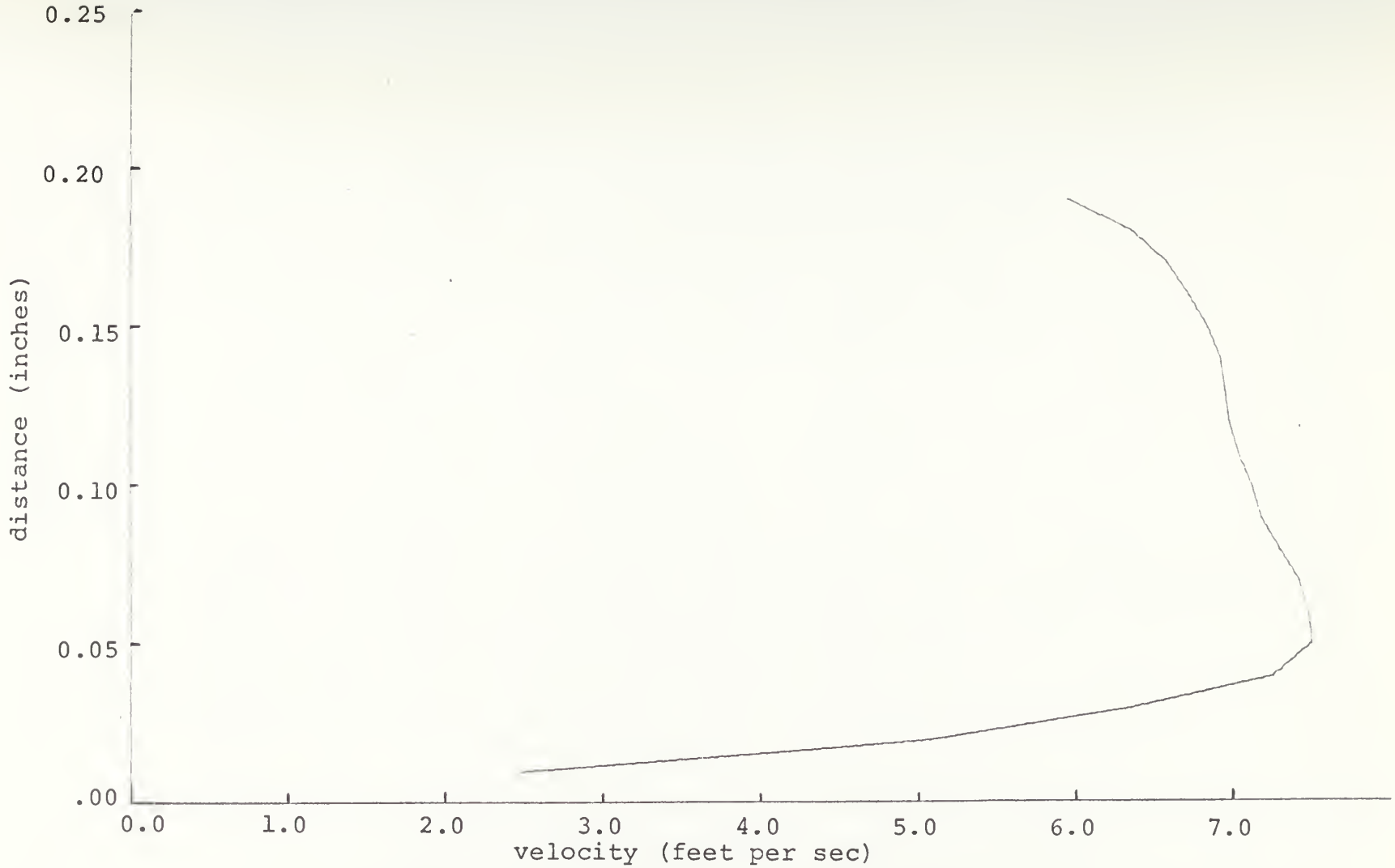

Figure 21. Velocity Profile Re = 1722.

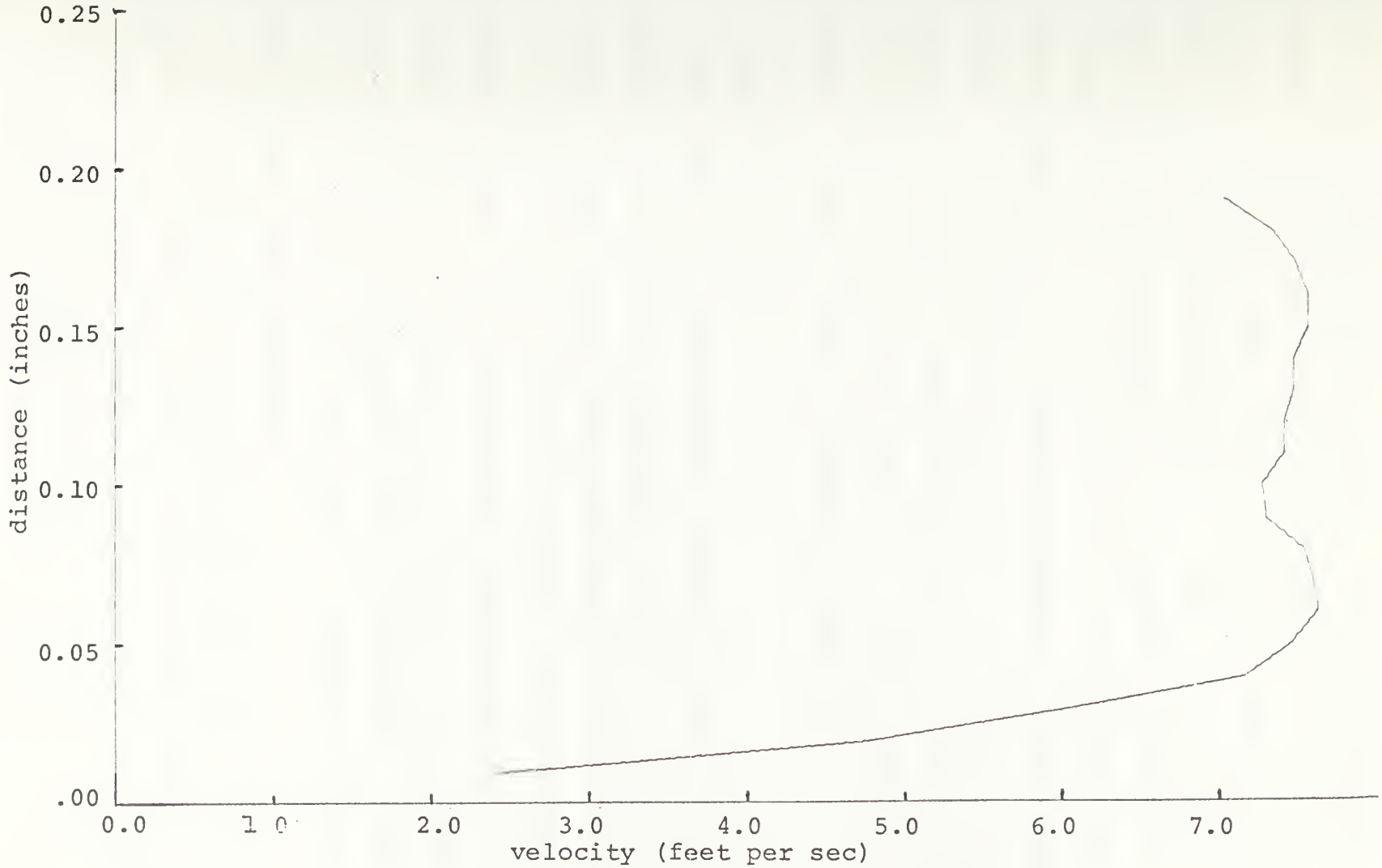

Figure 22. Velocity Profile Re = 1934.

moving through the edge of a vortex. Near the wall the outward radial velocity would increase the mean velocity measured. In the center of the vortex there may be little effect on the hot wire anemometer. Near the top of the vortex the radial component of the velocity would again affect the probe. At the other edge of this vortex, the inward movement of the fluid would produce the same velocity profile. The length of the hot wire, 0.063 inches, would be sufficiently small to traverse the vortices in this manner. A schematic drawing of the probe in a typical position relative to the vortices is shown in Figure 23.

C. TURBULENCE LEVELS

The turbulence intensity was defined as the root-mean-square of the velocity fluctuation divided by the mean velocity. These values were calculated by the data reduction program from the RMS meter readings and the bridge output voltages. The results were plotted against the distance from the concave wall in Figures 24 through 30. The turbulence level was quite low in the center of the channel and higher near the walls as a result of the low mean velocity near the walls.

The change in the turbulence level near the wall in Figure 24 was due to the step change in the velocity profile for that location and Reynolds number. Otherwise, Figures 24, 25, and 26 are self explanatory. In Figure 27, the curve representing the turbulence intensity is not as smooth as the other curves. Large increases in the fluctuations of

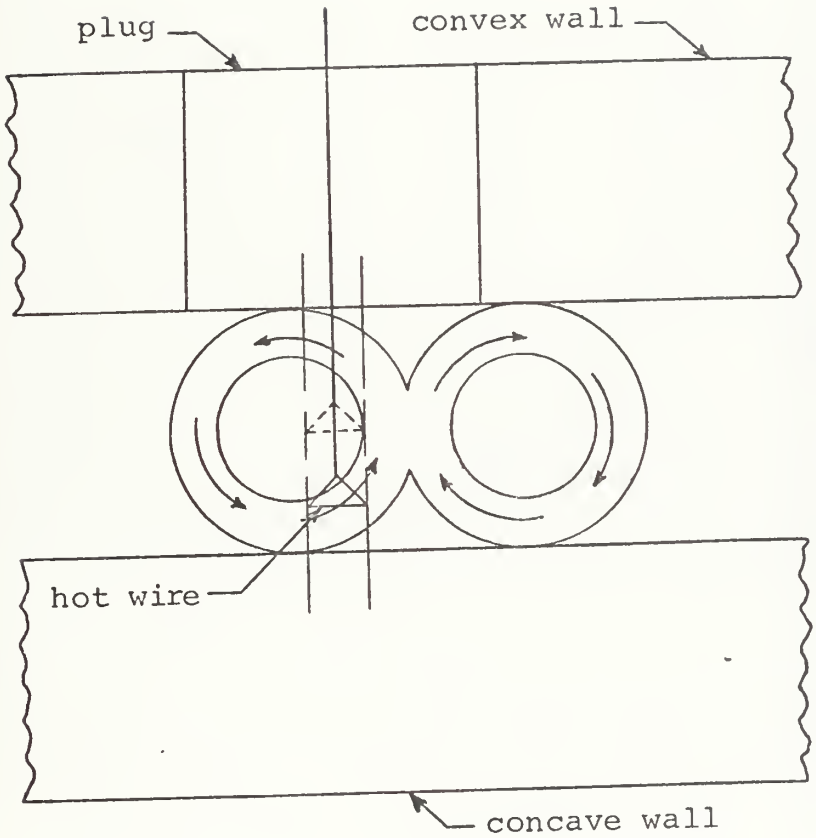

Figure 23. Typical Position of Hot Wire.

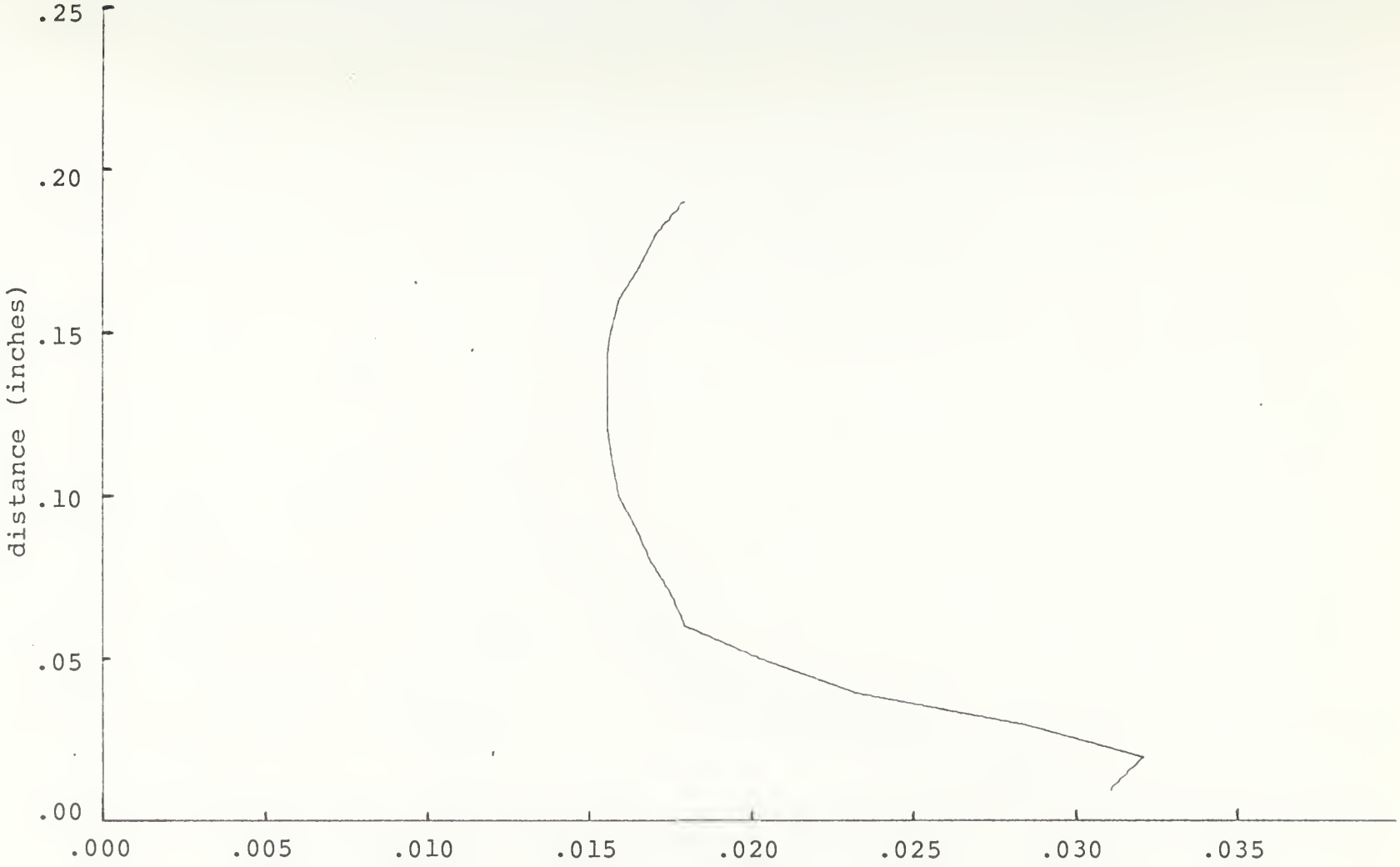

Figure 24. Turbulence Intensity Re = 609.

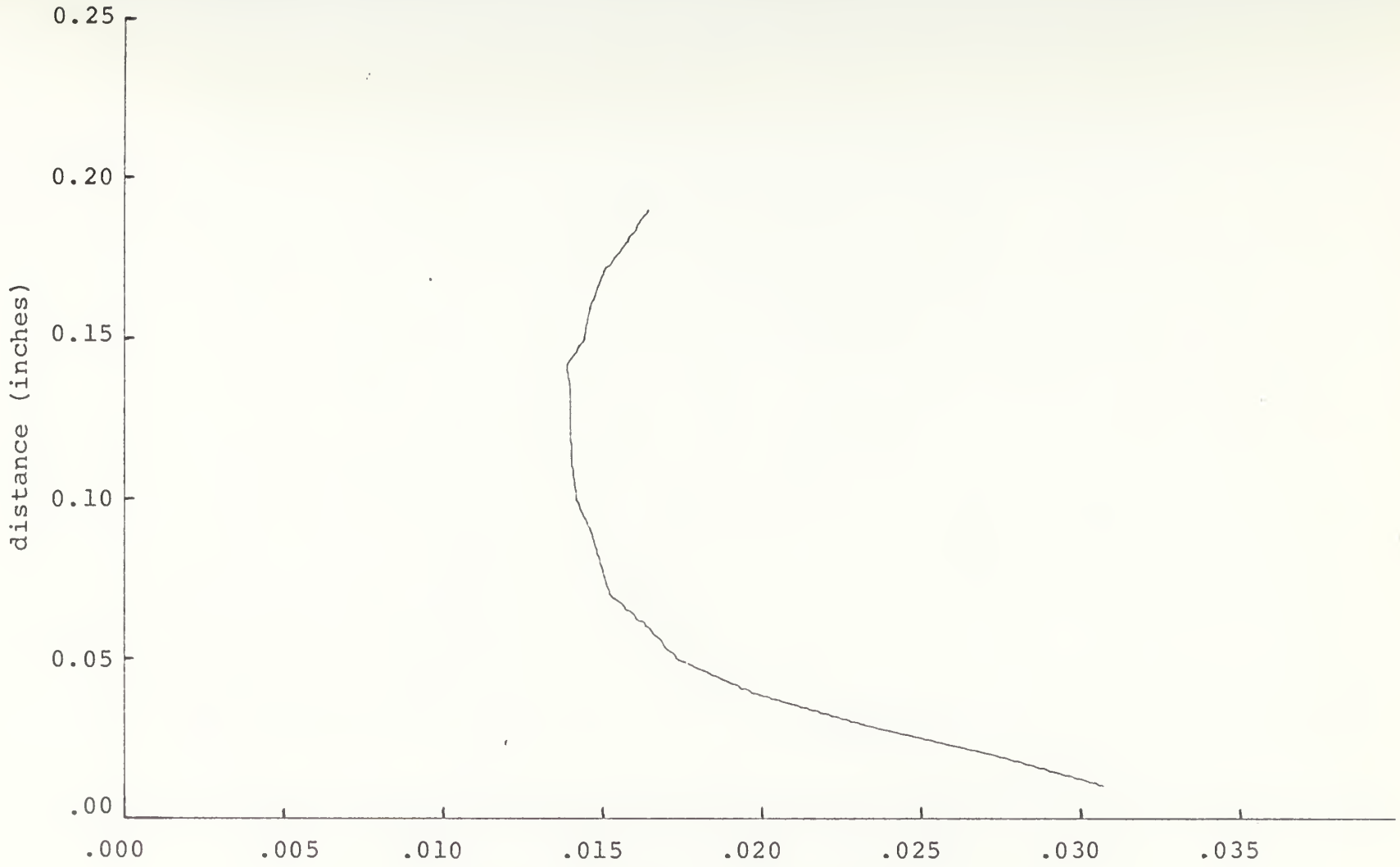

Figure 25. Turbulence Intensity Re = 875.

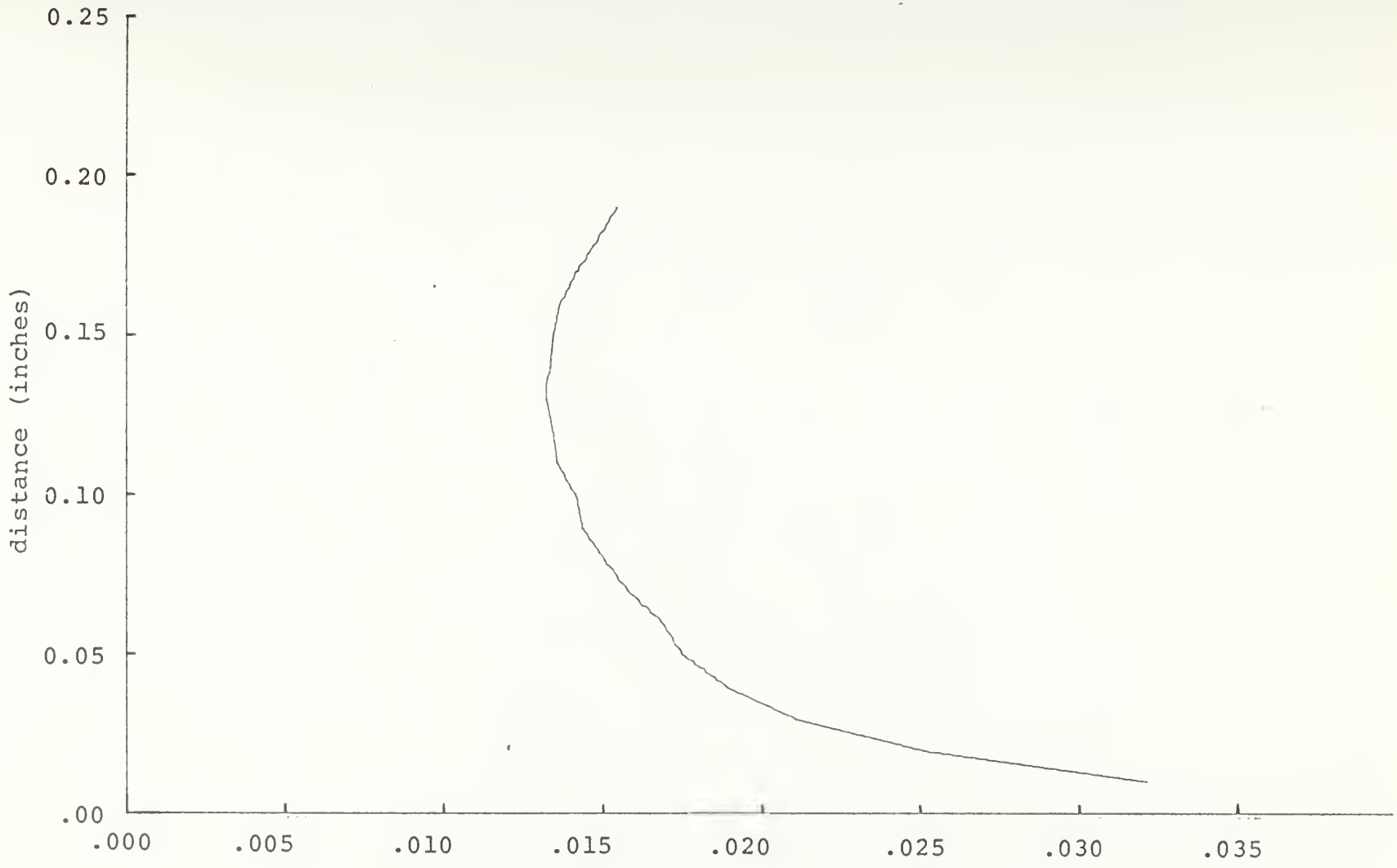

Figure 26. Turbulence Intensity Re = 1166.

Figure 27. Turbulence Intensity Re = 1298.

the RMS meter started at this flow rate, resulting in an increased uncertainty in the level of turbulence. With the RMS meter reading at the 0.00350 volt level, the value would suddenly increase as much as 0.010 and drop back again. The frequency of this random increase was of the order of 30 cycles per minute. One possible cause of these large jumps in the local velocity would be the sideways oscillatory motion of the vortices. During such sideways motion, different portions of the vortices could cross the hot wire anemometer causing the fluctuations. These fluctuations were present during the measurements that led to Figure 28. This figure represents a uniform turbulence level across the channel. In Figures 29 and 30, the level of the turbulence was larger than in the previous cases. The magnitude of the fluctuations was also doubled or larger. The occasionally high value of the turbulence intensity would indicate turbulent flow. In other words, there was bursting to turbulent flow at the higher flow rates.

The growth and motion of the vortices within the channel has been indicated by the mean velocity profiles and turbulence levels presented here. Evidence for the transition to turbulent flow has also appeared.

Figure 28. Turbulence Intensity Re = 1457.

Figure 29. Turbulence Intensity Re = 1722.

Figure 30. Turbulence Intensity Re = 1934.

V. PRESSURE DROP MEASUREMFNTS

A. EXPERIMENTAL PROCEDURES

To measure the pressure drop along the channel required a great deal of care. Each of the 28 pressure taps were cleaned and checked for tightness with high pressure air. The flow rate in the channel was adjusted and allowed to stabilize for approximately one hour before data was taken. The micromanometer was positioned on the table, leveled, and filled with the special fluid provided by the manufacturer.

The meniscus of this instrument was viewed under a magnifying glass and carefully adjusted so that the curve of the meniscus just touched the hair line on the glass tube. This was established as the zero position. It was found that the movement of even a small weight on the laboratory table would effect the level and therefore the zero of this micromanometer. Once the micromanometer was zeroed, no weight movement was permitted and the investigator did not touch the table while measurements were taken.

The pressure fittings for each of the pressure taps were numbered and taped to the edge of the channel. The pressure drop between pairs of pressure taps at one foot intervals was measurable, but contained too much uncertainty to be of use. Typical values of 0.007 inches of water were measured as the pressure drop per foot. However, values of 0.001

inches higher or lower could be obtained in the same position of the channel at the same flow rate. It is possible that part of these variations were due to small fluctuations in the flow rate caused by the centrifical blower. Other causes were considered, but such fluctuations could not be positively identified or eliminated.

The difference between the local pressure at each tap and atmospheric pressure proved to be more useful. At successive locations down the channel the magnitude of this pressure difference became larger and hence the relative error was less. In taking each pressure reading, the zero of the manometer was checked and then the flexible tubing from the micromanometer was connected to the pressure fitting. The pressure tap number was checked and the inlet temperature reading was taken and both were recorded. The manometer reservoir level was adjusted with the fine screw dial until the meniscus of the fluid had returned to its zero location. The rotometer was checked to insure that the flow rate was correct and stable. The meniscus of the fluid was then rechecked and if it had remained in the zero position, the pressure indicated by the dial was recorded along with that flow rate. The micromanometer was disconnected from the pressure fitting and then adjusted to return the meniscus to its zero position. If the dial indication was again zero, the pressure difference obtained was considered to be correct. Occasionally the micromanometer would not re-zero and the pressure measurement at that location was retaken after the instrument was adjusted.

The pressure drop over two foot portions of both the straight section and the curved section were taken to verify the other results. For measurement over these intervals the upstream pressure tap was connected to the top of the micromanometer. The downstream tap was connected to the reservoir of the micromanometer as in the previous setup.

B. PRESSURE DROP

The pressures measured were plotted downward on Figure 31. The top of this graph represents atmospheric pressure, and the amount that the static pressure in the channel was below the atmospheric level can be seen. The pressures are plotted against pressure tap number. The 28 pressure taps were three inches apart along the channel, and numbers one through 16 were on the straight portion of the channel. The pressure for six different Reynolds numbers were plotted, and the same patterns can be seen in each. The irregularities in the curves around pressure taps 14 and 15 and around taps 18 and 19 were of a smaller magnitude than the uncertainty for these measurements. Pressure taps 14 and 15 were in the straight portion of the channel and no cause for the irregularities were apparent. However, burs or other disturbances which were undetected during construction of the channel may have caused these irregularities. Pressure taps 18 and 19 were in the curved portion of the channel. In this case, the cause for the pressure irregularities may have been a difference in the position of the pressure taps relative to the vortices. A pressure tap that was being

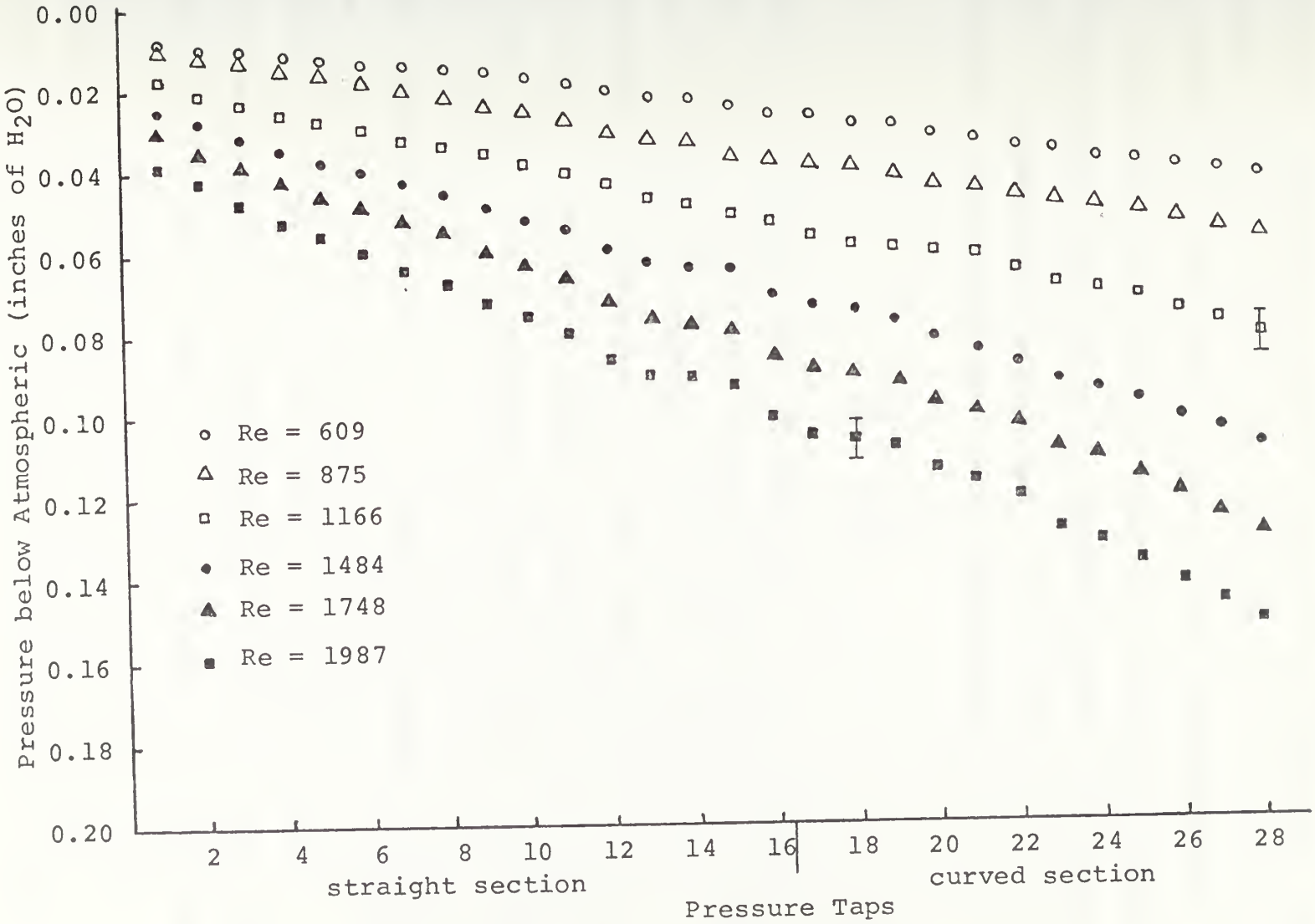

Figure 31. Pressure Below Atmospheric vs. Pressure Taps.

affected by the stagnation of outward moving fluid and one under the influence of moving fluid would probably give different pressure indications. Further study would be required to confirm that this was the cause of the irregularities.

The slope of the pressure curve in the straight section should compare with the exact analytic solution for laminar flow between parallel flat plates. The results of such an analysis [Ref. 6] show that the pressure drop is

$$\frac{dp}{dx} = 3 \frac{\mu U}{a^2}$$

where a is half the plate spacing and μ is the viscosity of the fluid. U is the mean velocity of the parabolic velocity profile between the parallel flat plates. However, the experimentally determined U was the volumetric flow rate through the rectangular channel divided by the cross sectional area. For a rectangular channel of aspect ratio 40, the difference in these two values of U would be small. The analytic value of U for a rectangular channel could be obtained from an infinite series given in the literature [Ref. 19]. The first term of this series would reduce U for the rectangular channel to 98.5315 percent of the value for an infinite parallel plate construction. The remaining terms of this series would rapidly become smaller. The experimental uncertainty was larger than this analytic difference, so that no correction was applied to the theoretical pressure drop.

The experimental pressure drop was calculated by a computer program for both the straight and the curved portions. This program fit a least square straight line to nine consecutive pressures representing a two foot section of the channel. The straight section of the channel was represented by pressure taps three through eleven inclusive. This avoided both the entrance region and the irregularities that were noted before. The curved portion was represented by pressure taps 19 through 27, where the vortices were most developed. The slope of each line was considered as the pressure drop in that portion of the channel. This program and its results are shown in Appendix C. These pressure drops in inches of water per foot of length, along with the analytic pressure drop calculated with the experimental values of U are shown in Table I. The percentage increase in the pressure drop for the curved section was calculated with respect to both the theoretical value and the measured value of pressure in the straight section. These results were also tabulated in Table I. The negative values shown were probably due to experimental uncertainties.

Because more significance might be obtained from a comparison of pressure drops in the straight section with pressure drops in the curved section, where the vortices were fully developed, the same computer program was used to consider one foot section of the channel. The straight portion was represented by pressure taps six through ten, and the curved section by the last one foot, pressure taps

Reynolds Number	Velocity (ft/sec)	Pressure Drop Calculated	Pressure Drop Straight Section	Pressure Drop Curved Section	Percentage Increase from Calculated Values	Percentage Increase from Measured Values
609	2.45	0.0050	0.00387	0.00553	10.6	42.9
875	3.52	0.0071	0.00737	0.00680	- 4.2	- 7.7
1166	4.69	0.0095	0.00890	0.00980	3.2	10.1
1484	5.97	0.0122	0.01140	0.01340	9.8	17.5
1748	7.03	0.0143	0.01400	0.01613	12.8	15.2
1987	7.99	0.0163	0.01613	0.01940	19.0	20.3

TABLE I

PRESSURE DROP PER FOOT FOR TWO FOOT INTERVALS CALCULATED BY LEAST SQUARES

24 through 28. The computer results for these calculations are shown in Appendix C. The resulting pressure drops and percentage increases are shown in Table II. These results showed no negative values for the increase, and had the same magnitude as the other results.

To verify and compare the other results, direct measurements of the pressure drop in the two foot intervals used above were made. The error in this type of measurement could have a magnitude as high as 0.002 inches of water. Nevertheless, the results, along with the resulting percentage increases in the pressure drop, are presented in Table III. The values of the pressure drop measured in the straight section of the channel compared moderately well with the theoretical values. This comparison further supported the methods used to obtain the data.

The percentage increase in the pressure drop from the straight section to the curved section was arrived at with three different measurements, and calculated with both the theoretical and the measured values in each case. The six different sets of percentage increases were plotted against the Reynolds numbers in Figure 32. The average increase for each Reynolds number is also identified in Figure 32. These results have considerable scatter due to the effects of experimental uncertainty. With an increase in the Reynolds number, there was an increased influence of the Taylor-Goertler vortices on the pressure drop. Even though the secondary flow was present, the increase in pressure drop in the curved section was small at the lower flow rates. At

Reynolds Number	Velocity (ft/sec)	Pressure Drop Calculated	Pressure Drop Straight Section	Pressure Drop Curved Section	Percentage Increase from Calculated Values	Percentage Increase from Measured Values
609	2.45	0.0050	0.00400	0.00500	0.0	25.0
875	3.52	0.0071	0.00760	0.00800	12.7	5.3
1166	4.69	0.0095	0.00840	0.01120	17.9	33.3
1484	5.97	0.0122	0.12000	0.01400	14.8	16.7
1748	7.03	0.0143	0.01440	0.01840	28.7	27.8
1987	7.99	0.0163	0.01640	0.02000	22.7	22.0

TABLE II

PRESSURE DROP PER FOOT FOR ONE FOOT INTERVALS CALCULATED BY LEAST SQUARES

Reynolds Number	Velocity (ft/sec)	Pressure Drop Calculated	Pressure Drop Straight Section	Pressure Drop Curved Section	Percentage Increase from Calculated Values	Percentage Increase from Measured Values
609	2.45	0.0050	0.00500	0.0450	-10.0	-10.0
875	3.52	0.0071	0.00750	0.00750	5.6	0.0
1166	4.69	0.0095	0.00900	0.00950	0.0	5.6
1484	5.97	0.0122	0.01150	0.01350	10.7	17.4
1748	7.03	0.0143	0.01350	0.01700	18.9	25.9
1987	7.99	0.0163	0.01600	0.01950	19.6	21.9

TABLE III

PRESSURE DROP PER FOOT FOR TWO FOOT INTERVALS MEASURED VALUES

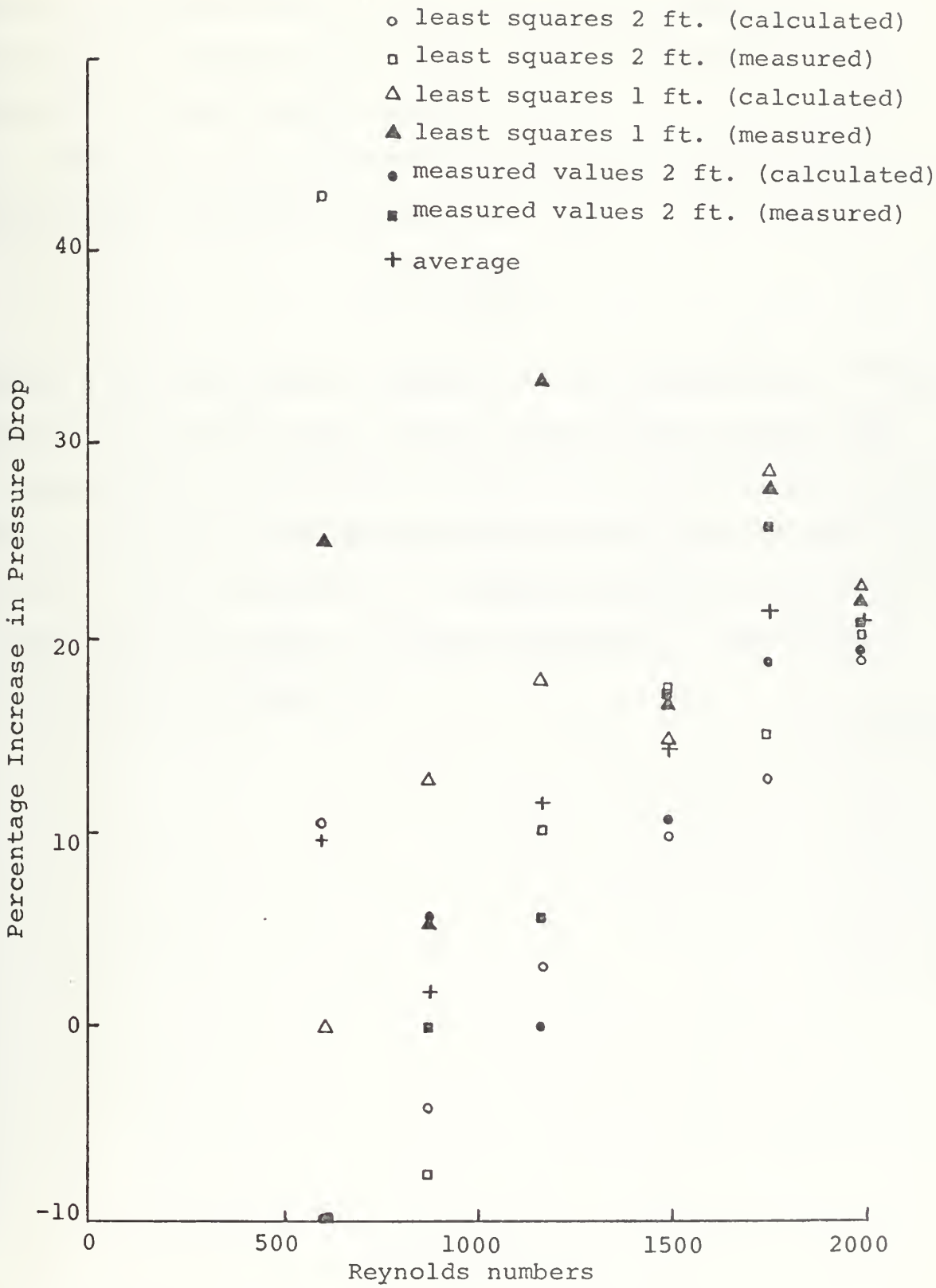

Figure 32. Percentage Increase in Pressure Drop vs. Reynolds Number.

higher Reynolds numbers, where the vortices became more active, the pressure drop in the curved section increased more than in the straight section.

This data was nondimensionalized as the pressure drop coefficient, which was defined as

$$Cp = \frac{p}{\frac{1}{2}\rho\ U^2}$$

where p was the pressure measured at each pressure tap. There was a larger error bound on these values because the uncertainty in U was added to that in the pressure drop. The calculation of the pressure drop coefficient was done by hand on a desk calculator. A sample calculation for the lowest Reynolds number is given in Appendix C. The results were plotted in Figure 33.

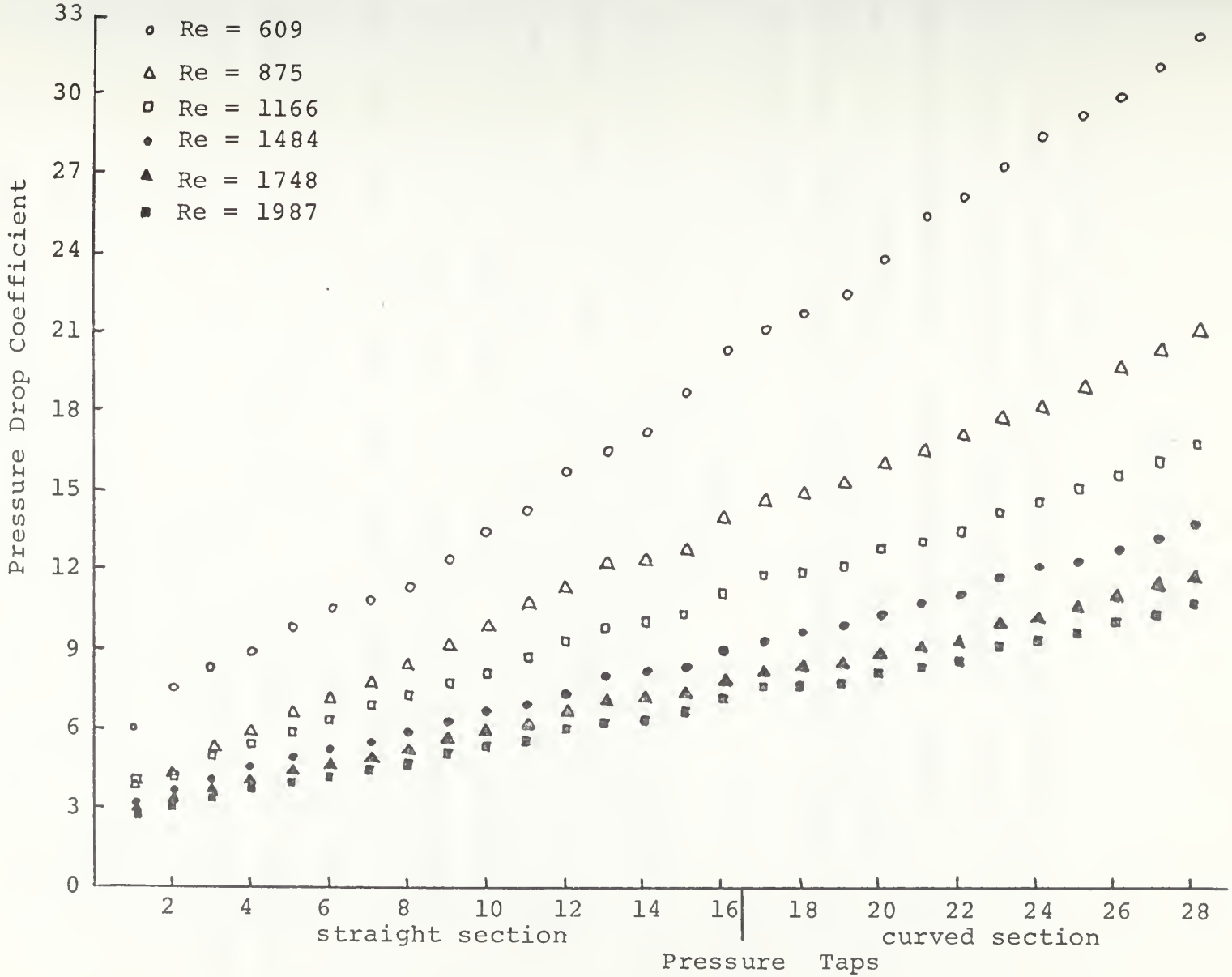

Figure 33. Pressure Drop Coefficient vs. Pressure Taps.

VI. HEAT TRANSFER

A. EXPERIMENTAL PROCEDURES

In order to determine the effect of Taylor-Goertler vortices on heat transfer it was necessary to measure the heat transferred from a uniform temperature surface in one wall of the straight portion of the rectangular channel. The heat transfer coefficients of interest were defined by the equation

$$Q = H * A*\Delta T$$

where Q was the heat convected, H was the heat transfer coefficient and A was the area of the heated surface. The temperature difference, ΔT, used depended on the particular heat transfer coefficient to be found. For the overall heat transfer coefficient, the log mean temperature difference was used. The mean heat transfer coefficient was defined with the difference equal to the wall temperature minus the inlet bulk temperature of the fluid. The temperature difference used for the local heat transfer coefficient was the difference between the temperature of the individual heating element and the bulk temperature of the fluid entering the control volume below that element. The differences in these definitions and the areas used will become clear during the discussion of the results.

A heater plate with 16 separate resistance heating elements placed along the downstream length of the heater

was designed and built as described earlier. To measure the heat transferred from a uniform temperature surface it was necessary to control the voltage to each of the 16 heating elements. The resistance and voltage at each heating strip was to be measured to determine the power generated. The temperatures were to be measured at two locations on each heating elements.

After the heater was in place in the channel wall, the resistance of each heating elements was measured with a Rosemont Commutating Bridge, Model 920A. The high current, regulated D.C. power supply fed the power controller which governed the voltage across each heating element. This specially constructed equipment had never been previously used or tested. The output level of each of the 20 circuits was set as low as possible. The input voltage was adjusted until the power controller's reference voltage was between the maximum recommended value of 8.800 volts and 8.700 volts. To insure that the heater plate did not become too hot, flow was established in the channel. The voltage in each of the first 16 power circuits was slowly increased, and the temperature along the plate was checked frequently. At any given power setting, four to five hours were required for the heated to come to equilibrium. As expected, in order to maintain the same temperature for each strip, the circuits near the leading edge of the plate required more power than the other circuits. If the variation of the power settings was not correct, the temperature distribution approached by

the plate was not uniform. When it was determined that the temperature would not be uniform, the power to the low temperature heating elements was increased and another settling period was allowed. Considerable time was required to obtain the first uniform temperature distribution. Thereafter, to obtain higher temperatures across the plate, each potentiometer's adjustment screw was turned equal amounts. As equilibrium was approached, small adjustments were made to remove temperature irregularities along the plate. In this manner, a uniform temperature could be achieved in a minimum time of about six hours.

During continued testing of the equipment, it was found that the heater plate could sustain temperatures as high as 200° F without damage. Higher operating temperatures were not attempted. During the early testing of the power controller the power circuit voltages were found to fluctuate even when the reference voltage was steady. Examination of the power circuit voltage showed a 60 cycle A.C. voltage superimposed on the controlled D.C. voltage. The source of this A.C. voltage was the grounded side of the regulated power supply. Consequently, downstream from the protective diodes, a 0.05 μf capacitive connection was made across the inputs to the power controller. This connection removed the A.C. voltage and the fluctuation in the power levels. When the power circuits were loaded, the stability was found to be approximately ±.004 volts over a 30 minute period. The power available was actually more than required for these tests.

After the equipment was tested, data collecting began. At the beginning of each data run, the flow rate was established and power was supplied to the heater. After two hours, an ice bath was made and the temperatures along the plate were periodically checked. During the third hour, adjustments were made in the temperature and flow rate. The reference voltage was also checked at this time so that its variation could be determined later.

The temperatures measured and recorded included the bulk temperatures of the entering and exiting air, the temperatures at the 32 thermocouple locations along the heater, and the temperatures of the four locations on the outside of the heater plate. The thermocouples were connected to a digital voltmeter by a set of switches. The switching and recording of the thermocouple outputs were accomplished by hand. As equilibrium was approached, the temperatures were recorded at 30 minute intervals. When the temperatures had stopped changing within the limits of accuracy of this experiment, the values were recorded as data. The reference voltage and flow rate were rechecked to insure no change had taken place. Then the digital voltmeter was connected to the power controller and the voltage across each heating element was recorded. The digital voltmeter was reconnected to the switches. The temperatures were recorded one additional time, and the flow rate was again checked. The data was considered valid if no changes had taken place. The process of taking data took approximately 30 minutes.

B. RESULTS

In order to calculate heat transfer coefficients from the data collected, it was necessary to account for the heat losses. In the geometry of this experiment, there were several potential losses. The largest was expected to be the conduction through the back side of the heater plate. For this reason, the insulation, described earlier was placed over the heated area. To obtain an estimate of the conduction losses through the plate, a finite difference model of the experimental situation was used.

A computer program was used to obtain a numerical solution of the transient and steady state temperature distributions and the heat flows of the three dimensional model. The program used is entitled TRUMP and was developed at the Lawrence Radiation Laboratory [Ref. 23]. This program was implemented for the IBM 360 computer at the Naval Postgraduate School by C. Erbayram [Ref. 24]. Because of the length of this program and its output, only the steady state results of one run are included in Appendix D.

In the computer program, one half of the symmetric arrangement of the heater plate, the insulation, and the surroundings were modeled by a total of 197 node points and 606 thermal connections. The initial temperature of all the nodes, the heat generated at the nodes representing the heating elements, and the heat transfer coefficients representing convection to the surroundings, were input data. The results were the steady state temperature at, and the

heat flow from each of the nodes. The time to reach steady state was also given by the TRUMP program, and compared well with the six hours required in the actual experiment.

After the TRUMP program was tested, the heat generation rates actually measured were input to the program. The heat transfer coefficients representing the convection to the air in the channel were initially estimated and then iterated until the wall temperature arrived at by the computer program was the same as that actually measured. In this way, the TRUMP program was used to model each experimental run. The heat flows from the nodes representing the heating elements were used to calculate losses in the reduction of the experimental data. This process will be described next.

Temperatures and several heat transfer coefficients were computed from the data collected by the computer program in Appendix D. A table of the thermocouple calibration data was included in the computer program. All of the temperatures were calculated by interpolating the thermocouple readings in this table. The local temperatures along the wall and the average wall temperatures are shown in the computer results contained in Appendix D.

The log mean temperature difference was calculated from the equation

$$T\ell m = \frac{Tbo - Tbi}{Ln \dfrac{Tw - Tbi}{Tw - Tbo}}$$

where Tw was the average wall temperature, and Tbi and Tbo were the bulk temperatures of the air into and out of the

test section respectively. Using a table of fluid properties vs. temperatures, the fluid properties were evaluated at the average bulk temperature. The overall heat transfer coefficient was then calculated from the equation

$$Ho = \frac{\rho * cp * \dot{V} * (Tbo - Tbi)}{Aw * T\ell m}$$

where $\dot{V}$ is the volumetric flow rate, and Aw is the area of the heated surface. The mean heat transfer coefficient was also calculated in the program. With the mean temperature difference defined as

$$Tm = Tw - Tbi$$

the mean heat transfer coefficient was calculated from the equation

$$Hm = \frac{\rho * cp * \dot{V} (Tbo - Tbi)}{Aw * Tm} .$$

The symbols are the same as used for the overall heat transfer coefficient. These two values appear in the computer output.

To calculate the local heat transfer coefficients, the power generated at each heating element was calculated from the resistance of the strip and the voltage across it. Two values of heat flow obtained from the TRUMP program were also read into the computer for each heating element. Since one node in the TRUMP program represented two adjacent heating elements, the heat flow values from the TRUMP program were divided in half to represent the losses from the individual heating elements. At the end elements, the conduction

losses along the channel wall were attributed entirely to the first and last heating element. The two heat flows for each heating element represented the conduction loss and the heat convection into the channel. A loss factor was calculated by the computer program by dividing the conduction loss by the sum of the heat flows. The power generated in each strip was multiplied by one minus the loss factor to give the useful heat at each element.

The radiation loss was accounted for by the equation

$$Qr = \varepsilon * \sigma * As * (Tw^4 - Tbi^4)$$

where ε was the emissivity of the nichrome taken as 0.7 and where As was the surface area of each heating element, 0.014783 square feet. The temperatures used were converted to degrees Rankine, and the Stefan-Boltzmann Constant, σ, was equal to 0.199967×10^{-10} BTU/min ft^2 °R. The radiation loss was subtracted from the heat generated at each element less the heat conducted out of the plate to give the heat convected into the channel.

The last loss accounted for was the convection from the heated air in the channel to the surroundings. Two thermal resistances were calculated for this type of loss. The first included terms for the forced convection in the channel, the conduction through the plexiglas lower wall, and the free convection from the horizontal outside surface of the plexiglas. The second thermal resistance included terms for the forced convection in the channel, the conduction

through the aluminum side walls, and the free convection from the vertical outside surfaces. The forced convection was represented by the mean heat transfer coefficient calculated by the program. The free convection was represented by correlation formulas given in the text, Heat Transfer, by J. Holman [Ref. 20]. The convection loss from the air through the walls of the channel was calculated from

$$Qc = \frac{A * (Tb - 70.0)}{R}$$

where Tb was the bulk temperature of air entering the control volume below each heating element, R was the thermal resistance for each case, and A was the corresponding area. The total loss of this type was the sum of the two Qc's calculated with each of the two thermal resistances. In summary the heat convected into the channel from each heating element, designated as p(j), was the power generated at each element minus the conduction losses through the plate and the radiation losses. The heat which raised the bulk temperature of the air, was this convected heat, p(j), minus the convection losses from the air.

The new bulk temperature of the fluid after passing a heating element was therefore calculated by the computer according to

$$Tb(j+1) = Tb(j) + \frac{[p(j)-Qc(j)]}{\rho * cp * \dot{V}} .$$

The local heat transfer coefficient was then easily calculated from the equation

$$H(j) = \frac{\rho * cp * \dot{V} * [Tb(j+1) - Tb(j)]}{As * [Tw - Tb(j)]}$$

where As was the area of one heating element. The distance of each heating element from the leading edge of the plate was also calculated and printed out along with the power convected, the bulk temperature of the fluid, and the local heat transfer coefficient. The average of these local heat transfer coefficients was also displayed on the computer outputs found in Appendix D.

Five data runs were taken and reduced in the manner described above. The five runs cover four different Reynolds numbers and a moderate range of wall temperatures. The resulting local heat transfer coefficients were plotted against the heating element numbers in Figures 34 through 38. The center of the first heating element was 0.137 inches from the leading edge of the plate, and each following element was 0.274 inches farther downstream.

The local heat transfer coefficients tend to be large at the beginning of the plate, decreasing more slowly with increasing distance along the heater plate. There is considerable scatter on these graphs due to the experimental uncertainty.

The heat transfer coefficient at the second heating element appeared consistantly low. This was due primarily to the method of calculating loss factors, which did not charge this heating element for any of the end losses. However, insufficient information about the heat flow was available to improve the technique. Other factors affecting

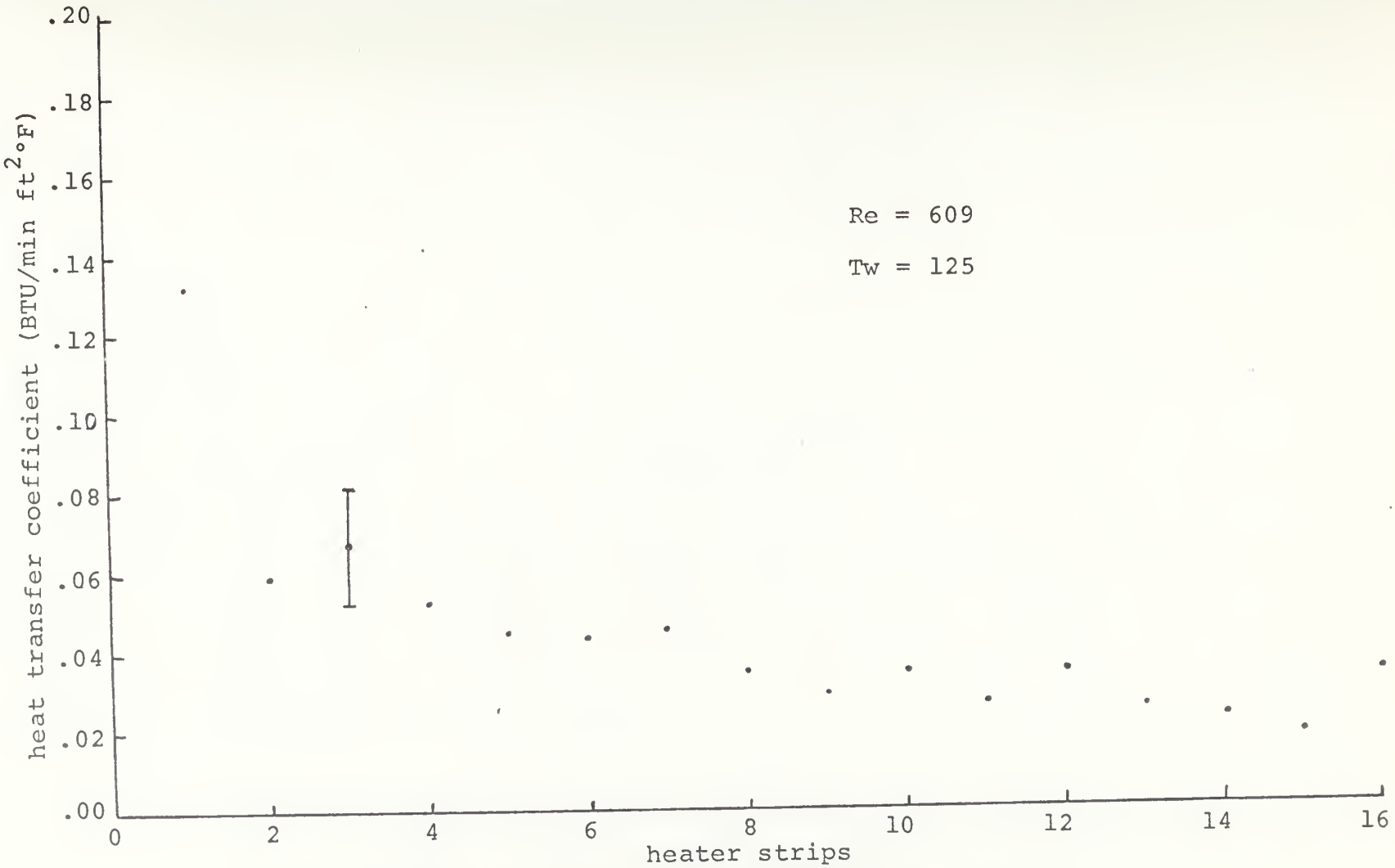

Figure 34. Heat Transfer Coefficient Tw = 125.

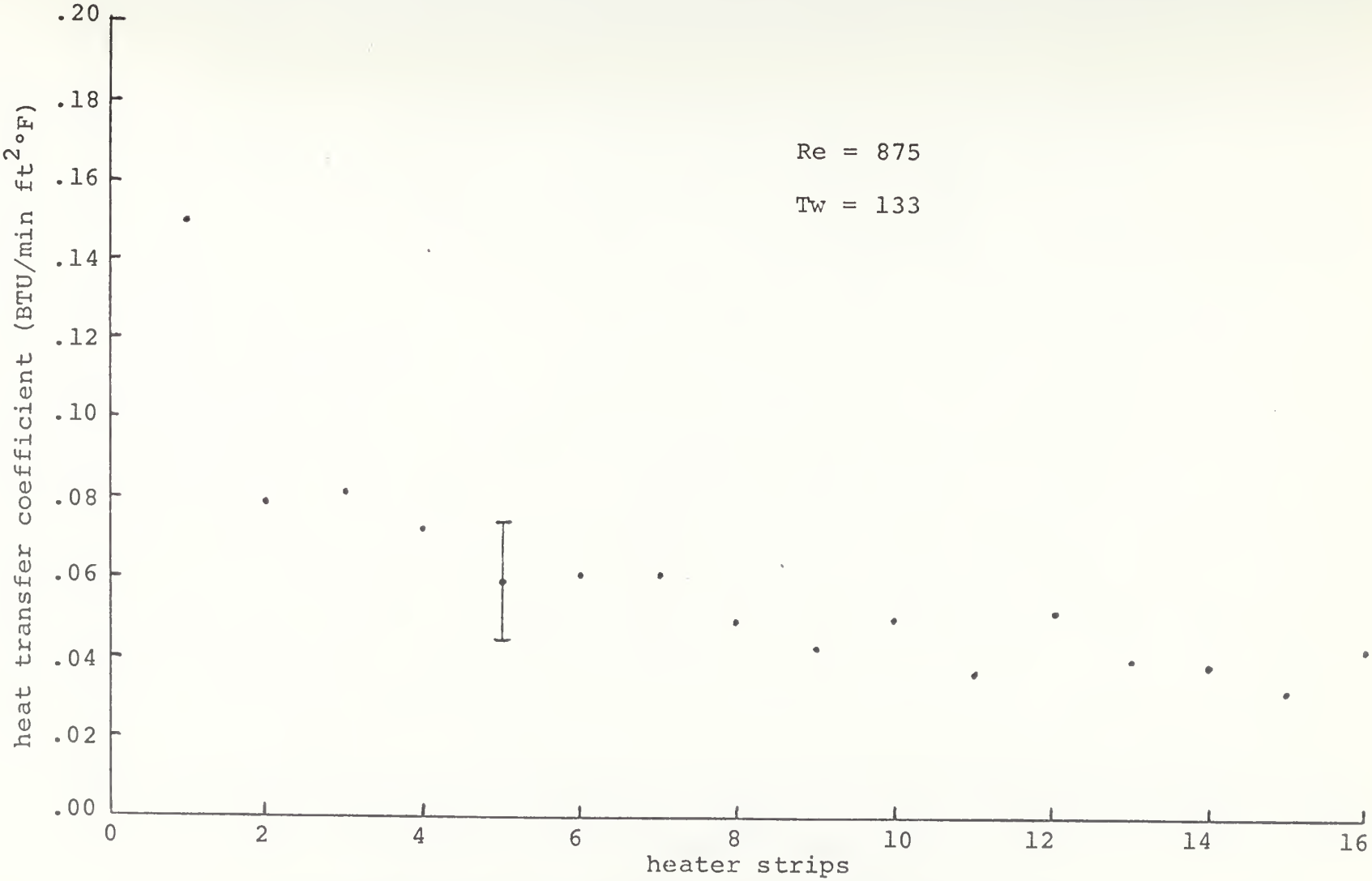

Figure 35. Heat Transfer Coefficient Tw = 133.

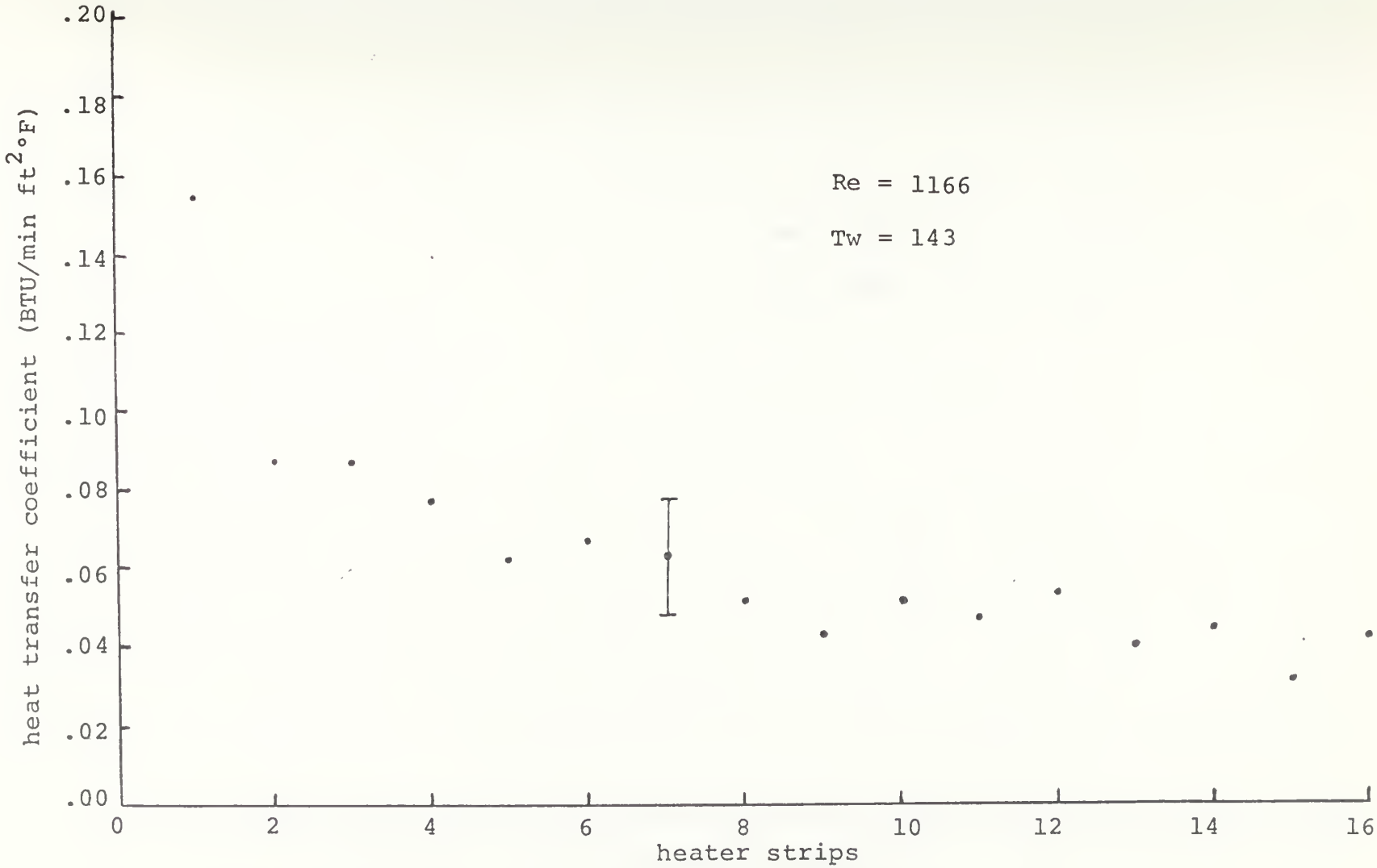

Figure 36. Heat Transfer Coefficient Tw = 143.

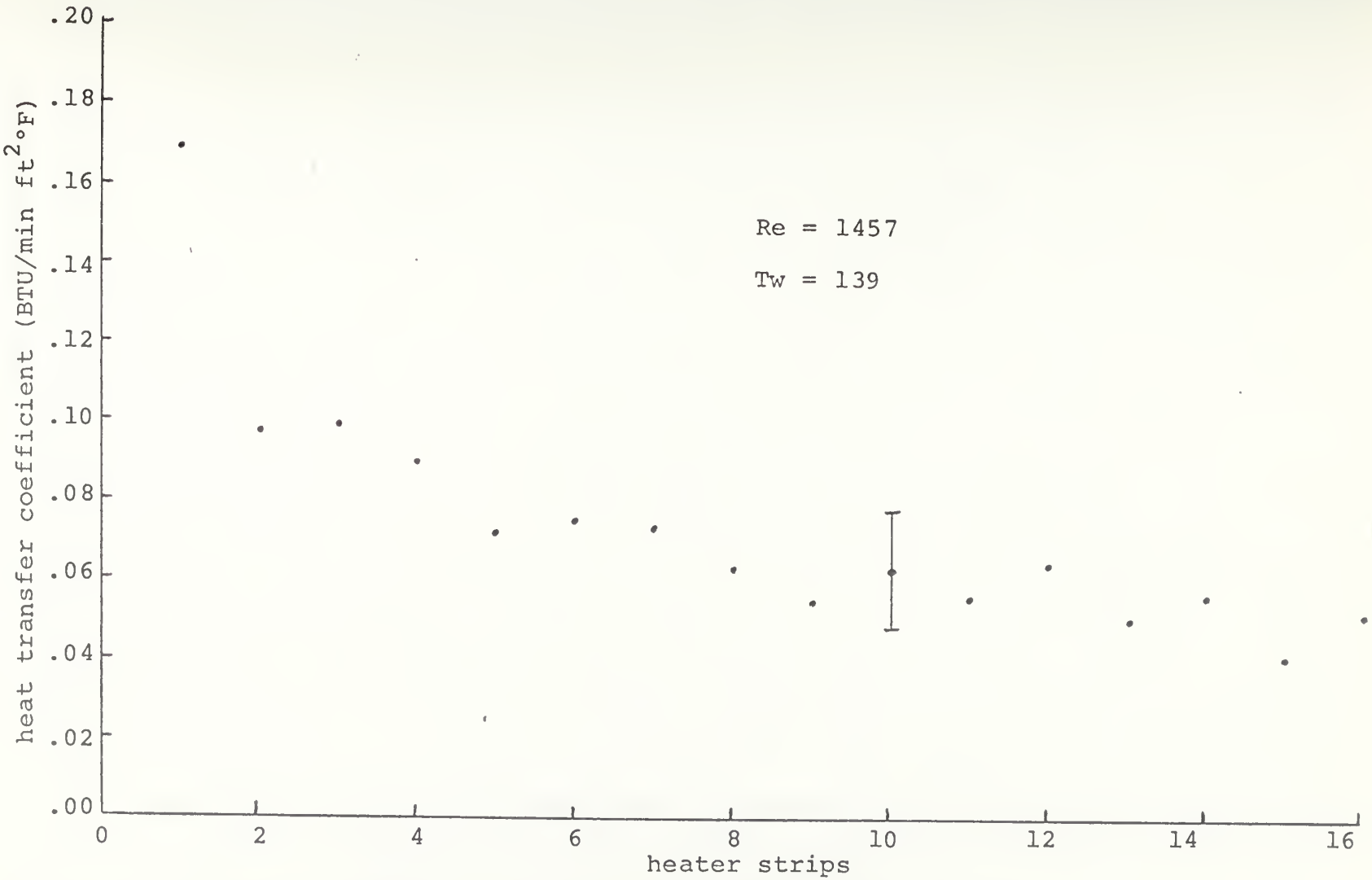

Figure 37. Heat Transfer Coefficient Tw = 139.

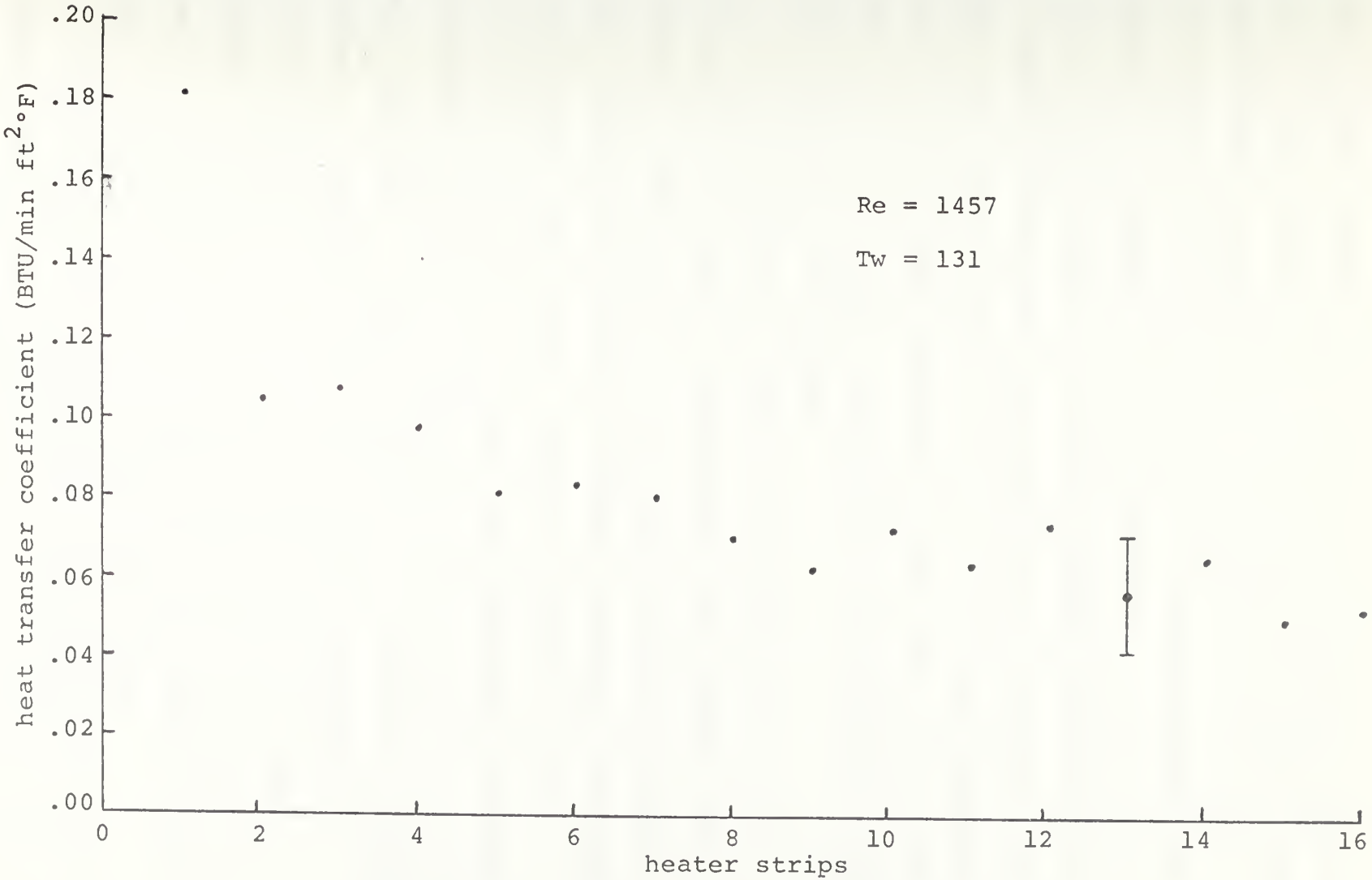

Figure 38. Heat Transfer Coefficient Tw = 131.

the scatter included the variation of temperature along the wall. This variation was as high as ±2.0° F and was probably due to small irregularities in the surface of the plate. The first nichrome strip on the fifth heating element was known to be indented, and its temperature was usually 1.5 to 2.0 degrees higher than the surrounding nichrome ribbons.

Typical error bounds are included in each graph. Dispite the scatter, the decrease in the local heat transfer coefficient is very much like that for a flat plate. However, the heat transfer coefficients are consistantly higher than those for a flat plate.

A brief attempt was made to find some result in the literature with which to compare the heat transfer coefficients. The majority of the literature for developing heat transfer in rectangular channels considers both walls being heated. The Nusselt number of thermally fully developed flow between parallel flat plates with one wall at constant temperature was found to be 4.0 [Ref. 16]. For this experiment, a Nusselt number of 4.0, based on hydraulic diameter, corresponds to a heat transfer coefficient of 0.0244 BTU/min ft^2 °F. For the lowest Reynolds number tested, the local heat transfer approaches this value. For the other Reynolds numbers, the local heat transfer coefficient is higher than the fully developed value.

This data was not nondimensionalized because it was not compared to any other results. The intended use of this data was for comparison with similar heated plate data from

the curved section of the channel. The procedures used to obtain these results were considered adequate for comparison to later work. However, several possible improvements were identified by this testing. Such improvements would include designing a system with fewer heating losses and developing a construction technique with would result in a smoother heated surface.

VII. CONCLUSIONS

The observations made during this investigation have led to several conclusions about the nature of Taylor-Goertler vortices in a curved rectangular channel. The vortices were observed to develop with distance along the channel. The importance of this observation was that an analytic description of the flow would have to account for this growth. The vortices were observed to increase in amplitude and complexity with increasing flow rate. Thus at a higher Reynolds number, less distance along the channel was required to obtain the same degree of development. Several identifiable patterns of the developing flow were observed. The patterns were useful in determining the degree of development of the vortices.

The study of the velocity profiles in the channel indicated that Taylor-Goertler vortices are a complex laminar flow. Furthermore, at flow rates below that necessary to sustain turbulent flow, momentary bursting to turbulent flow was observed.

The effect of Taylor-Goertler vortices on the pressure drop in the curved rectangular channel was observed to vary from no effect to approximately a 20 percent increase. The amount of the increase in pressure drop due to the Taylor-Goertler vortices increased with increasing Reynolds numbers. This seems reasonable considering that as the secondary flow

increases in activity the interaction of the Reynolds stresses with the mean flow intensifies.

The investigation of heat transfer from a constant temperature plate in one wall of the channel resulted in a procedure that would be adequate for determining the effects of Taylor-Goertler vortices on heat transfer. The heat transfer coefficients obtained for the straight section of the channel showed the trends expected and compared with the limiting data available. Improvements in the heat transfer measuring procedures could be made.

VIII. RECOMMENDATIONS

At the end of this investigation, it was clear that several recommendations could be made regarding continued study of Taylor-Goertler vortices in a curved rectangular channel. More flow visualization should be done to clarify the patterns in the vortex flow. Different aerosol injection techniques, including a wall slot, should be tried. More intense lighting and perhaps narrower slits should be used to obtain clearer pictures of the flow. An improved flow visualization technique should then be used to examine more locations along the curved portion of the channel. Due to the fact that there were motions in the flow patterns, still photography could not indicate all of the observations. A motion picture study of flow patterns would be ideal.

More could be learned from a hot wire anemometer study where the probe could be moved sideways across the channel as well as radially in and out. In this manner, the periodic variation in the spanwise direction could be determined. The size of the vortices and their locations could then be determined. In addition, by knowing where the probe was in a vortex, the magnitude of the other velocity components could be determined.

With respect to pressure drop, the placement of more pressure taps along the last portion of the straight section and along the entire curved section would improve the

reliability of the average pressure drop obtained. An investigation should be made to determine if the pressure variation in the direction perpendicular to the flow could be measured.

It was clear that work should continue towards determining the effect of Taylor-Goertler vortices on heat transfer. A heater plate for the curved section could be built in the same manner as the flat heater plate used in this experiment. However, it is recommended that a casting material with less shrinkage and better thermal insulation properties be used. If this is done, a smoother heated surface and fewer thermal losses would result. It is recommended that the development of a good heat transfer measuring technique be given considerable thought.

For any analytic solution attempted, it was felt that it should account for the development of the vortices with distance and flow rate. If the magnitudes of the velocity components are determined, as suggested above, they should compare with any analytic solution obtained. The interaction of the Reynolds stresses with the mean flow would have to be accounted for to predict the increase in pressure drop. Only a non-linear analysis such as J. Stuart's work [Ref. 25] could be expected to give such results. Other analytic techniques including numerical methods ought to be tried.

APPENDIX A

ERROR ANALYSIS

A calculation of the uncertainty for each of the major variables of this experiment was made in accordance with the methods of S. Kline and F. McClintoch [Ref. 26]. The estimates of the uncertainty in the measured quantities were made quite conservative so that there was considerable confidence in the uncertainties arrived at. As an example of the calculations the uncertainty in Reynolds number is calculated below. The Reynolds number is given by

$$Re = \frac{U * Dh}{\nu}$$

and the uncertainty is taken as

$$\frac{dRe}{Re} = \sqrt{\frac{dU}{U}^2 + \frac{dDh}{Dh}^2 + \frac{d\nu}{\nu}^2}$$

The uncertainty in the flow velocity is obtained from other calculations like this one based on estimates of the uncertainty in reading the volumetric flow rate through the rotometer and the uncertainty in the cross sectional area of the channel. The results of those calculations were $\frac{dU}{U} = 0.02805$. The uncertainty in hydraulic diameter and kinematic viscosity are obtained from estimates as 0.00426 and 0.00136 respectively. Then the uncertainty in the Reynolds number is

$$\frac{dRe}{Re} = \sqrt{(7.868 + 0.1815 + 0.0185) \times 10^{-4}} = 0.02840$$

Other quantities and their uncertainties are given below. The error bound for any quantity can be obtained by multiplying its magnitude by its uncertainty.

Quantity	Uncertainty
Ac	0.00412
Aw	0.00320
Cp	0.07515
cp	0.00010
De	0.02838
dH	0.00426
H	0.27150
Ho	0.03517
p (pressure)	0.05000
Ph (heat generated)	0.00502
p(j) (heat convected)	0.25502
Re	0.02840
T	0.00750
Tℓm	0.02000
Tw	0.01667
U	0.02805
$\dot{V}$	0.02775
ρ	0.00080

APPENDIX B

COMPUTER RESULTS FOR VELOCITY AND TURBULENCE

The computer program for reducing the hot wire anemometer calibration data is shown below. This program was adopted from a program written by Mr. Loyd Smith while he was studying at the Naval Postgraduate School. The resulting calibration curve is also shown.

The hot wire anemometer data reduction program was also adapted from a program by Mr. Smith and is shown below. The reduced data for the seven velocity and turbulence profiles is then included.

```
      DIMENSION PD(20),DATE(20)
      DIMENSION X(16),Y(16)
      DIMENSION XG(6),VG2(6)
      REAL*8 LABEL1/8H        /
      REAL LABEL2/4H    /
      REAL*8 ITITLE(12)
      DATA XG/0.0,1.0,2.0,3.0,4.0,5.0/
      DATA SUMX,SUMX2,SUMY,SUMXY/0.0,0.0,0.0,0.0/
      DATA A/3.55447/
C     READS IN PROBE DATA AND CALIBRATION DATA
      READ(5,1000)PD
      READ(5,1000)DATE
 1000 FORMAT(20A4)
      WRITE(6,2000)PD
 2000 FORMAT('1','PROBE DATA: ',20A4)
      WRITE(6,2001)DATE
 2001 FORMAT(' ','DATE: ',20A4)
      READ(5,1001)N
 1001 FORMAT(I10)
      WRITE(6,2002)A,N
 2002 FORMAT(' ','FLOW CONSTANT: ',8X,F10.3,/,' NUMBER OF DA
     1TA POINTS: ',I10,//,6X,'H',9X,'V',9X,'U',9X,'X',9X,
     2'Y',//)
      DO 10 I=1,N
C     READS IN EXPERIMENTAL VALUES OF THE MANOMETER READING
C     AND THE DC VOLTAGE OUTPUT OF THE ANEMOMETER.  THE CON-
C     STANT A IS SET FOR H IN IN. OF H2O ON A STANDARD DAY
      READ(5,1002)H,V
 1002 FORMAT(2F10.3)
      U=A*SQRT(H)
      X(I)=SQRT(U)
      Y(I)=V**2
      X2=X(I)**2
      XY=X(I)*Y(I)
      SUMX=SUMX+X(I)
      SUMX2=SUMX2+X2
      SUMY=SUMY+Y(I)
      SUMXY=SUMXY+XY
      WRITE(6,2003)H,V,U,X(I),Y(I)
 2003 FORMAT(5F10.3,/)
   10 CONTINUE
C     COMPUTE CONSTANTS BY LEAST SQUARES ANALYSIS
      D=N*SUMX2-(SUMX**2)
      BETA=(N*SUMXY-SUMX*SUMY)/D
      VC2=(SUMY*SUMX2-SUMXY*SUMX)/D
      WRITE(6,2004)BETA,VC2
 2004 FORMAT(' ','BETA = ',F10.3,10X,' VC2 = ',F10.3)
      READ(5,1003)(ITITLE(I),I=1,6)
      READ(5,1003)(ITITLE(I),I=7,12)
 1003 FORMAT(6A8)
C     POINT PLOTS DATA
      CALL DRAW(N,X,Y,1,2,LABEL1,ITITLE,1.0,1.0,1,1,0,0,4,
     35,0,LAST)
C     THE LEAST SQUARES EQUATION IS USED TO COMPUTE SIX
C     POINTS FOR A STRIGHT LINE
      DO 20 I=1,6
      VG2(I)=VC2+BETA*XG(I)
   20 CONTINUE
      CALL DRAW(6,XG,VG2,3,0,LABEL2,ITITLE,1.0,1.0,1,1,0,0,
     44,5,0,LAST)
      STOP
      END
```

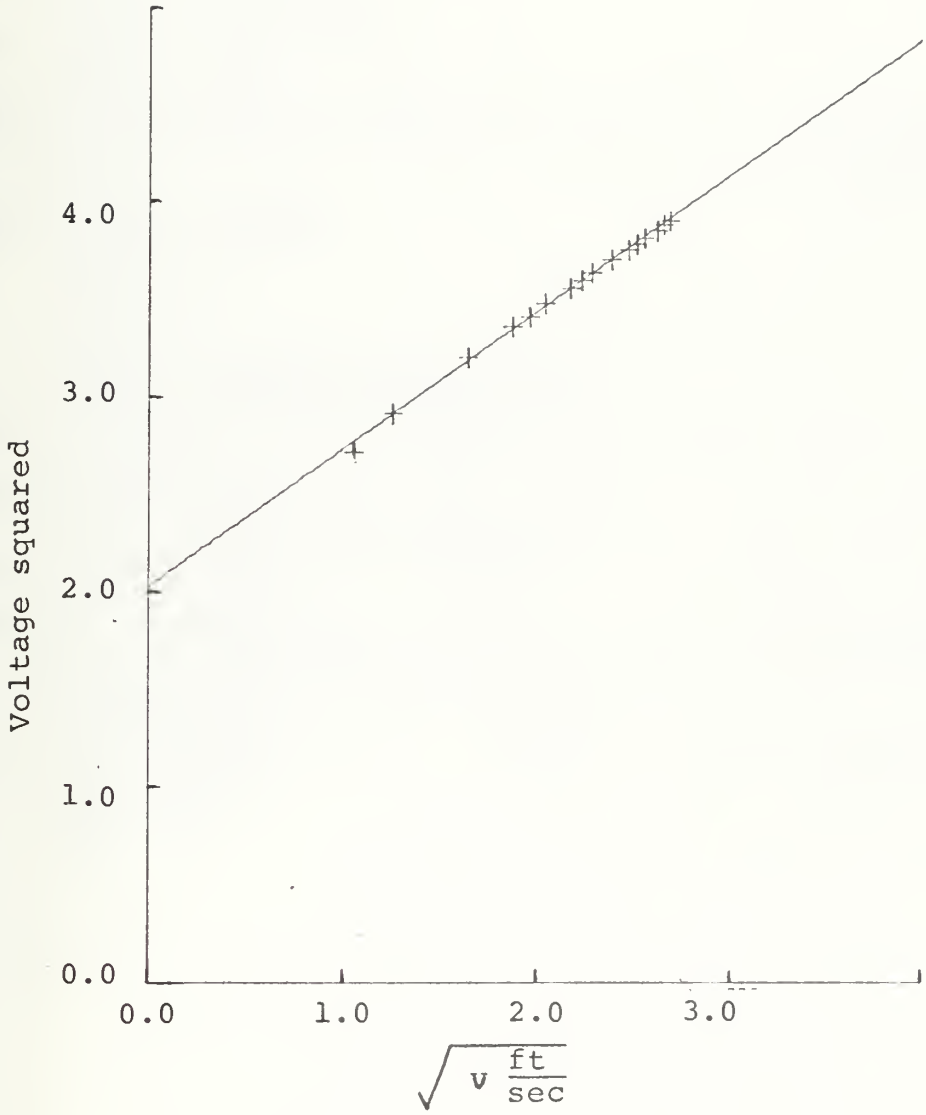

Hot wire anemometer calibration curve

```
      DIMENSICN DATA1(20),CATA2(20),H(25),U(25),T(25)
      REAL*8 ITITL1(12),ITITL2(12)
      REAL LABEL/4H    /
   3C READ(5,900)NPROB
  9CC FCRMAT(I1C)
      IF(NPROB.LT.0) STOP
      READ(5,10CC)DATA1
      READ(5,100C)DATA2
 1000 FCRMAT(20A4)
      WRITE(6,2000)
 2000 FCRMAT('1',//////////)
      WRITE(6,2001)DATA1
      WRITE(6,2001)DATA2
 20C1 FCRMAT(' ',21X,20A4)
      READ(5,1001) RO,VC2,BETA
 1CC1 FCRMAT(3F10.6)
      WRITE(6,2002) RO,VC2,BETA
 2002 FCRMAT(33X,'INITICAL PCSITICN=',F7.3,/,24X,' VO2 = ',
     2F1C.6,9X,'BETA =',F10.6,//,30X,'H',19X,'U',19X,'T',//)
      NCP=0
   1C READ(5,1CC2)R,V,E
 1CC2 FCRMAT(3F10.6)
      IF(R.LT.0.0) GO TO 20
      NCP=NDP+1
      I=NCP
      H(I)=R-RO
      U(I)=(((V**2)-VO2)/BETA)**2
      T(I)=(4.C*V*E)/((V**2)-VO2)
      WRITE(6,2003)H(I),U(I),T(I)
 20C3 FCRMAT(21X,F10.6,1CX,F10.6,10X,F1C.6,/)
      GC TO 10
   2C WRITE(6,2004)
 20C4 FCRMAT(//////////)
      READ(5,1CC3)(ITITL1(I),I=1,6)
      READ(5,1003)(ITITL1(I),I=7,12)
 1CC3 FCRMAT(6A8)
      WRITE(6,2005)
 20C5 FCRMAT(//////////////)
      CALL DRAW(NDP,U,H,C,0,LABEL,ITITL1,1.0,0.C5,C,C,0,0,
     88,5,0,LAST)
      READ(5,1CC4)(ITITL2(I),I=1,6)
      READ(5,1CC4)(ITITL2(I),I=7,12)
 1CC4 FCRMAT(6A8)
      CALL DRAW(NDP,T,H,0,0,LABEL,ITITL2,0.010,.C5,0,0,0,0,
     68,5,0,LAST)
      GC TO 3C
      END
```

CONCAVE TO CONVEX WALL DISTANCE, VELOCITY AND TURBULENCE
PROBE NO. TSI1279 DATE 5 FEB 73 23% FLOW RATE RE= 609
INITICAL POSITION= 0.270
VO2 = 2.020000 BETA = 0.710000

H	U	T
0.010000	0.613295	0.031175
0.020000	0.620402	0.032164
0.030000	0.951606	0.028536
0.040000	1.536921	0.023217
0.050000	1.958789	0.020265
0.060000	2.504096	0.017990
0.070000	2.665120	0.017536
0.080000	2.900582	0.016941
0.090000	3.111880	0.016465
0.100000	3.239269	0.015917
0.110000	3.332104	0.015737
0.120000	3.407528	0.015596
0.130000	3.426528	0.015561
0.140000	3.407528	0.015596
0.150000	3.332104	0.015737
0.160000	3.202550	0.015990
0.170000	3.040466	0.016621
0.180000	2.815131	0.017149
0.190000	2.504096	0.017990

CONCAVE TO CONVEX WALL DISTANCE, VELOCITY AND TURBULENCE
PROBE NO. TSI1279 DATE 5 FEB 73 33% FLOW RATE RE= 875
INITICAL POSITION= 0.270
VO2 = 2.020000 BETA = 0.710000

H	U	T
0.010000	0.701554	0.030997
0.020000	1.298702	0.027440
0.030000	1.945134	0.023128
0.040000	2.665120	0.019690
0.050000	3.111880	0.017332
0.060000	3.580913	0.016380
0.070000	3.943310	0.015237
0.080000	4.153802	0.014926
0.090000	4.370939	0.014629
0.100000	4.549487	0.014152
0.110000	4.640411	0.014043
0.120000	4.686278	0.013989
0.130000	4.663301	0.014016
0.140000	4.572118	0.013877
0.150000	4.459676	0.014514
0.160000	4.283268	0.014746
0.170000	4.026724	0.015111
0.180000	3.719356	0.015865
0.190000	3.369696	0.016505

CONCAVE TO CONVEX WALL DISTANCE, VELOCITY AND TURBULENCE
PROBE NO. TSI1279 DATE 5 FEB 73 44% FLOW RATE RE=1166
INITICAL POSITION= 0.270
VC2 = 2.020000 BETA = 0.710000

H	U	T
0.010000	0.942583	0.032475
0.020000	1.958789	0.025157
0.030000	2.815131	0.021060
0.040000	3.659631	0.018945
0.050000	4.153802	0.017500
0.060000	4.594827	0.016818
0.070000	5.015061	0.015774
0.080000	5.258296	0.015016
0.090000	5.483244	0.014313
0.100000	5.688062	0.014111
0.110000	5.844732	0.013514
0.120000	5.977282	0.013398
0.130000	6.003999	0.013152
0.140000	5.950615	0.013421
0.150000	5.844732	0.013514
0.160000	5.636421	0.013704
0.170000	5.282988	0.014286
0.180000	4.919745	0.014929
0.190000	4.459676	0.015515

CONCAVE TO CONVEX WALL DISTANCE, VELOCITY AND TURBULENCE
PROBE NO. TSI1279 DATE 7 FEB 73 49% FLOW RATE RE=1298
INITICAL POSITION= 0.270
VO2 = 2.020000 BETA = 0.710000

H	U	T
0.010000	1.320405	0.030549
0.020000	2.084258	0.027238
0.030000	3.600484	0.024517
0.040000	4.825512	0.021835
0.050000	5.407611	0.020888
0.060000	5.871078	0.017987
0.070000	6.057706	0.017772
0.080000	6.111675	0.017269
0.090000	6.220504	0.016712
0.100000	6.302920	0.016191
0.110000	6.385982	0.015239
0.120000	6.497812	0.015138
0.130000	6.582447	0.014633
0.140000	6.667787	0.014133
0.150000	6.639285	0.014156
0.160000	6.554168	0.014226
0.170000	6.302920	0.014440
0.180000	5.977282	0.015184
0.190000	5.457953	0.015726

CONCAVE TO CONVEX WALL DISTANCE, VELOCITY AND TURBULENCE
PROBE NO. TSI1279 DATE 6 FEB 73 55% FLOW RATE RE=1457
INITICAL POSITION= 0.270
VC2 = 2.020000 BETA = 0.710000

H	U	T
0.010000	2.348951	0.023978
0.020000	4.872481	0.019336
0.030000	6.138762	0.017681
0.040000	6.811521	0.014869
0.050000	7.045468	0.014679
0.060000	6.927876	0.014773
0.070000	6.869542	0.014821
0.080000	6.725045	0.014941
0.090000	6.497812	0.015138
0.100000	6.441764	0.015188
0.110000	6.330523	0.015290
0.120000	6.302920	0.015316
0.130000	6.275369	0.014903
0.140000	6.247911	0.014928
0.150000	6.247911	0.014928
0.160000	6.193172	0.014938
0.170000	6.030813	0.014687
0.180000	5.766069	0.014943
0.190000	5.357558	0.016305

CONCAVE TO CONVEX WALL DISTANCE, VELOCITY AND TURBULENCE
PROBE NO. TSI1279 DATE 6 FEB 73 65% FLOW RATE RE=1722
INITICAL POSITION= 0.270
VO2 = 2.020000 BETA = 0.710000

H	U	T
0.010000	2.488311	0.050629
0.020000	5.087305	0.047533
0.030000	6.358225	0.043613
0.040000	7.254210	0.041479
0.050000	7.497396	0.032772
0.060000	7.466739	0.032823
0.070000	7.405624	0.024694
0.080000	7.284319	0.020707
0.090000	7.164276	0.020838
0.100000	7.104720	0.020904
0.110000	7.015953	0.018903
0.120000	6.957165	0.018964
0.130000	6.927876	0.016884
0.140000	6.898683	0.016911
0.150000	6.811521	0.016993
0.160000	6.696387	0.017103
0.170000	6.554168	0.019399
0.180000	6.330523	0.024027
0.190000	5.924045	0.024647

CONCAVE TO CONVEX WALL DISTANCE, VELOCITY AND TURBULENCE
PROBE NO. TSI1279 DATE 6 FEB 73 73% FLOW RATE RE=1934
INITICAL POSITION= 0.270
VC2 = 2.020000 BETA = 0.710000

H	U	T
0.010000	2.425794	0.095928
0.020000	4.778824	0.097417
0.030000	6.030813	0.089011
0.040000	7.164276	0.075016
0.050000	7.466739	0.061543
0.060000	7.620902	0.052928
0.070000	7.589893	0.053009
0.080000	7.528167	0.049083
0.090000	7.284319	0.041414
0.100000	7.254210	0.041479
0.110000	7.405624	0.037041
0.120000	7.405624	0.028809
0.130000	7.466739	0.028720
0.140000	7.466739	0.024617
0.150000	7.558975	0.020420
0.160000	7.558975	0.020420
0.170000	7.466739	0.020514
0.180000	7.314532	0.020675
0.190000	7.015953	0.025204

APPENDIX C

CALCULATIONS AND COMPUTER RESULTS FOR PRESSURE DROP

The computer program written to find the slope of the pressure curve is shown below. The results for six different Reynolds numbers are shown. The first set of results represent nine pressure readings or two foot intervals. The second complete set represents selected one foot intervals. The last item shown in this appendix is a tabular calculation of the pressure drop coefficient for the lowest Reynolds number tested.

```
C
C
C     CALCULATION OF THE LEAST SQUARES SLOPE FOR PRESSURE
C     DROP DATA.  DATA READ IN IS NUMBER OF DATA POINTS,
C     REYNOLDS NUMBER, POSITION OF PRESSURE TAP IN INCHES
C     AND PRESSURE IN INCHES OF WATER.
C
C
      DIMENSION TYPE(2)
      WRITE(6,11)
   11 FORMAT('1',////)
      L=0
  200 READ(5,10) N,RE,TYPE(1),TYPE(2)
   10 FORMAT(I8,F8.1,2A4)
      IF(N.LT.1) GO TO 300
      SUMX=0.0
      SUMY=0.0
      SUMX2=0.0
      SUMXY=0.0
      L=L+1
      IF(L.GT.3) GO TO 310
      GO TO 210
  310 WRITE(6,11)
      L=1
  210 WRITE(6,20) RE
   20 FORMAT(' ',31X,'SLOPE OF PRESSURE DROP CURVE FOR ',
     1'REYNOLDS NUMBER =',F7.1,///,35X,'POSITION (FT)',20X,
     2'PRESSURE (IN H2O)',//)
      C=N
      DO 100 I=1,N
      READ(5,22) T,Y
   22 FORMAT(2F10.5)
      X=T/12.0
      WRITE(6,23) X,Y
   23 FORMAT(39X,F7.5,25X,F7.5)
      X2=X**2
      XY=X*Y
      SUMX=SUMX+X
      SUMY=SUMY+Y
      SUMX2=SUMX2+X2
      SUMXY=SUMXY+XY
  100 CONTINUE
      D=(SUMX)**2-C*SUMX2
      AO=(SUMX*SUMXY-SUMY*SUMX2)/D
      A1=(SUMX*SUMY-C*SUMXY)/D
      WRITE(6,24) TYPE(1), TYPE(2), A1
   24 FORMAT(5X,//,33X,'THE PRESSURE DROP IN THE ',2A4,1X,
     3'SECTION IS',F12.6,////)
      GO TO 200
  300 STOP
      END
```

SLOPE OF PRESSURE DROP CURVE FOR REYNOLDS NUMBER = 609.0

POSITION (FT)	PRESSURE (IN H2O)
0.0	0.01100
0.25000	0.01200
0.50000	0.01300
0.75000	0.01400
1.00000	0.01450
1.25000	0.01500
1.50000	0.01650
1.75000	0.01800
2.00000	0.01900

THE PRESSURE DROP IN THE STRIGHT SECTION IS 0.003867

SLOPE OF PRESSURE DROP CURVE FOR REYNOLDS NUMBER = 609.0

POSITION (FT)	PRESSURE (IN H2O)
0.0	0.03000
0.25000	0.03200
0.50000	0.03400
0.75000	0.03500
1.00000	0.03650
1.25000	0.03800
1.50000	0.03900
1.75000	0.04000
2.00000	0.04150

THE PRESSURE DROP IN THE CURVED SECTION IS 0.005533

SLOPE OF PRESSURE DROP CURVE FOR REYNOLDS NUMBER = 875.0

POSITION (FT)	PRESSURE (IN H2O)
0.0	0.01400
0.25000	0.01600
0.50000	0.01800
0.75000	0.01950
1.00000	0.02100
1.25000	0.02300
1.50000	0.02500
1.75000	0.02700
2.00000	0.02900

THE PRESSURE DROP IN THE STRIGHT SECTION IS 0.007367

SLCPE OF PRESSURE DROP CURVE FOR REYNCLCS NUMBER = 875.C

PCSITION (FT)	PRESSURE (IN H2O)
0.0	C.0420C
0.25000	0.04400
0.500CC	0.04550
0.750CO	C.047CC
1.00000	0.049CC
1.250CC	0.05000
1.500CC	C.C52CC
1.75000	0.C540C
2.000CC	0.05600

THE PRESSURE DROP IN THE CURVED SECTION IS 0.0068CO

SLOPE OF PRESSURE DROP CURVE FOR REYNCLCS NUMBER = 1166.0

POSITION (FT)	PRESSURE (IN H2O)
0.0	0.02400
0.250CO	0.C260C
0.50000	C.028CC
0.750CC	0.03050
1.00000	0.03300
1.25000	0.035CO
1.500CC	0.03700
1.750CC	C.C3900
2.00000	0.04200

THE PRESSURE DROP IN THE STRIGHT SECTION IS 0.CC89CO

SLCPE OF PRESSURE DROP CURVE FOR REYNCLCS NUMBER = 1166.C

PCSITION (FT)	PRESSURE (IN H2O)
0.0	C.C59CO
C.25000	0.06200
0.50000	C.06300
0.75000	C.066CC
1.00000	0.06900
1.25000	0.071CC
1.50000	0.073CO
1.75000	0.07600
2.00000	C.079CO

THE PRESSURE DROP IN THE CURVED SECTICN IS 0.009800

SLCPE OF PRESSURE DROP CURVE FOR REYNCLDS NUMBER = 1484.0

PCSITION (FT)	PRESSURE (IN H2O)
0.0	0.03200
0.25000	0.03500
0.50000	0.03800
0.75000	0.04000
1.00000	0.04300
1.25000	0.04600
1.50000	0.04900
1.75000	0.05200
2.00000	0.05500

THE PRESSURE DROP IN THE STRIGHT SECTICN IS 0.011400

SLCPE OF PRESSURE DROP CURVE FOR REYNCLDS NUMBER = 1484.0

POSITION (FT)	PRESSURE (IN H2O)
0.0	0.07800
0.25000	0.08200
0.50000	0.08500
0.75000	0.08800
1.00000	0.09300
1.25000	0.09500
1.50000	0.09800
1.75000	0.10200
2.00000	0.10500

THE PRESSURE DROP IN THE CURVED SECTION IS 0.013400

SLCPE OF PRESSURE DROP CURVE FOR REYNCLDS NUMBER = 1748.0

POSITION (FT)	PRESSURE (IN H2O)
0.0	0.03900
0.25000	0.04300
0.50000	0.04700
0.75000	0.05000
1.00000	0.05300
1.25000	0.05700
1.50000	0.06100
1.75000	0.06400
2.00000	0.06700

THE PRESSURE DROP IN THE STRIGHT SECTICN IS 0.014000

SLCPE OF PRESSURE DRCP CURVE FCR REYNCLCS NUMEER = 1748.0

POSITION (FT)	PRESSURE (IN H2O)
0.0	0.C93CC
0.25000	0.09800
0.50000	C.10CCO
0.75000	0.103CC
1.00000	C.11000
1.25000	C.112CC
1.50000	0.116CC
1.75000	C.12100
2.00000	C.12600

THE PRESSURE DROP IN THE CURVED SECTICN IS 0.016133

SLCPE CF PRESSURE DROP CURVE FOR REYNCLCS NUMBER = 1987.C

PCSITION (FT)	PRESSURE (IN H2O)
0.0	C.048CO
0.25000	0.C52CC
0.50000	0.05600
0.75000	C.C6CCC
1.00000	0.064CC
1.25000	0.06800
1.50000	C.073CC
1.75000	C.076CC
2.00000	0.08000

THE PRESSURE DROP IN THE STRIGHT SECTION IS 0.016133

SLOPE OF PRESSURE DROP CURVE FOR REYNCLCS NUMBER = 1987.0

POSITION (FT)	PRESSURE (IN H2C)
0.0	0.10800
0.25000	0.114CC
0.50000	C.117CC
0.75000	0.12100
1.00000	0.129CO
1.25000	0.13200
1.50000	0.13700
1.75000	0.142CO
2.00000	0.147CO

THE PRESSURE DROP IN THE CURVED SECTION IS 0.0194CC

SLOPE OF PRESSURE DROP CURVE FOR REYNOLDS NUMBER = 609.0

POSITION (FT)	PRESSURE (IN H2O)
0.0	0.01400
0.25000	0.01450
0.50000	0.01500
0.75000	0.01650
1.00000	0.01800

THE PRESSURE DROP IN THE STRIGHT SECTION IS 0.004000

SLOPE OF PRESSURE DROP CURVE FOR REYNOLDS NUMBER = 609.0

POSITION (FT)	PRESSURE (IN H2O)
0.0	0.03800
0.25000	0.03900
0.50000	0.04000
0.75000	0.04150
1.00000	0.04300

THE PRESSURE DROP IN THE CURVED SECTION IS 0.005000

SLOPE OF PRESSURE DROP CURVE FOR REYNOLDS NUMBER = 875.0

POSITION (FT)	PRESSURE (IN H2O)
0.0	0.01950
0.25000	0.02100
0.50000	0.02300
0.75000	0.02500
1.00000	0.02700

THE PRESSURE DROP IN THE STRIGHT SECTION IS 0.007600

SLOPE OF PRESSURE DROP CURVE FOR REYNOLDS NUMBER = 875.0

POSITION (FT)	PRESSURE (IN H2O)
0.0	0.05000
0.25000	0.05200
0.50000	0.05400
0.75000	0.05600
1.00000	0.05800

THE PRESSURE DROP IN THE CURVED SECTION IS 0.008000

SLCPE OF PRESSURE DROP CURVE FOR REYNCLCS NUMBER = 1166.0

PCSITION (FT)	PRESSURE (IN H2O)
0.0	C.03C50
0.25000	0.03300
0.500CC	0.C3500
0.75000	C.037CC
1.000CC	0.03900

THE PRESSURE DROP IN THE STRIGHT SECTION IS C.CC84CC

SLOPE OF PRESSURE DROP CURVE FOR REYNCLCS NUMBER = 1166.0

POSITION (FT)	PRESSURE (IN H2O)
0.0	0.07100
0.25000	C.073C0
0.50000	C.076CC
0.75000	0.07900
1.00CC0	0.C82C0

THE PRESSURE DROP IN THE CURVED SECTICN IS 0.011200

SLCPE OF PRESSURE DROP CURVE FOR REYNCLCS NUMBER = 1484.0

POSITION (FT)	PRESSURE (IN H2C)
0.0	0.04000
0.25000	C.043CC
0.50000	0.0460C
0.75CCC	0.049C0
1.00000	C.C52CC

THE PRESSURE DROP IN THE STRIGHT SECTICN IS 0.012000

SLCPE CF PRESSURE DROP CURVE FOR REYNCLCS NUMBER = 1484.0

POSITION (FT)	PRESSURE (IN H2O)
0.0	C.095CC
0.25000	C.098CC
0.500CC	0.10200
0.75000	C.105CC
1.00000	0.10900

THE PRESSURE DROP IN THE CURVED SECTION IS 0.014CC0

SLOPE OF PRESSURE DROP CURVE FOR REYNOLDS NUMBER = 1748.0

POSITION (FT)	PRESSURE (IN H2O)
0.0	0.05000
0.25000	0.05300
0.50000	0.05700
0.75000	0.06100
1.00000	0.06400

THE PRESSURE DROP IN THE STRIGHT SECTION IS 0.014400

SLOPE OF PRESSURE DROP CURVE FOR REYNOLDS NUMBER = 1748.0

POSITION (FT)	PRESSURE (IN H2O)
0.0	0.11200
0.25000	0.11600
0.50000	0.12100
0.75000	0.12600
1.00000	0.13000

THE PRESSURE DROP IN THE CURVED SECTION IS 0.018400

SLOPE OF PRESSURE DROP CURVE FOR REYNOLDS NUMBER = 1987.0

POSITION (FT)	PRESSURE (IN H2O)
0.0	0.06000
0.25000	0.06400
0.50000	0.06800
0.75000	0.07300
1.00000	0.07600

THE PRESSURE DROP IN THE STRIGHT SECTION IS 0.016400

SLOPE OF PRESSURE DROP CURVE FOR REYNOLDS NUMBER = 1987.0

POSITION (FT)	PRESSURE (IN H2O)
0.0	0.13200
0.25000	0.13700
0.50000	0.14200
0.75000	0.14700
1.00000	0.15200

THE PRESSURE DROP IN THE CURVED SECTION IS 0.020000

Pressure Tap	T(volts)	T (°F)	ρ	Percentage Flow Rate	U	$\frac{1}{2} \rho U^2$	Pressure Difference	Cp
1	0.948	75.0	0.00231	23	2.45	0.00133	0.0080	6.00
2	0.948	75.0					0.0100	7.50
3	0.948	75.0					0.0110	8.25
4	0.947	75.0					0.0120	9.00
5	0.948	75.0					0.0130	9.75
6	0.947	75.0					0.0140	10.50
7	0.947	75.0					0.0145	10.87
8	0.947	75.0					0.0150	11.24
9	0.947	75.0					0.0165	12.37
10	0.947	75.0					0.0180	13.49
11	0.947	75.0					0.0190	14.24
12	0.947	75.0					0.0210	15.74
13	0.947	75.0					0.0220	16.49
14	0.947	75.0					0.0230	17.24
15	0.948	75.0					0.0250	18.74
16	0.948	75.0					0.0270	20.24
17	0.948	75.0					0.0280	20.99
18	0.948	75.0					0.0290	21.74
19	0.949	75.0					0.0300	22.49
20	0.949	75.0					0.03200	23.99
21	0.949	75.0					0.0340	25.49
22	0.949	75.0					0.0350	26.24
23	0.950	75.1					0.0365	27.36
24	0.950	75.1					0.0380	28.49
25	0.950	75.1					0.0390	29.24
26	0.950	75.1					0.0400	29.99
27	0.951	75.1					0.0415	31.11
28	0.951	75.1	0.00231	23	2.45	0.00133	0.0430	32.24

APPENDIX D

COMPUTER RESULTS FOR HEAT TRANSFER

The final results for one run of the TRUMP program are shown on pages 130 through 144. The computer program for the calculation of the heat transfer coefficients follows the TRUMP program. The five sets of heating data results are presented with the temperature distribution shown on the first page and the heat transfer coefficients on the second page of each of the results.

TRUMP OUTPUT DATA DATA DECK 1

* TRUMP SOLUTION TO FLAT PLATE HEATER LOSSES TW=120.0 U=2.0

PRINTOUT	CYCLE	TOO FAST	TOO SLOW	KWIT	DELTMX	SMALL	TVARY	NUTS
7	46	0	5	4	6.00000E 01	9.99999E-07	5.00000E 00	0

TOTAL TIME	TIME STEP	HEAT FLOW	TEMP FROM FLUX	FLUX RATE	TEMP RATE
3.72629E 02	6.00000E 01	-1.45627E 02	-8.58139E 02	-3.90809E-01	-2.30293E 00

AVG TEMP	HEAT CAPACITY	HEAT CONTENT	GEN RATE	HEAT GEN	TEMP FROM GEN
9.40752E 01	1.69701D-01	1.59646E 01	4.08068E-01	1.52058E 02	8.96035E 02

NODE	TEMP	DT	DDT	GEN RATE	W	H	F	DLRE AT 280 F
1	0.1158D 03	0.2655D-03	0.7946D-06	0.0	0.1034E 00	0.4095E-01	0.4094E-01	0.0
2	0.1180D 03	-0.2235D-04	-0.6688D-07	0.0	0.1053E 00	0.4282E-01	0.4280E-01	0.0
3	0.1181D 03	-0.1079D-03	-0.3230D-06	0.0	0.1054E 00	0.4295E-01	0.4291E-01	0.0
4	0.1182D 03	-0.1405D-03	-0.4205D-06	0.0	0.1055E 00	0.4298E-01	0.4294E-01	0.0
5	0.1179D 03	-0.1654D-03	-0.4951D-06	0.0	0.1052E 00	0.4272E-01	0.4267E-01	0.0
6	0.1182D 03	-0.1858D-03	-0.5560D-06	0.0	0.1055E 00	0.4303E-01	0.4298E-01	0.0
7	0.1172D 03	-0.1989D-03	-0.5952D-06	0.0	0.1047E 00	0.4219E-01	0.4213E-01	0.0
8	0.1147D 03	-0.1900D-03	-0.5686D-06	0.0	0.1023E 00	0.3985E-01	0.3980E-01	0.0
9	0.9898D 02	-0.1085D-03	-0.3246D-06	0.0	0.8834E-01	0.2587E-01	0.2583E-01	0.0
10	0.9191D 02	0.2057D-03	0.6155D-06	0.0	0.8203E-01	0.1955E-01	0.1957E-01	0.0
11	0.1158D 03	0.2664D-03	0.7973D-06	0.0	0.1034E 00	0.4095E-01	0.4094E-01	0.0
12	0.1180D 03	-0.2262D-04	-0.6769D-07	0.0	0.1053E 00	0.4282E-01	0.4280E-01	0.0
13	0.1181D 03	-0.1082D-03	-0.3238D-06	0.0	0.1054E 00	0.4295E-01	0.4291E-01	0.0
14	0.1182D 03	-0.1408D-03	-0.4213D-06	0.0	0.1055E 00	0.4298E-01	0.4294E-01	0.0
15	0.1179D 03	-0.1657D-03	-0.4960D-06	0.0	0.1052E 00	0.4272E-01	0.4267E-01	0.0
16	0.1182D 03	-0.1861D-03	-0.5569D-06	0.0	0.1055E 00	0.4303E-01	0.4298E-01	0.0
17	0.1173D 03	-0.1992D-03	-0.5963D-06	0.0	0.1047E 00	0.4219E-01	0.4213E-01	0.0
18	0.1147D 03	-0.1904D-03	-0.5697D-06	0.0	0.1023E 00	0.3985E-01	0.3979E-01	0.0
19	0.9898D 02	-0.1089D-03	-0.3260D-06	0.0	0.8834E-01	0.2587E-01	0.2583E-01	0.0
20	0.9191D 02	0.2062D-03	0.6172D-06	0.0	0.8203E-01	0.1955E-01	0.1957E-01	0.0
21	0.1158D 03	0.2664D-03	0.7973D-06	0.0	0.1034E 00	0.4089E-01	0.4092E-01	0.0
22	0.1180D 03	-0.2254D-04	-0.6745D-07	0.0	0.1053E 00	0.4280E-01	0.4278E-01	0.0
23	0.1181D 03	-0.1081D-03	-0.3236D-06	0.0	0.1054E 00	0.4293E-01	0.4289E-01	0.0
24	0.1181D 03	-0.1407D-03	-0.4210D-06	0.0	0.1054E 00	0.4297E-01	0.4292E-01	0.0
25	0.1179D 03	-0.1656D-03	-0.4957D-06	0.0	0.1052E 00	0.4271E-01	0.4266E-01	0.0
26	0.1182D 03	-0.1860D-03	-0.5566D-06	0.0	0.1055E 00	0.4302E-01	0.4296E-01	0.0
27	0.1172D 03	-0.1991D-03	-0.5959D-06	0.0	0.1046E 00	0.4217E-01	0.4211E-01	0.0
28	0.1146D 03	-0.1903D-03	-0.5694D-06	0.0	0.1023E 00	0.3983E-01	0.3978E-01	0.0
29	0.9897D 02	-0.1088D-03	-0.3258D-06	0.0	0.8833E-01	0.2586E-01	0.2582E-01	0.0
30	0.9190D 02	0.2063D-03	0.6173D-06	0.0	0.8202E-01	0.1955E-01	0.1956E-01	0.0
31	0.1150D 03	0.2655D-03	0.7946D-06	0.0	0.1026E 00	0.4013E-01	0.4017E-01	0.0
32	0.1170D 03	-0.2025D-04	-0.6061D-07	0.0	0.1044E 00	0.4193E-01	0.4191E-01	0.0
33	0.1171D 03	-0.1052D-03	-0.3149D-06	0.0	0.1045E 00	0.4204E-01	0.4201E-01	0.0
34	0.1171D 03	-0.1373D-03	-0.4108D-06	0.0	0.1046E 00	0.4208E-01	0.4203E-01	0.0
35	0.1169D 03	-0.1616D-03	-0.4835D-06	0.0	0.1043E 00	0.4182E-01	0.4177E-01	0.0
36	0.1172D 03	-0.1814D-03	-0.5429D-06	0.0	0.1046E 00	0.4213E-01	0.4207E-01	0.0
37	0.1163D 03	-0.1942D-03	-0.5812D-06	0.0	0.1038E 00	0.4130E-01	0.4124E-01	0.0
38	0.1137D 03	-0.1855D-03	-0.5553D-06	0.0	0.1015E 00	0.3904E-01	0.3898E-01	0.0
39	0.9842D 02	-0.1053D-03	-0.3151D-06	0.0	0.8783E-01	0.2536E-01	0.2532E-01	0.0
40	0.9155D 02	0.2064D-03	0.6178D-06	0.0	0.8170E-01	0.1923E-01	0.1925E-01	0.0
41	0.7841D 02	0.1765D-03	0.5283D-06	0.0	0.6998E-01	0.7508E-02	0.7539E-02	0.0
42	0.7694D 02	0.1737D-04	0.5200D-07	0.0	0.6867E-01	0.6193E-02	0.6192E-02	0.0
43	0.7680D 02	-0.1308D-04	-0.3914D-07	0.0	0.6854E-01	0.6069E-02	0.6064E-02	0.0
44	0.7679D 02	-0.1806D-04	-0.5405D-07	0.0	0.6853E-01	0.6056E-02	0.6050E-02	0.0

NCDE	TEMP	DT	DDT	GE N RATE	W	H	F	CLRE AT 280 F
45	0.7678D 02	-0.1934D-04	-0.5788D-07	0.0	0.6852E-01	0.6048E-02	0.6041E-02	0.0
46	0.7678D 02	-0.2008D-04	-0.6010D-07	0.0	0.6853E-01	0.6052E-02	0.6045E-02	0.0
47	0.7675D 02	-0.2028D-04	-0.6069D-07	0.0	0.6849E-01	0.6022E-02	0.6015E-02	0.0
48	0.7665D 02	-0.1706D-04	-0.5105D-07	0.0	0.6840E-01	0.5930E-02	0.5924E-02	0.0
49	0.7625D 02	0.1176D-04	0.3520D-07	0.0	0.6805E-01	0.5581E-02	0.5579E-02	0.0
50	0.7652D 02	0.1562D-03	0.4674D-06	0.0	0.6829E-01	0.5818E-02	0.5847E-02	0.0
61	0.7304D 02	-0.2933D-03	-0.8778D-06	0.0	0.4889E-01	0.2037E-02	0.1950E-02	0.0
62	0.7239D 02	-0.3398D-03	-0.1017D-05	0.0	0.4845E-01	0.1597E-02	0.1492E-02	0.0
63	0.7235D 02	-0.3465D-03	-0.1037D-05	0.0	0.4843E-01	0.1575E-02	0.1467E-02	0.0
64	0.7234D 02	-0.3489D-03	-0.1044D-05	0.0	0.4842E-01	0.1567E-02	0.1459E-02	0.0
65	0.7233D 02	-0.3497D-03	-0.1047D-05	0.0	0.4842E-01	0.1562E-02	0.1453E-02	0.0
66	0.7233D 02	-0.3495D-03	-0.1046D-05	0.0	0.4841E-01	0.1558E-02	0.1450E-02	0.0
67	0.7232D 02	-0.3482D-03	-0.1042D-05	0.0	0.4841E-01	0.1556E-02	0.1448E-02	0.0
68	0.7232D 02	-0.3454D-03	-0.1034D-05	0.0	0.4841E-01	0.1555E-02	0.1447E-02	0.0
69	0.7233D 02	-0.3388D-03	-0.1014D-05	0.0	0.4841E-01	0.1559E-02	0.1453E-02	0.0
70	0.7259D 02	-0.2968D-03	-0.8881D-06	0.0	0.4859E-01	0.1736E-02	0.1647E-02	0.0
71	0.1217D 03	0.2689D-03	0.8049D-06	0.0	0.1086E 00	0.4611E-01	0.4619E-01	0.0
72	0.1228D 03	-0.2313D-04	-0.6923D-07	0.0	0.1096E 00	0.4716E-01	0.4711E-01	0.0
73	0.1229D 03	-0.1103D-03	-0.3301D-06	0.0	0.1097E 00	0.4721E-01	0.4712E-01	0.0
74	0.1230D 03	-0.1452D-03	-0.4346D-06	0.0	0.1097E 00	0.4726E-01	0.4715E-01	0.0
75	0.1225D 03	-0.1727D-03	-0.5170D-06	0.0	0.1094E 00	0.4695E-01	0.4677E-01	0.0
76	0.1231D 03	-0.1953D-03	-0.5846D-06	0.0	0.1098E 00	0.4737E-01	0.4724E-01	0.0
77	0.1220D 03	-0.2104D-03	-0.6297D-06	0.0	0.1089E 00	0.4639E-01	0.4624E-01	0.0
78	0.1196D 03	-0.2016D-03	-0.6033D-06	0.0	0.1067E 00	0.4425E-01	0.4411E-01	0.0
79	0.9963D 02	-0.1165D-03	-0.3486D-06	0.0	0.8891E-01	0.2644E-01	0.2634E-01	0.0
80	0.9213D 02	0.2181D-03	0.6528D-06	0.0	0.8222E-01	0.1975E-01	0.1979E-01	0.0
81	0.1217D 03	0.2693D-03	0.8060D-06	0.0	0.1086E 00	0.4611E-01	0.4619E-01	0.0
82	0.1228D 03	-0.2329D-04	-0.6971D-07	0.0	0.1096E 00	0.4716E-01	0.4711E-01	0.0
83	0.1229D 03	-0.1105D-03	-0.3306D-06	0.0	0.1097E 00	0.4721E-01	0.4712E-01	0.0
84	0.1230D 03	-0.1454D-03	-0.4351D-06	0.0	0.1097E 00	0.4726E-01	0.4715E-01	0.0
85	0.1225D 03	-0.1729D-03	-0.5176D-06	0.0	0.1094E 00	0.4695E-01	0.4677E-01	0.0
86	0.1231D 03	-0.1955D-03	-0.5852D-06	0.0	0.1098E 00	0.4737E-01	0.4723E-01	0.0
87	0.1220D 03	-0.2106D-03	-0.6304D-06	0.0	0.1089E 00	0.4639E-01	0.4624E-01	0.0
88	0.1196D 03	-0.2018D-03	-0.6040D-06	0.0	0.1067E 00	0.4425E-01	0.4411E-01	0.0
89	0.9963D 02	-0.1167D-03	-0.3494D-06	0.0	0.8891E-01	0.2644E-01	0.2633E-01	0.0
90	0.9213D 02	0.2184D-03	0.6535D-06	0.0	0.8222E-01	0.1975E-01	0.1979E-01	0.0
91	0.1217D 03	0.2693D-03	0.8060D-06	0.0	0.1086E 00	0.4610E-01	0.4618E-01	0.0
92	0.1228D 03	-0.2328D-04	-0.6968D-07	0.0	0.1096E 00	0.4715E-01	0.4710E-01	0.0
93	0.1229D 03	-0.1104D-03	-0.3305D-06	0.0	0.1097E 00	0.4720E-01	0.4711E-01	0.0
94	0.1229D 03	-0.1453D-03	-0.4350D-06	0.0	0.1097E 00	0.4725E-01	0.4714E-01	0.0
95	0.1225D 03	-0.1729D-03	-0.5174D-06	0.0	0.1094E 00	0.4685E-01	0.4676E-01	0.0
96	0.1231D 03	-0.1955D-03	-0.5851D-06	0.0	0.1098E 00	0.4737E-01	0.4723E-01	0.0
97	0.1220D 03	-0.2106D-03	-0.6303D-06	0.0	0.1089E 00	0.4638E-01	0.4623E-01	0.0
98	0.1196D 03	-0.2018D-03	-0.6039D-06	0.0	0.1067E 00	0.4424E-01	0.4410E-01	0.0
99	0.9962D 02	-0.1167D-03	-0.3493D-06	0.0	0.8891E-01	0.2643E-01	0.2633E-01	0.0
100	0.9212D 02	0.2184D-03	0.6535D-06	0.0	0.8222E-01	0.1974E-01	0.1978E-01	0.0
101	0.1211D 03	0.2685D-03	0.8037D-06	0.0	0.1081E 00	0.4565E-01	0.4573E-01	0.0
102	0.1223D 03	-0.2096D-04	-0.6272D-07	0.0	0.1091E 00	0.4664E-01	0.4659E-01	0.0
103	0.1223D 03	-0.1089D-03	-0.3259D-06	0.0	0.1092E 00	0.4668E-01	0.4659E-01	0.0
104	0.1224D 03	-0.1434D-03	-0.4291D-06	0.0	0.1092E 00	0.4673E-01	0.4663E-01	0.0
105	0.1220D 03	-0.1705D-03	-0.5104D-06	0.0	0.1088E 00	0.4637E-01	0.4625E-01	0.0
106	0.1225D 03	-0.1928D-03	-0.5771D-06	0.0	0.1093E 00	0.4685E-01	0.4671E-01	0.0
107	0.1214D 03	-0.2078D-03	-0.6218D-06	0.0	0.1083E 00	0.4587E-01	0.4573E-01	0.0
108	0.1190D 03	-0.1990D-03	-0.5957D-06	0.0	0.1062E 00	0.4377E-01	0.4363E-01	0.0
109	0.9930D 02	-0.1147D-03	-0.3432D-06	0.0	0.8862E-01	0.2615E-01	0.2604E-01	0.0
110	0.9191D 02	0.2183D-03	0.6534D-06	0.0	0.8203E-01	0.1956E-01	0.1960E-01	0.0
111	0.7439D 02	0.1453D-03	0.4348D-06	0.0	0.6639E-01	0.3918E-02	0.3982E-02	0.0
112	0.7336D 02	0.2076D-04	0.6214D-07	0.0	0.6547E-01	0.2995E-02	0.3003E-02	0.0

NODE	TEMP	DT	DDT	GE N RATE	W	H	F	CLRE AT 280 F
113	0.7327D 02	-0.1369D-05	-0.4057D-08	0.0	0.6539E-01	0.2914E-02	0.2909E-02	0.0
114	0.7325D 02	-0.5325D-05	-0.1594D-07	0.0	0.6538E-01	0.2904E-02	0.2898E-02	0.0
115	0.7325D 02	-0.6201D-05	-0.1856D-07	0.0	0.6537E-01	0.2898E-02	0.2891E-02	0.0
116	0.7325D 02	-0.6746D-05	-0.2019D-07	0.0	0.6537E-01	0.2902E-02	0.2895E-02	0.0
117	0.7323D 02	-0.6895D-05	-0.2064D-07	0.0	0.6535E-01	0.2880E-02	0.2873E-02	0.0
118	0.7315D 02	-0.4482D-05	-0.1341D-07	0.0	0.6529E-01	0.2815E-02	0.2809E-02	0.0
119	0.7286D 02	0.1690D-04	0.5057D-07	0.0	0.6502E-01	0.2549E-02	0.2551E-02	0.0
120	0.7308D 02	0.1302D-03	0.3896D-06	0.0	0.6522E-01	0.2748E-02	0.2805E-02	0.0
131	0.7172D 02	0.1685D-03	0.5043D-06	0.0	0.4800E-01	0.1149E-02	0.1230E-02	0.0
132	0.7104D 02	0.1347D-03	0.4031D-06	0.0	0.4755E-01	0.6974E-03	0.7646E-03	0.0
133	0.7101D 02	0.1322D-03	0.3957D-06	0.0	0.4753E-01	0.6767E-03	0.7431E-03	0.0
134	0.7100D 02	0.1329D-03	0.3976D-06	0.0	0.4752E-01	0.6705E-03	0.7369E-03	0.0
135	0.7100D 02	0.1335D-03	0.3995D-06	0.0	0.4752E-01	0.6660E-03	0.7325E-03	0.0
136	0.7099D 02	0.1336D-03	0.3999D-06	0.0	0.4752E-01	0.6631E-03	0.7295E-03	0.0
137	0.7099D 02	0.1334D-03	0.3992D-06	0.0	0.4752E-01	0.6613E-03	0.7275E-03	0.0
138	0.7099D 02	0.1333D-03	0.3989D-06	0.0	0.4752E-01	0.6606E-03	0.7267E-03	0.0
139	0.7099D 02	0.1360D-03	0.4071D-06	0.0	0.4752E-01	0.6648E-03	0.7318E-03	0.0
140	0.7128D 02	0.1658D-03	0.4962D-06	0.0	0.4771E-01	0.8559E-03	0.9359E-03	0.0
151	0.1256D 03	0.2124D-03	0.6357D-06	0.9033D-01	0.3278E-01	0.1453E-02	-0.3366E 02	0.0
152	0.1253D 03	-0.1557D-04	-0.4660D-07	0.6044D-01	0.3271E-01	0.1385E-02	-0.2252E 02	0.0
153	0.1253D 03	-0.9723D-04	-0.2910D-06	0.4935D-01	0.3271E-01	0.1379E-02	-0.1839E 02	0.0
154	0.1254D 03	-0.1307D-03	-0.3912D-06	0.4606D-01	0.3273E-01	0.1401E-02	-0.1716E 02	0.0
155	0.1249D 03	-0.1571D-03	-0.4702D-06	0.4064D-01	0.3260E-01	0.1269E-02	-0.1514E 02	0.0
156	0.1256D 03	-0.1787D-03	-0.5348D-06	0.4071D-01	0.3278E-01	0.1453E-02	-0.1517E 02	0.0
157	0.1244D 03	-0.1934D-03	-0.5788D-06	0.3618D-01	0.3247E-01	0.1141E-02	-0.1348E 02	0.0
158	0.1226D 03	-0.1843D-03	-0.5516D-06	0.4435D-01	0.3201E-01	0.6782E-03	-0.1652E 02	0.0
159	0.9956D 02	-0.1006D-03	-0.3009D-06	0.0	0.2599E-01	-0.5337E-02	-0.5658E-02	0.0
160	0.9241D 02	0.1885D-03	0.5640D-06	0.0	0.2413E-01	-0.7202E-02	-0.7109E-02	0.0
181	0.7145D 02	0.5819D-04	0.1742D-06	0.0	0.4663E-02	0.9451E-04	0.1544E-03	0.0
182	0.7118D 02	0.1446D-04	0.4326D-07	0.0	0.4646E-02	0.7699E-04	0.8815E-04	0.0
183	0.7113D 02	0.2959D-05	0.8857D-08	0.0	0.4643E-02	0.7384E-04	0.7403E-04	0.0
184	0.7112D 02	0.8827D-06	0.2642D-08	0.0	0.4642E-02	0.7337E-04	0.7176E-04	0.0
185	0.7112D 02	0.4328D-06	0.1295D-08	0.0	0.4642E-02	0.7314E-04	0.7096E-04	0.0
186	0.7112D 02	0.2008D-06	0.6011D-09	0.0	0.4642E-02	0.7322E-04	0.7067E-04	0.0
187	0.7111D 02	0.2209D-06	0.6612D-09	0.0	0.4641E-02	0.7246E-04	0.6982E-04	0.0
188	0.7108D 02	0.1822D-05	0.5453D-08	0.0	0.4639E-02	0.7024E-04	0.6895E-04	0.0
189	0.7095D 02	0.1265D-04	0.3785D-07	0.0	0.4631E-02	0.6209E-04	0.7108E-04	0.0
190	0.7098D 02	0.5276D-04	0.1579D-06	0.0	0.4633E-02	0.6420E-04	0.1188E-03	0.0
201	0.7033D 02	0.3698D-03	0.1107D-05	0.0	0.3443E-02	0.1624E-04	0.7285E-01	0.0
202	0.7032D 02	0.3711D-03	0.1111D-05	0.0	0.3442E-02	0.1564E-04	0.7303E-01	0.0
203	0.7031D 02	0.3735D-03	0.1118D-05	0.0	0.3442E-02	0.1517E-04	0.7332E-01	0.0
204	0.7030D 02	0.3756D-03	0.1124D-05	0.0	0.3441E-02	0.1479E-04	0.7356E-01	0.0
205	0.7030D 02	0.3769D-03	0.1128D-05	0.0	0.3441E-02	0.1450E-04	0.7366E-01	0.0
206	0.7029D 02	0.3771D-03	0.1128D-05	0.0	0.3441E-02	0.1431E-04	0.7360E-01	0.0
207	0.7029D 02	0.3761D-03	0.1126D-05	0.0	0.3441E-02	0.1421E-04	0.7339E-01	0.0
208	0.7029D 02	0.3745D-03	0.1121D-05	0.0	0.3441E-02	0.1420E-04	0.7311E-01	0.0
209	0.7029D 02	0.3729D-03	0.1116D-05	0.0	0.3441E-02	0.1428E-04	0.7286E-01	0.0
210	0.7030D 02	0.3721D-03	0.1114D-05	0.0	0.3441E-02	0.1449E-04	0.7273E-01	0.0
211	0.7033D 02	0.3700D-03	0.1107D-05	0.0	0.7004E-01	0.3287E-03	0.1248E 00	0.0
212	0.7032D 02	0.3714D-03	0.1111D-05	0.0	0.7003E-01	0.3176E-03	0.1281E 00	0.0
213	0.7031D 02	0.3737D-03	0.1118D-05	0.0	0.7002E-01	0.3080E-03	0.1286E 00	0.0
214	0.7030D 02	0.3758D-03	0.1125D-05	0.0	0.7002E-01	0.3003E-03	0.1290E 00	0.0
215	0.7030D 02	0.3771D-03	0.1129D-05	0.0	0.7001E-01	0.2944E-03	0.1292E 00	0.0
216	0.7029D 02	0.3773D-03	0.1129D-05	0.0	0.7001E-01	0.2904E-03	0.1291E 00	0.0
217	0.7029D 02	0.3763D-03	0.1126D-05	0.0	0.7000E-01	0.2884E-03	0.1287E 00	0.0
218	0.7029D 02	0.3748D-03	0.1122D-05	0.0	0.7000E-01	0.2883E-03	0.1283E 00	0.0
219	0.7029D 02	0.3732D-03	0.1117D-05	0.0	0.7000E-01	0.2900E-03	0.1278E 00	0.0
220	0.7029D 02	0.3723D-03	0.1114D-05	0.0	0.7001E-01	0.2937E-03	0.1246E 00	0.0

NODE	TEMP	DT	DDT	GEN RATE	h	H	F	CURE AT 280 F
221	0.7033D 02	0.3701D-03	0.1108D-05	0.0	0.7004E-01	0.3278E-03	0.5205E-01	0.0
222	0.7032D 02	0.3715D-03	0.1112D-05	0.0	0.7003E-01	0.3173E-03	0.5522E-01	0.0
223	0.7031D 02	0.3738D-03	0.1119D-05	0.0	0.7002E-01	0.3078E-03	0.5542E-01	0.0
224	0.7030D 02	0.3759D-03	0.1125D-05	0.0	0.7001E-01	0.3001E-03	0.5559E-01	0.0
225	0.7030D 02	0.3772D-03	0.1129D-05	0.0	0.7001E-01	0.2942E-03	0.5566E-01	0.0
226	0.7029D 02	0.3773D-03	0.1129D-05	0.0	0.7001E-01	0.2902E-03	0.5561E-01	0.0
227	0.7029D 02	0.3764D-03	0.1127D-05	0.0	0.7000E-01	0.2882E-03	0.5545E-01	0.0
228	0.7029D 02	0.3749D-03	0.1122D-05	0.0	0.7000E-01	0.2881E-03	0.5525E-01	0.0
229	0.7029D 02	0.3733D-03	0.1117D-05	0.0	0.7000E-01	0.2898E-03	0.5506E-01	0.0
230	0.7029D 02	0.3724D-03	0.1115D-05	0.0	0.7001E-01	0.2932E-03	0.5193E-01	0.0
231	0.7301D 02	-0.5732D-03	-0.1715D-05	0.0	0.7272E-01	0.3003E-02	-0.7831E-03	0.0
232	0.7300D 02	-0.5795D-03	-0.1734D-05	0.0	0.7270E-01	0.2985E-02	-0.4538E-02	0.0
233	0.7298D 02	-0.5853D-03	-0.1752D-05	0.0	0.7268E-01	0.2970E-02	-0.4616E-02	0.0
234	0.7297D 02	-0.5891D-03	-0.1763D-05	0.0	0.7267E-01	0.2958E-02	-0.4664E-02	0.0
235	0.7296D 02	-0.5908D-03	-0.1768D-05	0.0	0.7266E-01	0.2949E-02	-0.4690E-02	0.0
236	0.7295D 02	-0.5906D-03	-0.1767D-05	0.0	0.7266E-01	0.2943E-02	-0.4695E-02	0.0
237	0.7295D 02	-0.5884D-03	-0.1761D-05	0.0	0.7265E-01	0.2939E-02	-0.4677E-02	0.0
238	0.7295D 02	-0.5843D-03	-0.1749D-05	0.0	0.7265E-01	0.2939E-02	-0.4640E-02	0.0
239	0.7295D 02	-0.5785D-03	-0.1731D-05	0.0	0.7266E-01	0.2941E-02	-0.4573E-02	0.0
240	0.7296D 02	-0.5722D-03	-0.1713D-05	0.0	0.7266E-01	0.2946E-02	-0.8363E-03	0.0
300	0.9269D 02	-0.4603D-04	-0.1378D-06	0.0	0.1073E 01	0.2626E 00	0.2624E 00	0.0
310	0.7126D 02	-0.1263D-03	-0.3779D-06	0.0	0.3093E-01	0.5452E-03	0.4854E-03	0.0
320	0.9229D 02	0.4527D-03	0.1355D-05	0.0	0.9888E 00	0.2388E 00	0.2388E 00	0.0
330	0.8030D 02	0.3797D-03	0.1136D-05	0.0	0.8604E 00	0.1104E 00	0.1104E 00	0.0

MATERIAL DATA

NAME	MATL	TOT CAP	TOT HEAT	AVG TEMP	TMELT	HMELT
THSE	1	1.02633E-01	1.04929E 01	1.02238E 02	0.0	0.0
NICR	2	3.75292E-03	3.91741E-01	1.04383E 02	0.0	0.0
PXGL	3	2.14293E-02	1.84921E 00	8.62934E 01	0.0	0.0
ALUM	4	2.98778E-02	2.12701E 00	7.11902E 01	0.0	0.0
INSL	5	1.20080E-02	1.10376E 00	9.19181E 01	0.0	0.0

INTERNAL CONNECTION DATA

NOD1	NOD2	AREA	HINT	RINT	TRAN	HEAT FLOW	AVG RATE
1	11	0.4340D-03	0.1000E 13	0.0	0.8401D-05	-0.9699E-06	-0.2603E-08
2	12	0.4340D-03	0.1000E 13	0.0	0.8401D-05	-0.1221E-05	-0.3277E-08
3	13	0.4340D-03	0.1000E 13	0.0	0.8401D-05	-0.1259E-05	-0.3379E-08
4	14	0.4340D-03	0.1000E 13	0.0	0.8401D-05	-0.1261E-05	-0.3384E-08
5	15	0.4340D-03	0.1000E 13	0.0	0.8401D-05	-0.1253E-05	-0.3364E-08
6	16	0.4340D-03	0.1000E 13	0.0	0.8401D-05	-0.1251E-05	-0.3358E-08
7	17	0.4340D-03	0.1000E 13	0.0	0.8401D-05	-0.1213E-05	-0.3254E-08
8	18	0.4340D-03	0.1000E 13	0.0	0.8401D-05	-0.1088E-05	-0.2920E-08
9	19	0.4340D-03	0.1000E 13	0.0	0.8401D-05	-0.7105E-06	-0.1907E-08
10	20	0.4340D-03	0.1000E 13	0.0	0.8401D-05	-0.4281E-06	-0.1149E-08
11	21	0.4340D-03	0.1000E 13	0.0	0.8401D-05	-0.5061E-04	-0.1358E-06
12	22	0.4340D-03	0.1000E 13	0.0	0.8401D-05	-0.6160E-04	-0.1653E-06
13	23	0.4340D-03	0.1000E 13	0.0	0.8401D-05	-0.6302E-04	-0.1691E-06
14	24	0.4340D-03	0.1000E 13	0.0	0.8401D-05	-0.6313E-04	-0.1694E-06
15	25	0.4340D-03	0.1000E 13	0.0	0.8401D-05	-0.6279E-04	-0.1685E-06
16	26	0.4340D-03	0.1000E 13	0.0	0.8401D-05	-0.6294E-04	-0.1689E-06
17	27	0.4340D-03	0.1000E 13	0.0	0.8401D-05	-0.6126E-04	-0.1644E-06
18	28	0.4340D-03	0.1000E 13	0.0	0.8401D-05	-0.5573E-04	-0.1496E-06
19	29	0.4340D-03	0.1000E 13	0.0	0.8401D-05	-0.3550E-04	-0.9527E-07
20	30	0.4340D-03	0.1000E 13	0.0	0.8401D-05	-0.2166E-04	-0.5814E-07
21	31	0.4340D-03	0.1000E 13	0.0	0.8401D-05	-0.2588E-02	-0.6946E-05
22	32	0.4340D-03	0.1000E 13	0.0	0.8401D-05	-0.2987E-02	-0.8017E-05
23	33	0.4340D-03	0.1000E 13	0.0	0.8401D-05	-0.3025E-02	-0.8119E-05
24	34	0.4340D-03	0.1000E 13	0.0	0.8401D-05	-0.3028E-02	-0.8125E-05
25	35	0.4340D-03	0.1000E 13	0.0	0.8401D-05	-0.3008E-02	-0.8072E-05
26	36	0.4340D-03	0.1000E 13	0.0	0.8401D-05	-0.3023E-02	-0.8113E-05
27	37	0.4340D-03	0.1000E 13	0.0	0.8401D-05	-0.2950E-02	-0.7917E-05
28	38	0.4340D-03	0.1000E 13	0.0	0.8401D-05	-0.2724E-02	-0.7310E-05
29	39	0.4340D-03	0.1000E 13	0.0	0.8401D-05	-0.1679E-02	-0.4506E-05
30	40	0.4340D-03	0.1000E 13	0.0	0.8401D-05	-0.1075E-02	-0.2885E-05
31	41	0.4340D-03	0.1000E 13	0.0	0.8401D-05	-0.1124E 00	-0.3017E-03
32	42	0.4340D-03	0.1000E 13	0.0	0.8401D-05	-0.1229E 00	-0.3297E-03
33	43	0.4340D-03	0.1000E 13	0.0	0.8401D-05	-0.1235E 00	-0.3314E-03
34	44	0.4340D-03	0.1000E 13	0.0	0.8401D-05	-0.1235E 00	-0.3315E-03
35	45	0.4340D-03	0.1000E 13	0.0	0.8401D-05	-0.1226E 00	-0.3289E-03
36	46	0.4340D-03	0.1000E 13	0.0	0.8401D-05	-0.1235E 00	-0.3315E-03
37	47	0.4340D-03	0.1000E 13	0.0	0.8401D-05	-0.1207E 00	-0.3240E-03
38	48	0.4340D-03	0.1000E 13	0.0	0.8401D-05	-0.1133E 00	-0.3041E-03
39	49	0.4340D-03	0.1000E 13	0.0	0.8401D-05	-0.6730E-01	-0.1806E-03
40	50	0.4340D-03	0.1000E 13	0.0	0.8401D-05	-0.4549E-01	-0.1221E-03
41	61	0.4340D-03	0.1000E 13	0.0	0.9601D-05	-0.1862E-01	-0.4998E-04
42	62	0.4340D-03	0.1000E 13	0.0	0.9601D-05	-0.1596E-01	-0.4283E-04
43	63	0.4340D-03	0.1000E 13	0.0	0.9601D-05	-0.1561E-01	-0.4189E-04
44	64	0.4340D-03	0.1000E 13	0.0	0.9601D-05	-0.1560E-01	-0.4185E-04
45	65	0.4340D-03	0.1000E 13	0.0	0.9601D-05	-0.1559E-01	-0.4183E-04
46	66	0.4340D-03	0.1000E 13	0.0	0.9601D-05	-0.1562E-01	-0.4192E-04
47	67	0.4340D-03	0.1000E 13	0.0	0.9601D-05	-0.1551E-01	-0.4163E-04
48	68	0.4340D-03	0.1000E 13	0.0	0.9601D-05	-0.1516E-01	-0.4068E-04
49	69	0.4340D-03	0.1000E 13	0.0	0.9601D-05	-0.1375E-01	-0.3691E-04
50	70	0.4340D-03	0.1000E 13	0.0	0.9601D-05	-0.1365E-01	-0.3663E-04
71	81	0.4340D-03	0.1000E 13	0.0	0.8401D-05	-0.4391E-06	-0.1178E-08
72	82	0.4340D-03	0.1000E 13	0.0	0.8401D-05	-0.5491E-06	-0.1473E-08
73	83	0.4340D-03	0.1000E 13	0.0	0.8401D-05	-0.5655E-06	-0.1518E-08
74	84	0.4340D-03	0.1000E 13	0.0	0.8401D-05	-0.5661E-06	-0.1519E-08
75	85	0.4340D-03	0.1000E 13	0.0	0.8401D-05	-0.5623E-06	-0.1509E-08
76	86	0.4340D-03	0.1000E 13	0.0	0.8401D-05	-0.5613E-06	-0.1506E-08
77	87	0.4340D-03	0.1000E 13	0.0	0.8401D-05	-0.5438E-06	-0.1459E-08

NCD1	NCD2	AREA	HINT	RINT	TRAN	HEAT FLOW	AVG RATE
78	88	0.4340D-03	0.1000E 13	0.0	0.8401D-05	-0.4882E-06	-0.1310E-08
79	89	0.4340D-03	0.1000E 13	0.0	0.8401D-05	-0.3178E-06	-0.8530E-09
80	90	0.4340D-03	0.1000E 13	0.0	0.8401D-05	-0.1933E-06	-0.5186E-09
81	91	0.4340D-03	0.1000E 13	0.0	0.8401D-05	-0.2428E-04	-0.6516E-07
82	92	0.4340D-03	0.1000E 13	0.0	0.8401D-05	-0.2925E-04	-0.7850E-07
83	93	0.4340D-03	0.1000E 13	0.0	0.8401D-05	-0.2989E-04	-0.8020E-07
84	94	0.4340D-03	0.1000E 13	0.0	0.8401D-05	-0.2994E-04	-0.8034E-07
85	95	0.4340D-03	0.1000E 13	0.0	0.8401D-05	-0.2977E-04	-0.7988E-07
86	96	0.4340D-03	0.1000E 13	0.0	0.8401D-05	-0.2985E-04	-0.8011E-07
87	97	0.4340D-03	0.1000E 13	0.0	0.8401D-05	-0.2906E-04	-0.7800E-07
88	98	0.4340D-03	0.1000E 13	0.0	0.8401D-05	-0.2652E-04	-0.7116E-07
89	99	0.4340D-03	0.1000E 13	0.0	0.8401D-05	-0.1678E-04	-0.4504E-07
90	100	0.4340D-03	0.1000E 13	0.0	0.8401D-05	-0.1034E-04	-0.2774E-07
91	101	0.4340D-03	0.1000E 13	0.0	0.8401D-05	-0.1569E-02	-0.4199E-05
92	102	0.4340D-03	0.1000E 13	0.0	0.8401D-05	-0.1757E-02	-0.4714E-05
93	103	0.4340D-03	0.1000E 13	0.0	0.8401D-05	-0.1773E-02	-0.4759E-05
94	104	0.4340D-03	0.1000E 13	0.0	0.8401D-05	-0.1774E-02	-0.4762E-05
95	105	0.4340D-03	0.1000E 13	0.0	0.8401D-05	-0.1762E-02	-0.4727E-05
96	106	0.4340D-03	0.1000E 13	0.0	0.8401D-05	-0.1773E-02	-0.4758E-05
97	107	0.4340D-03	0.1000E 13	0.0	0.8401D-05	-0.1731E-02	-0.4646E-05
98	108	0.4340D-03	0.1000E 13	0.0	0.8401D-05	-0.1612E-02	-0.4326E-05
99	109	0.4340D-03	0.1000E 13	0.0	0.8401D-05	-0.9744E-03	-0.2615E-05
100	110	0.4340D-03	0.1000E 13	0.0	0.8401D-05	-0.6411E-03	-0.1720E-05
101	111	0.4340D-03	0.1000E 13	0.0	0.8401D-05	-0.1444E 00	-0.3875E-03
102	112	0.4340D-03	0.1000E 13	0.0	0.8401D-05	-0.1506E 00	-0.4043E-03
103	113	0.4340D-03	0.1000E 13	0.0	0.8401D-05	-0.1508E 00	-0.4048E-03
104	114	0.4340D-03	0.1000E 13	0.0	0.8401D-05	-0.1509E 00	-0.4049E-03
105	115	0.4340D-03	0.1000E 13	0.0	0.8401D-05	-0.1495E 00	-0.4013E-03
106	116	0.4340D-03	0.1000E 13	0.0	0.8401D-05	-0.1511E 00	-0.4054E-03
107	117	0.4340D-03	0.1000E 13	0.0	0.8401D-05	-0.1477E 00	-0.3965E-03
108	118	0.4340D-03	0.1000E 13	0.0	0.8401D-05	-0.1408E 00	-0.3778E-03
109	119	0.4340D-03	0.1000E 13	0.0	0.8401D-05	-0.8058E-01	-0.2162E-03
110	120	0.4340D-03	0.1000E 13	0.0	0.8401D-05	-0.5722E-01	-0.1536E-03
111	131	0.4340D-03	0.1000E 13	0.0	0.9601D-05	-0.9315E-02	-0.2500E-04
112	132	0.4340D-03	0.1000E 13	0.0	0.9601D-05	-0.8158E-02	-0.2189E-04
113	133	0.4340D-03	0.1000E 13	0.0	0.9601D-05	-0.7944E-02	-0.2132E-04
114	134	0.4340D-03	0.1000E 13	0.0	0.9601D-05	-0.7935E-02	-0.2129E-04
115	135	0.4340D-03	0.1000E 13	0.0	0.9601D-05	-0.7928E-02	-0.2128E-04
116	136	0.4340D-03	0.1000E 13	0.0	0.9601D-05	-0.7957E-02	-0.2135E-04
117	137	0.4340D-03	0.1000E 13	0.0	0.9601D-05	-0.7877E-02	-0.2114E-04
118	138	0.4340D-03	0.1000E 13	0.0	0.9601D-05	-0.7628E-02	-0.2047E-04
119	139	0.4340D-03	0.1000E 13	0.0	0.9601D-05	-0.6550E-02	-0.1758E-04
120	140	0.4340D-03	0.1000E 13	0.0	0.9601D-05	-0.6277E-02	-0.1685E-04
151	181	0.1389D-04	0.1000E 13	0.0	0.1000D-04	-0.1996E 00	-0.5356E-03
152	182	0.1389D-04	0.1000E 13	0.0	0.1000D-04	-0.1992E 00	-0.5346E-03
153	183	0.1389D-04	0.1000E 13	0.0	0.1000D-04	-0.1989E 00	-0.5339E-03
154	184	0.1389D-04	0.1000E 13	0.0	0.1000D-04	-0.1991E 00	-0.5343E-03
155	185	0.1389D-04	0.1000E 13	0.0	0.1000D-04	-0.1970E 00	-0.5288E-03
156	186	0.1389D-04	0.1000E 13	0.0	0.1000D-04	-0.1995E 00	-0.5355E-03
157	187	0.1389D-04	0.1000E 13	0.0	0.1000D-04	-0.1951E 00	-0.5236E-03
158	188	0.1389D-04	0.1000E 13	0.0	0.1000D-04	-0.1888E 00	-0.5067E-03
159	189	0.1389D-04	0.1000E 13	0.0	0.1000D-04	-0.1041E 00	-0.2793E-03
160	190	0.1389D-04	0.1000E 13	0.0	0.1000D-04	-0.7775E-01	-0.2086E-03
181	201	0.1389D-04	0.1000E 13	0.0	0.2857D-04	-0.1169E-01	-0.3138E-04
182	202	0.1389D-04	0.1000E 13	0.0	0.2857D-04	-0.9157E-02	-0.2457E-04
183	203	0.1389D-04	0.1000E 13	0.0	0.2857D-04	-0.8770E-02	-0.2354E-04
184	204	0.1389D-04	0.1000E 13	0.0	0.2857D-04	-0.8771E-02	-0.2354E-04

NCC1	NCC2	AREA	HINT	RINT	TRAN	HEAT FLCW	AVG RATE
185	205	C.1389D-C4	0.1000E 13	0.0	0.2857D-04	-0.8788E-C2	-0.2358E-C4
186	206	0.1389D-C4	0.1000E 13	0.0	0.2857D-C4	-0.8837E-02	-0.2372E-04
187	207	C.1389D-04	0.1000E 13	0.0	0.2857D-C4	-0.8733E-C2	-0.2344E-04
188	208	C.1389D-C4	0.1000E 13	0.0	0.2857D-C4	-0.8378E-C2	-0.2248E-04
189	209	C.1389D-04	0.1000E 13	0.0	0.2857D-C4	-C.7032E-C2	-C.1887E-04
190	210	0.1389D-04	0.1000E 13	0.0	0.2857D-C4	-0.7241E-C2	-C.1943E-04
61	310	C.4340D-C3	0.10CCE 13	C.C	0.8575D-C5	-0.5354E-C2	-0.1437E-04
62	310	0.4340D-03	0.1000E 13	0.0	0.8575D-C5	-C.3385E-C2	-C.9083E-05
63	310	C.434CD-C3	0.10C0E 13	0.0	0.8575D-05	-0.3284E-C2	-C.8814E-05
64	310	0.434CD-C3	0.1000E 13	0.C	0.8575D-05	-0.3250E-C2	-0.8721E-05
65	310	0.4340D-03	0.1000E 13	0.0	0.8575D-C5	-C.3225E-C2	-C.8655E-C5
66	310	0.434CD-C3	0.1000E 13	0.0	0.8575D-05	-0.3209E-02	-0.8611E-05
67	310	C.434CD-03	0.1000E 13	0.0	0.8575D-C5	-C.3198E-C2	-0.8583E-05
68	310	C.4340D-03	0.1000E 13	0.0	0.8575D-C5	-0.3194E-C2	-C.8571E-05
69	310	C.434CD-C3	0.1000E 13	0.0	0.8575D-C5	-0.3210E-02	-0.8613E-05
70	310	0.4340D-03	0.1000E 13	0.0	0.8575D-C5	-C.3986E-C2	-C.107CE-04
131	310	C.4340D-03	0.1000E 13	0.0	0.8575D-05	-0.1346E-02	-C.3612E-05
132	310	C.434CD-C3	0.10C0E 13	0.C	0.8575D-C5	0.6743E-03	0.1810E-05
133	310	0.4340D-03	0.1000E 13	0.0	0.8575D-C5	C.7662E-C3	0.2C56E-05
134	310	C.434CD-C3	0.10C0E 13	0.0	0.8575D-05	0.7939E-03	0.2131E-05
135	310	C.434CD-C3	0.10C0E 13	0.0	0.8575D-C5	0.8136E-03	0.2183E-05
136	310	0.4340D-03	0.1000E 13	0.0	0.8575D-C5	C.8265E-C3	C.2218E-05
137	310	C.434CD-C3	0.10CCE 13	0.0	0.8575D-05	0.8344E-03	0.2239E-05
138	310	0.4340D-03	0.1000E 13	0.0	0.8575D-C5	C.8375E-C3	0.2248E-05
139	310	C.434CD-C3	0.1000E 13	0.0	0.8575D-C5	0.82CCE-C3	C.2201E-05
140	310	0.434CD-C3	0.100CE 13	0.0	0.8575D-C5	-0.2010E-C4	-0.5395E-07
211	310	0.8681D-03	0.1000E 13	0.0	0.2777D-C4	C.9129E-C2	0.245CE-04
212	310	C.8681D-C3	0.1000E 13	0.0	0.2777D-C4	0.9237E-02	0.2479E-04
213	310	C.8681D-C3	0.1000E 13	0.0	0.2777D-C4	C.9329E-02	0.2503E-04
214	310	C.8681D-03	0.1000E 13	0.0	0.2777D-04	C.9403E-C2	0.2523E-04
215	310	C.8681D-C3	0.100CE 13	0.0	0.2777D-C4	0.9458E-02	0.2538E-04
216	310	0.8681D-C3	0.1000E 13	0.0	0.2777D-C4	0.9496E-C2	0.2548E-04
217	310	C.8681D-03	0.1000E 13	0.0	0.2777D-04	0.9515E-C2	0.2553E-04
218	310	C.8681D-C3	0.1CC0E 13	0.C	0.2777D-C4	0.9516E-C2	0.2554E-04
219	310	0.8681D-03	0.1000E 13	0.0	0.2777D-C4	C.950CE-02	0.2549E-04
220	310	C.8681D-C3	0.1C00E 13	0.0	0.2777D-04	0.9464E-C2	0.2540E-04
221	310	C.8681D-C3	0.1000E 13	0.0	0.2777D-C4	0.9139E-02	0.2452E-04
222	310	C.8681D-03	0.1000E 13	0.0	0.2777D-C4	C.924CE-C2	C.2480E-04
223	310	C.8681D-C3	0.10C0E 13	0.0	0.2777D-04	0.9331E-02	0.2504E-04
224	310	0.8681D-03	0.1C00E 13	0.0	0.2777D-04	C.9405E-02	0.2524E-04
225	310	C.8681D-03	0.100CE 13	0.0	0.2777D-04	0.9460E-C2	C.2539E-04
226	310	C.8681D-C3	0.1CCCE 13	0.0	0.2777D-C4	0.9498E-02	0.2549E-04
227	310	0.8681D-03	0.1000E 13	0.0	0.2777D-C4	C.9517E-02	0.2554E-04
228	310	C.8681D-C3	0.1000E 13	0.0	0.2777D-C4	0.9518E-C2	C.2554E-04
229	310	C.8681D-C3	0.1000E 13	0.0	0.2777D-C4	C.9502E-02	0.2550E-04
230	310	C.8681D-03	0.1000E 13	0.0	0.2777D-C4	C.9469E-C2	C.2541E-C4
231	300	C.8681D-C3	0.1000E 13	C.0	0.2777D-04	0.1986E CO	0.5328E-03
232	300	0.8681D-03	0.100CE 13	0.0	0.2777D-C4	0.1987E CO	0.5333E-03
233	300	C.8681D-03	0.1000E 13	0.0	0.2777D-04	0.1989E CO	C.5337E-03
234	300	C.8681D-C3	0.10C0E 13	0.0	0.2777D-C4	0.1990E 00	0.5340E-03
235	300	0.8681D-C3	0.10C0E 13	0.0	0.2777D-C4	0.1991E CO	0.5343E-03
236	300	C.8681D-C3	0.100CE 13	0.0	0.2777D-C4	0.1991E CC	C.5344E-03
237	300	C.8681D-C3	0.10CCE 13	0.0	0.2777D-C4	0.1992E CO	0.5345E-03
238	300	C.8681D-03	0.1000E 13	0.0	0.2777D-C4	0.1992E CC	C.5345E-03
239	300	C.8681D-C3	0.100CE 13	0.0	0.2777D-04	0.1992E 00	0.5345E-03
240	300	0.8681D-03	0.1000E 13	0.0	0.2777D-C4	C.1991E CO	0.5343E-03
201	310	C.1389D-04	0.1000E 13	0.0	0.4416D-06	0.1449E-C3	0.3889E-06

NCD1	NCD2	AREA	HINT	RINT	TRAN	HEAT FLCW	AVG RATE
202	310	0.1389D-04	0.1000E 13	0.0	0.4416D-06	0.1468E-03	0.3940E-06
203	310	0.1389D-04	0.1000E 13	0.0	0.4416D-06	0.1483E-03	0.3979E-06
204	310	0.1389D-04	0.1000E 13	0.0	0.4416D-06	0.1494E-03	0.4010E-06
205	310	0.1389D-04	0.1000E 13	0.0	0.4416D-06	0.1503E-03	0.4034E-06
206	310	0.1389D-04	0.1000E 13	0.0	0.4416D-06	0.1509E-03	0.4050E-06
207	310	0.1389D-04	0.1000E 13	0.0	0.4416D-06	0.1512E-03	0.4058E-06
208	310	0.1389D-04	0.1000E 13	0.0	0.4416D-06	0.1512E-03	0.4059E-06
209	310	0.1389D-04	0.1000E 13	0.0	0.4416D-06	0.1510E-03	0.4052E-06
210	310	0.1389D-04	0.1000E 13	0.0	0.4416D-06	0.1504E-03	0.4035E-06
1	71	0.3472D-02	0.1000E 13	0.0	0.5377D-03	0.1203E 01	0.3228E-02
2	72	0.3472D-02	0.1000E 13	0.0	0.5377D-03	0.1003E 01	0.2692E-02
3	73	0.3472D-02	0.1000E 13	0.0	0.5377D-03	0.9819E 00	0.2635E-02
4	74	0.3472D-02	0.1000E 13	0.0	0.5377D-03	0.9848E 00	0.2643E-02
5	75	0.3472D-02	0.1000E 13	0.0	0.5377D-03	0.9602E 00	0.2577E-02
6	76	0.3472D-02	0.1000E 13	0.0	0.5377D-03	0.9965E 00	0.2674E-02
7	77	0.3472D-02	0.1000E 13	0.0	0.5377D-03	0.9643E 00	0.2588E-02
8	78	0.3472D-02	0.1000E 13	0.0	0.5377D-03	0.1008E 01	0.2705E-02
9	79	0.3472D-02	0.1000E 13	0.0	0.5377D-03	0.1467E 00	0.3937E-03
10	80	0.3472D-02	0.1000E 13	0.0	0.5377D-03	0.6021E-01	0.1616E-03
11	81	0.3472D-02	0.1000E 13	0.0	0.5377D-03	0.1203E 01	0.3228E-02
12	82	0.3472D-02	0.1000E 13	0.0	0.5377D-03	0.1003E 01	0.2692E-02
13	83	0.3472D-02	0.1000E 13	0.0	0.5377D-03	0.9820E 00	0.2635E-02
14	84	0.3472D-02	0.1000E 13	0.0	0.5377D-03	0.9848E 00	0.2643E-02
15	85	0.3472D-02	0.1000E 13	0.0	0.5377D-03	0.9603E 00	0.2577E-02
16	86	0.3472D-02	0.1000E 13	0.0	0.5377D-03	0.9966E 00	0.2674E-02
17	87	0.3472D-02	0.1000E 13	0.0	0.5377D-03	0.9643E 00	0.2588E-02
18	88	0.3472D-02	0.1000E 13	0.0	0.5377D-03	0.1008E 01	0.2705E-02
19	89	0.3472D-02	0.1000E 13	0.0	0.5377D-03	0.1467E 00	0.3938E-03
20	90	0.3472D-02	0.1000E 13	0.0	0.5377D-03	0.6022E-01	0.1616E-03
21	91	0.3472D-02	0.1000E 13	0.0	0.5377D-03	0.1204E 01	0.3232E-02
22	92	0.3472D-02	0.1000E 13	0.0	0.5377D-03	0.1005E 01	0.2698E-02
23	93	0.3472D-02	0.1000E 13	0.0	0.5377D-03	0.9841E 00	0.2641E-02
24	94	0.3472D-02	0.1000E 13	0.0	0.5377D-03	0.9869E 00	0.2649E-02
25	95	0.3472D-02	0.1000E 13	0.0	0.5377D-03	0.9624E 00	0.2583E-02
26	96	0.3472D-02	0.1000E 13	0.0	0.5377D-03	0.9987E 00	0.2680E-02
27	97	0.3472D-02	0.1000E 13	0.0	0.5377D-03	0.9664E 00	0.2593E-02
28	98	0.3472D-02	0.1000E 13	0.0	0.5377D-03	0.1010E 01	0.2710E-02
29	99	0.3472D-02	0.1000E 13	0.0	0.5377D-03	0.1479E 00	0.3970E-03
30	100	0.3472D-02	0.1000E 13	0.0	0.5377D-03	0.6095E-01	0.1636E-03
31	101	0.3472D-02	0.1000E 13	0.0	0.5377D-03	0.1270E 01	0.3408E-02
32	102	0.3472D-02	0.1000E 13	0.0	0.5377D-03	0.1084E 01	0.2909E-02
33	103	0.3472D-02	0.1000E 13	0.0	0.5377D-03	0.1064E 01	0.2856E-02
34	104	0.3472D-02	0.1000E 13	0.0	0.5377D-03	0.1067E 01	0.2864E-02
35	105	0.3472D-02	0.1000E 13	0.0	0.5377D-03	0.1042E 01	0.2797E-02
36	106	0.3472D-02	0.1000E 13	0.0	0.5377D-03	0.1079E 01	0.2895E-02
37	107	0.3472D-02	0.1000E 13	0.0	0.5377D-03	0.1044E 01	0.2803E-02
38	108	0.3472D-02	0.1000E 13	0.0	0.5377D-03	0.1081E 01	0.2901E-02
39	109	0.3472D-02	0.1000E 13	0.0	0.5377D-03	0.1931E 00	0.5181E-03
40	110	0.3472D-02	0.1000E 13	0.0	0.5377D-03	0.8874E-01	0.2381E-03
41	111	0.3472D-02	0.1000E 13	0.0	0.5377D-03	-0.7726E 00	-0.2073E-02
42	112	0.3472D-02	0.1000E 13	0.0	0.5377D-03	-0.6914E 00	-0.1855E-02
43	113	0.3472D-02	0.1000E 13	0.0	0.5377D-03	-0.6833E 00	-0.1834E-02
44	114	0.3472D-02	0.1000E 13	0.0	0.5377D-03	-0.6826E 00	-0.1832E-02
45	115	0.3472D-02	0.1000E 13	0.0	0.5377D-03	-0.6821E 00	-0.1831E-02
46	116	0.3472D-02	0.1000E 13	0.0	0.5377D-03	-0.6823E 00	-0.1831E-02
47	117	0.3472D-02	0.1000E 13	0.0	0.5377D-03	-0.6805E 00	-0.1826E-02
48	118	0.3472D-02	0.1000E 13	0.0	0.5377D-03	-0.6745E 00	-0.1810E-02

NCD1	NCD2	AREA	HINT	RINT	TRAN	HEAT FLCW	AVG RATE
49	119	0.3472D-02	0.1000E 13	0.0	0.5377D-03	-0.6560E 00	-0.1760E-02
50	120	0.3472D-02	0.1000E 13	0.0	0.5377D-03	-0.6615E 00	-0.1775E-02
61	131	0.2604D-02	0.1000E 13	0.0	0.4032D-03	-0.1885E 00	-0.5059E-03
62	132	0.2604D-02	0.1000E 13	0.0	0.4032D-03	-0.1909E 00	-0.5123E-03
63	133	0.2604D-02	0.1000E 13	0.0	0.4032D-03	-0.1905E 00	-0.5112E-03
64	134	0.2604D-02	0.1000E 13	0.0	0.4032D-03	-0.1902E 00	-0.5104E-03
65	135	0.2604D-02	0.1000E 13	0.0	0.4032D-03	-0.1899E 00	-0.5097E-03
66	136	0.2604D-02	0.1000E 13	0.0	0.4032D-03	-0.1898E 00	-0.5092E-03
67	137	0.2604D-02	0.1000E 13	0.0	0.4032D-03	-0.1897E 00	-0.5090E-03
68	138	0.2604D-02	0.1000E 13	0.0	0.4032D-03	-0.1896E 00	-0.5088E-03
69	139	0.2604D-02	0.1000E 13	0.0	0.4032D-03	-0.1895E 00	-0.5086E-03
70	140	0.2604D-02	0.1000E 13	0.0	0.4032D-03	-0.1865E 00	-0.5005E-03
1	300	0.3472D-02	0.1000E 13	0.0	0.1007D-03	-0.8559E 00	-0.2297E-02
2	300	0.3472D-02	0.1000E 13	0.0	0.1007D-03	-0.9350E 00	-0.2509E-02
3	300	0.3472D-02	0.1000E 13	0.0	0.1007D-03	-0.9379E 00	-0.2517E-02
4	300	0.3472D-02	0.1000E 13	0.0	0.1007D-03	-0.9378E 00	-0.2517E-02
5	300	0.3472D-02	0.1000E 13	0.0	0.1007D-03	-0.9256E 00	-0.2484E-02
6	300	0.3472D-02	0.1000E 13	0.0	0.1007D-03	-0.9377E 00	-0.2516E-02
7	300	0.3472D-02	0.1000E 13	0.0	0.1007D-03	-0.9022E 00	-0.2421E-02
8	300	0.3472D-02	0.1000E 13	0.0	0.1007D-03	-0.8067E 00	-0.2165E-02
9	300	0.3472D-02	0.1000E 13	0.0	0.1007D-03	-0.2271E 00	-0.6096E-03
10	300	0.3472D-02	0.1000E 13	0.0	0.1007D-03	0.3372E-01	0.9050E-04
11	300	0.3472D-02	0.1000E 13	0.0	0.1007D-03	-0.8559E 00	-0.2297E-02
12	300	0.3472D-02	0.1000E 13	0.0	0.1007D-03	-0.9350E 00	-0.2509E-02
13	300	0.3472D-02	0.1000E 13	0.0	0.1007D-03	-0.9379E 00	-0.2517E-02
14	300	0.3472D-02	0.1000E 13	0.0	0.1007D-03	-0.9378E 00	-0.2517E-02
15	300	0.3472D-02	0.1000E 13	0.0	0.1007D-03	-0.9256E 00	-0.2484E-02
16	300	0.3472D-02	0.1000E 13	0.0	0.1007D-03	-0.9377E 00	-0.2516E-02
17	300	0.3472D-02	0.1000E 13	0.0	0.1007D-03	-0.9021E 00	-0.2421E-02
18	300	0.3472D-02	0.1000E 13	0.0	0.1007D-03	-0.8067E 00	-0.2165E-02
19	300	0.3472D-02	0.1000E 13	0.0	0.1007D-03	-0.2271E 00	-0.6095E-03
20	300	0.3472D-02	0.1000E 13	0.0	0.1007D-03	0.3373E-01	0.9051E-04
21	300	0.3472D-02	0.1000E 13	0.0	0.1007D-03	-0.8553E 00	-0.2295E-02
22	300	0.3472D-02	0.1000E 13	0.0	0.1007D-03	-0.9342E 00	-0.2507E-02
23	300	0.3472D-02	0.1000E 13	0.0	0.1007D-03	-0.9372E 00	-0.2515E-02
24	300	0.3472D-02	0.1000E 13	0.0	0.1007D-03	-0.9370E 00	-0.2515E-02
25	300	0.3472D-02	0.1000E 13	0.0	0.1007D-03	-0.9249E 00	-0.2482E-02
26	300	0.3472D-02	0.1000E 13	0.0	0.1007D-03	-0.9369E 00	-0.2514E-02
27	300	0.3472D-02	0.1000E 13	0.0	0.1007D-03	-0.9014E 00	-0.2419E-02
28	300	0.3472D-02	0.1000E 13	0.0	0.1007D-03	-0.8060E 00	-0.2163E-02
29	300	0.3472D-02	0.1000E 13	0.0	0.1007D-03	-0.2267E 00	-0.6084E-03
30	300	0.3472D-02	0.1000E 13	0.0	0.1007D-03	0.3399E-01	0.9121E-04
31	300	0.3472D-02	0.1000E 13	0.0	0.1007D-03	-0.8242E 00	-0.2212E-02
32	300	0.3472D-02	0.1000E 13	0.0	0.1007D-03	-0.8984E 00	-0.2411E-02
33	300	0.3472D-02	0.1000E 13	0.0	0.1007D-03	-0.9009E 00	-0.2418E-02
34	300	0.3472D-02	0.1000E 13	0.0	0.1007D-03	-0.9007E 00	-0.2417E-02
35	300	0.3472D-02	0.1000E 13	0.0	0.1007D-03	-0.8888E 00	-0.2385E-02
36	300	0.3472D-02	0.1000E 13	0.0	0.1007D-03	-0.9007E 00	-0.2417E-02
37	300	0.3472D-02	0.1000E 13	0.0	0.1007D-03	-0.8660E 00	-0.2324E-02
38	300	0.3472D-02	0.1000E 13	0.0	0.1007D-03	-0.7733E 00	-0.2075E-02
39	300	0.3472D-02	0.1000E 13	0.0	0.1007D-03	-0.2066E 00	-0.5544E-03
40	300	0.3472D-02	0.1000E 13	0.0	0.1007D-03	0.4688E-01	0.1258E-03
41	300	0.3472D-02	0.1000E 13	0.0	0.1007D-03	0.5242E 00	0.1407E-02
42	300	0.3472D-02	0.1000E 13	0.0	0.1007D-03	0.5753E 00	0.1544E-02
43	300	0.3472D-02	0.1000E 13	0.0	0.1007D-03	0.5801E 00	0.1557E-02
44	300	0.3472D-02	0.1000E 13	0.0	0.1007D-03	0.5807E 00	0.1558E-02
45	300	0.3472D-02	0.1000E 13	0.0	0.1007D-03	0.5810E 00	0.1559E-02

NCD1	NCD2	AREA	HINT	RINT	TRAN	HEAT FLCW	AVG RATE
46	3CC	0.3472D-02	0.1000E 13	0.0	0.1CC7D-03	0.5809E CO	C.1559E-C2
47	3CC	0.3472D-C2	0.1CC0E 13	0.0	0.1CC7D-C3	0.5821E 00	0.1562E-02
48	3CC	0.3472D-C2	0.1000E 13	0.0	0.1CC7D-C3	C.5859E CC	C.1572E-C2
49	3CC	C.3472D-C2	0.1000E 13	0.0	0.1CC7D-03	C.6005E CC	C.1611E-C2
5C	3CC	0.3472D-C2	0.1CCCE 13	C.C	0.1CC7D-C3	0.5924E CO	C.1590E-02
71	151	C.3472D-C2	0.1000E 13	0.0	0.1C75D-C2	C.1651E C1	0.4430E-02
72	152	C.3472D-C2	0.1000E 13	0.0	0.1C75D-02	0.1065E 01	0.2857E-02
73	153	C.3472D-02	0.1000E 13	0.0	0.1C75D-C2	0.1029E C1	0.2760E-02
74	154	C.3472D-02	0.1000E 13	0.0	0.1C75D-C2	C.1038E C1	C.2785E-C2
75	155	C.3472D-C2	0.1CC0E 13	0.C	0.1C75D-02	C.9951E CO	0.2671E-02
76	156	0.3472D-C2	0.1CC0E 13	0.0	0.1C75D-C2	0.1064E C1	C.2855E-02
77	157	C.3472D-C2	0.1CC0E 13	0.0	0.1C75D-02	0.1026E C1	C.2753E-C2
78	158	C.3472D-C2	0.1CC0E 13	0.0	0.1C75D-C2	0.1270E C1	0.3408E-02
79	159	0.3472D-C2	0.1CC0E 13	0.0	0.1C75D-C2	C.1833E-C1	C.4920E-04
8C	16C	C.3472D-C2	0.1000E 13	0.0	0.1C75D-02	0.1531E CO	0.4109E-03
81	151	C.3472D-C2	0.1000E 13	0.0	0.1C75D-C2	C.1651E C1	0.4431E-02
82	152	C.3472D-02	0.1000E 13	0.0	0.1C75D-C2	C.1065E C1	C.2857E-C2
83	153	C.3472D-C2	0.1CC0E 13	0.0	0.1C75D-C2	0.1029E 01	0.2760E-02
84	154	0.3472D-02	0.1000E 13	0.C	0.1C75D-C2	C.1038E 01	0.2785E-02
85	155	C.3472D-C2	0.1000E 13	0.0	0.1C75D-02	C.9952E CO	0.2671E-02
86	156	0.3472D-C2	0.1CC0E 13	C.C	0.1C75D-C2	0.1064E 01	0.2855E-02
87	157	0.3472D-C2	0.1000E 13	0.0	0.1C75D-C2	C.1026E C1	C.2753E-02
88	158	C.3472D-C2	0.1CC0E 13	0.0	0.1C75D-C2	0.127CE C1	0.3408E-02
89	159	0.3472D-C2	0.1000E 13	0.0	0.1C75D-C2	C.1837E-01	0.4931E-04
9C	16C	C.3472D-02	0.1000E 13	0.0	0.1C75D-C2	C.1531E CC	C.4110E-03
91	151	C.3472D-C2	0.1CC0E 13	0.0	0.1C75D-C2	0.1654E C1	0.4439E-02
92	152	0.3472D-02	0.1000E 13	0.0	0.1C75D-C2	C.1068E 01	0.2867E-02
93	153	C.3472D-C2	0.1000E 13	0.0	0.1C75D-02	0.1032E C1	C.2771E-C2
94	154	C.3472D-C2	0.1CC0E 13	0.C	0.1C75D-C2	0.1042E 01	0.2795E-02
95	155	0.3472D-C2	0.1000E 13	0.0	0.1C75D-C2	C.999CE CC	C.2681E-02
96	156	C.3472D-C2	0.1000E 13	0.0	0.1C75D-C2	C.1068E C1	0.2866E-02
97	157	C.3472D-C2	0.1000E 13	0.0	0.1C75D-C2	C.103CE C1	0.2763E-02
98	158	C.3472D-02	0.1000E 13	0.0	0.1C75D-C2	C.1273E C1	C.3417E-C2
99	159	C.3472D-C2	0.1CCCE 13	0.C	0.1C75D-02	0.2052E-C1	C.5507E-04
100	160	0.3472D-C2	0.1000E 13	0.0	0.1C75D-C2	C.1545E CO	0.4145E-03
1C1	151	C.3472D-02	0.1000E 13	0.0	0.1075D-02	C.1854E C1	C.4976E-C2
102	152	0.3472D-C2	0.1000E 13	0.C	0.1C75D-C2	0.1293E 01	0.3470E-02
103	153	0.3472D-C2	0.1000E 13	0.0	0.1C75D-C2	C.1259E C1	C.3380E-02
1C4	154	C.3472D-C2	0.1CCCE 13	0.0	0.1C75D-02	0.1269E C1	C.3404E-02
105	155	C.3472D-C2	0.1000E 13	0.0	0.1C75D-C2	C.1224E C1	0.3286E-02
106	156	0.3472D-02	0.1000E 13	0.0	0.1C75D-C2	C.1295E C1	0.3474E-C2
1C7	157	C.3472D-C2	0.1CCCE 13	0.C	0.1C75D-02	0.1251E C1	0.3358E-02
108	158	0.3472D-02	0.1000E 13	0.0	0.1C75D-C2	C.148CE C1	0.3971E-02
1C9	159	0.3472D-C2	0.1CC0E 13	0.0	0.1C75D-02	0.1452E CC	C.3897E-C3
11C	16C	0.3472D-C2	0.1CC0E 13	C.C	0.1C75D-C2	0.2365E CO	0.6347E-03
111	181	0.3472D-C2	0.1000E 13	0.0	0.1C75D-C2	-C.1125E C1	-C.3C18E-02
112	182	C.3472D-C2	0.1CC0E 13	0.0	0.1C75D-C2	-0.8417E CO	-C.2259E-02
113	183	0.3472D-C2	0.1000E 13	0.0	0.1C75D-C2	-C.8243E CO	-0.2212E-02
114	184	C.3472D-02	0.1000E 13	0.0	0.1C75D-C2	-C.8227E CO	-C.22C8E-02
115	185	C.3472D-C2	0.1000E 13	C.0	0.1C75D-02	-0.821CE 00	-0.2203E-02
116	186	0.3472D-C2	0.1000E 13	0.0	0.1C75D-C2	-C.8221E CO	-0.2206E-02
117	187	C.3472D-02	0.1CC0E 13	0.0	0.1075D-02	-0.8169E CC	-C.2192E-02
118	188	C.3472D-C2	C.1CC0E 13	0.C	0.1C75D-C2	-C.8021E 00	-0.2152E-02
119	189	0.3472D-C2	0.1000E 13	0.0	0.1C75D-C2	-C.7335E CC	-C.1968E-02
12C	19C	C.3472D-C2	0.1000E 13	0.0	0.1C75D-02	-0.7989E CC	-0.2144E-02
131	2C1	C.2604D-C2	0.1CC0E 13	0.0	0.8C62D-C3	-C.3912E CO	-0.1050E-02
132	2C2	C.26C4D-02	0.1000E 13	0.0	0.8C62D-03	-C.2046E CC	-0.5491E-03

NCD1	NCD2	AREA	HINT	RINT	TRAN	HEAT FLCW	AVG RATE
133	203	0.2604D-02	0.1000E 13	0.0	0.8062D-03	-0.1986E 00	-0.5331E-03
134	204	0.2604D-02	0.1000E 13	0.0	0.8062D-03	-0.1982E 00	-0.5319E-03
135	205	0.2604D-02	0.1000E 13	0.0	0.8062D-03	-0.1980E 00	-0.5313E-03
136	206	0.2604D-02	0.1000E 13	0.0	0.8062D-03	-0.1978E 00	-0.5309E-03
137	207	0.2604D-02	0.1000E 13	0.0	0.8062D-03	-0.1976E 00	-0.5304E-03
138	208	0.2604D-02	0.1000E 13	0.0	0.8062D-03	-0.1974E 00	-0.5297E-03
139	209	0.2604D-02	0.1000E 13	0.0	0.8062D-03	-0.1986E 00	-0.5329E-03
140	210	0.2604D-02	0.1000E 13	0.0	0.8062D-03	-0.2764E 00	-0.7418E-03
211	201	0.2604D-02	0.1000E 13	0.0	0.5918D 00	0.3451E 00	0.9262E-03
212	202	0.2604D-02	0.1000E 13	0.0	0.5918D 00	0.1410E 00	0.3783E-03
213	203	0.2604D-02	0.1000E 13	0.0	0.5918D 00	0.1343E 00	0.3604E-03
214	204	0.2604D-02	0.1000E 13	0.0	0.5918D 00	0.1336E 00	0.3585E-03
215	205	0.2604D-02	0.1000E 13	0.0	0.5918D 00	0.1333E 00	0.3577E-03
216	206	0.2604D-02	0.1000E 13	0.0	0.5918D 00	0.1333E 00	0.3577E-03
217	207	0.2604D-02	0.1000E 13	0.0	0.5918D 00	0.1332E 00	0.3574E-03
218	208	0.2604D-02	0.1000E 13	0.0	0.5918D 00	0.1329E 00	0.3565E-03
219	209	0.2604D-02	0.1000E 13	0.0	0.5918D 00	0.1329E 00	0.3568E-03
220	210	0.2604D-02	0.1000E 13	0.0	0.5918D 00	0.2178E 00	0.5846E-03
211	221	0.2604D-02	0.1000E 13	0.0	0.3958D 00	-0.1332E 00	-0.3574E-03
212	222	0.2604D-02	0.1000E 13	0.0	0.3958D 00	-0.3684E-01	-0.9887E-04
213	223	0.2604D-02	0.1000E 13	0.0	0.3958D 00	-0.3072E-01	-0.8243E-04
214	224	0.2604D-02	0.1000E 13	0.0	0.3958D 00	-0.3009E-01	-0.8075E-04
215	225	0.2604D-02	0.1000E 13	0.0	0.3958D 00	-0.2987E-01	-0.8017E-04
216	226	0.2604D-02	0.1000E 13	0.0	0.3958D 00	-0.2989E-01	-0.8022E-04
217	227	0.2604D-02	0.1000E 13	0.0	0.3958D 00	-0.2995E-01	-0.8039E-04
218	228	0.2604D-02	0.1000E 13	0.0	0.3958D 00	-0.2996E-01	-0.8041E-04
219	229	0.2604D-02	0.1000E 13	0.0	0.3958D 00	-0.3130E-01	-0.8401E-04
220	230	0.2604D-02	0.1000E 13	0.0	0.3958D 00	-0.7135E-01	-0.1915E-03
61	231	0.2604D-02	0.1000E 13	0.0	0.8057D-03	-0.5774E-02	-0.1549E-04
62	232	0.2604D-02	0.1000E 13	0.0	0.8057D-03	0.1743E 00	0.4678E-03
63	233	0.2604D-02	0.1000E 13	0.0	0.8057D-03	0.1794E 00	0.4816E-03
64	234	0.2604D-02	0.1000E 13	0.0	0.8057D-03	0.1793E 00	0.4811E-03
65	235	0.2604D-02	0.1000E 13	0.0	0.8057D-03	0.1790E 00	0.4804E-03
66	236	0.2604D-02	0.1000E 13	0.0	0.8057D-03	0.1788E 00	0.4798E-03
67	237	0.2604D-02	0.1000E 13	0.0	0.8057D-03	0.1788E 00	0.4797E-03
68	238	0.2604D-02	0.1000E 13	0.0	0.8057D-03	0.1790E 00	0.4804E-03
69	239	0.2604D-02	0.1000E 13	0.0	0.8057D-03	0.1782E 00	0.4782E-03
70	240	0.2604D-02	0.1000E 13	0.0	0.8057D-03	0.1067E 00	0.2862E-03
231	310	0.2604D-02	0.1000E 13	0.0	0.8334D-04	-0.5145E-01	-0.1381E-03
232	310	0.2604D-02	0.1000E 13	0.0	0.8334D-04	-0.5093E-01	-0.1367E-03
233	310	0.2604D-02	0.1000E 13	0.0	0.8334D-04	-0.5048E-01	-0.1355E-03
234	310	0.2604D-02	0.1000E 13	0.0	0.8334D-04	-0.5013E-01	-0.1345E-03
235	310	0.2604D-02	0.1000E 13	0.0	0.8334D-04	-0.4986E-01	-0.1338E-03
236	310	0.2604D-02	0.1000E 13	0.0	0.8334D-04	-0.4968E-01	-0.1333E-03
237	310	0.2604D-02	0.1000E 13	0.0	0.8334D-04	-0.4958E-01	-0.1330E-03
238	310	0.2604D-02	0.1000E 13	0.0	0.8334D-04	-0.4956E-01	-0.1330E-03
239	310	0.2604D-02	0.1000E 13	0.0	0.8334D-04	-0.4963E-01	-0.1332E-03
240	310	0.2604D-02	0.1000E 13	0.0	0.8334D-04	-0.4977E-01	-0.1336E-03
1	2	0.8681D-03	0.1000E 13	0.0	0.3360D-04	0.2640E-01	0.7085E-04
2	3	0.8681D-03	0.1000E 13	0.0	0.3360D-04	0.1006E-02	0.2698E-05
3	4	0.8681D-03	0.1000E 13	0.0	0.3360D-04	-0.4061E-04	-0.1090E-06
4	5	0.8681D-03	0.1000E 13	0.0	0.3360D-04	-0.4053E-02	-0.1088E-04
5	6	0.8681D-03	0.1000E 13	0.0	0.3360D-04	0.4021E-02	0.1079E-04
6	7	0.8681D-03	0.1000E 13	0.0	0.3360D-04	-0.1184E-01	-0.3179E-04
7	8	0.8681D-03	0.1000E 13	0.0	0.3360D-04	-0.3186E-01	-0.8549E-04
8	9	0.8681D-03	0.1000E 13	0.0	0.3360D-04	-0.1933E 00	-0.5186E-03
9	10	0.8681D-03	0.1000E 13	0.0	0.3360D-04	-0.8701E-01	-0.2335E-03

NOD1	NOD2	AREA	HINT	RINT	TRAN	HEAT FLOW	AVG RATE
11	12	0.8681D-03	0.1000E 13	0.0	0.336CD-04	0.2640E-01	0.7085E-04
12	13	0.8681D-03	0.1000E 13	0.0	0.3360D-04	0.1005E-02	0.2698E-05
13	14	0.8681D-03	0.1000E 13	0.0	0.336CD-04	-0.4062E-04	-0.1090E-06
14	15	0.8681D-03	0.1000E 13	0.0	0.336CD-04	-0.4053E-02	-0.1088E-04
15	16	0.8681D-03	0.1000E 13	0.0	0.336CD-04	0.4021E-02	0.1079E-04
16	17	0.8681D-03	0.1000E 13	0.0	0.336CD-04	-0.1184E-01	-0.3179E-04
17	18	0.8681D-03	0.1000E 13	0.0	0.3360D-04	-0.3186E-01	-0.8549E-04
18	19	0.8681D-03	0.1000E 13	0.0	0.336CD-04	-0.1933E 00	-0.5186E-03
19	20	0.8681D-03	0.1000E 13	0.0	0.336CD-04	-0.8701E-01	-0.2335E-03
21	22	0.8681D-03	0.1000E 13	0.0	0.336CD-04	0.2636E-01	0.7073E-04
22	23	0.8681D-03	0.1000E 13	0.0	0.336CD-04	0.9997E-03	0.2683E-05
23	24	0.8681D-03	0.1000E 13	0.0	0.336CD-04	-0.4106E-04	-0.1102E-06
24	25	0.8681D-03	0.1000E 13	0.0	0.336CD-04	-0.4051E-02	-0.1087E-04
25	26	0.8681D-03	0.1000E 13	0.0	0.336CD-04	0.4020E-02	0.1079E-04
26	27	0.8681D-03	0.1000E 13	0.0	0.336CD-04	-0.1184E-01	-0.3177E-04
27	28	0.8681D-03	0.1000E 13	0.0	0.336CD-04	-0.3183E-01	-0.8543E-04
28	29	0.8681D-03	0.1000E 13	0.0	0.336CD-04	-0.1932E 00	-0.5184E-03
29	30	0.8681D-03	0.1000E 13	0.0	0.336CD-04	-0.8695E-01	-0.2334E-03
31	32	0.8681D-03	0.1000E 13	0.0	0.336CD-04	0.2476E-01	0.6645E-04
32	33	0.8681D-03	0.1000E 13	0.0	0.336CD-04	0.8468E-03	0.2273E-05
33	34	0.8681D-03	0.1000E 13	0.0	0.336CD-04	-0.4923E-04	-0.1321E-06
34	35	0.8681D-03	0.1000E 13	0.0	0.336CD-04	-0.3972E-02	-0.1066E-04
35	36	0.8681D-03	0.1000E 13	0.0	0.336CD-04	0.3958E-02	0.1062E-04
36	37	0.8681D-03	0.1000E 13	0.0	0.336CD-04	-0.1155E-01	-0.3098E-04
37	38	0.8681D-03	0.1000E 13	0.0	0.336CD-04	-0.3093E-01	-0.8300E-04
38	39	0.8681D-03	0.1000E 13	0.0	0.336CD-04	-0.1889E 00	-0.5072E-03
39	40	0.8681D-03	0.1000E 13	0.0	0.336CD-04	-0.8454E-01	-0.2269E-03
41	42	0.8681D-03	0.1000E 13	0.0	0.336CD-04	-0.1704E-01	-0.4574E-04
42	43	0.8681D-03	0.1000E 13	0.0	0.336CD-04	-0.1615E-02	-0.4335E-05
43	44	0.8681D-03	0.1000E 13	0.0	0.336CD-04	-0.1858E-03	-0.4986E-06
44	45	0.8681D-03	0.1000E 13	0.0	0.336CD-04	-0.1270E-03	-0.3409E-06
45	46	0.8681D-03	0.1000E 13	0.0	0.336CD-04	0.5539E-04	0.1486E-06
46	47	0.8681D-03	0.1000E 13	0.0	0.336CD-04	-0.4187E-03	-0.1124E-05
47	48	0.8681D-03	0.1000E 13	0.0	0.336CD-04	-0.1256E-02	-0.3372E-05
48	49	0.8681D-03	0.1000E 13	0.0	0.336CD-04	-0.4863E-02	-0.1305E-04
49	50	0.8681D-03	0.1000E 13	0.0	0.336CD-04	0.2682E-02	0.7198E-05
61	62	0.6510D-03	0.1000E 13	0.0	0.252CD-04	-0.5790E-02	-0.1554E-04
62	63	0.6510D-03	0.1000E 13	0.0	0.252CD-04	-0.2947E-03	-0.7909E-06
63	64	0.6510D-03	0.1000E 13	0.0	0.252CD-04	-0.1015E-03	-0.2723E-06
64	65	0.6510D-03	0.1000E 13	0.0	0.252CD-04	-0.7288E-04	-0.1956E-06
65	66	0.6510D-03	0.1000E 13	0.0	0.252CD-04	-0.4861E-04	-0.1305E-06
66	67	0.6510D-03	0.1000E 13	0.0	0.252CD-04	-0.2998E-04	-0.8044E-07
67	68	0.6510D-03	0.1000E 13	0.0	0.252CD-04	-0.1310E-04	-0.3515E-07
68	69	0.6510D-03	0.1000E 13	0.0	0.252CD-04	0.4597E-04	0.1234E-06
69	70	0.6510D-03	0.1000E 13	0.0	0.252CD-04	0.2282E-02	0.6123E-05
71	72	0.8681D-03	0.1000E 13	0.0	0.336CD-04	0.1392E-01	0.3734E-04
72	73	0.8681D-03	0.1000E 13	0.0	0.3360D-04	-0.3397E-03	-0.9116E-06
73	74	0.8681D-03	0.1000E 13	0.0	0.336CD-04	0.1312E-03	0.3522E-06
74	75	0.8681D-03	0.1000E 13	0.0	0.336CD-04	-0.5593E-02	-0.1501E-04
75	76	0.8681D-03	0.1000E 13	0.0	0.3360D-04	0.6289E-02	0.1688E-04
76	77	0.8681D-03	0.1000E 13	0.0	0.336CD-04	-0.1386E-01	-0.3721E-04
77	78	0.8681D-03	0.1000E 13	0.0	0.336CD-04	-0.2914E-01	-0.7819E-04
78	79	0.8681D-03	0.1000E 13	0.0	0.336CD-04	-0.2472E 00	-0.6633E-03
79	80	0.8681D-03	0.1000E 13	0.0	0.336CD-04	-0.9244E-01	-0.2481E-03
81	82	0.8681D-03	0.1000E 13	0.0	0.336CD-04	0.1392E-01	0.3734E-04
82	83	0.8681D-03	0.1000E 13	0.0	0.336CD-04	-0.3398E-03	-0.9118E-06
83	84	0.8681D-03	0.1000E 13	0.0	0.336CD-04	0.1312E-03	0.3522E-06

NOD1	NOD2	AREA	HINT	RINT	TRAN	HEAT FLOW	AVG RATE
84	85	0.8681D-03	0.1000E 13	0.0	0.336CD-C4	-C.5593E-C2	-C.1501E-04
85	86	0.8681D-C3	0.1000E 13	0.0	0.336CD-04	0.6289E-C2	0.1688E-04
86	87	C.8681D-C3	0.10CCE 13	0.C	0.336CD-C4	-C.1386E-C1	-0.3721E-04
87	88	0.8681D-03	0.1000E 13	0.0	0.336CD-C4	-0.2914E-C1	-0.7819E-04
88	89	C.8681D-C3	0.1000E 13	0.0	0.336CD-04	-0.2472E C0	-0.6633E-03
89	90	0.8681D-03	0.1000E 13	0.0	0.336CD-C4	-C.9244E-C1	-C.2481E-03
91	92	C.8681D-03	0.1000E 13	0.0	0.336CD-04	0.1390E-C1	C.3729E-04
92	93	C.8681D-C3	0.1CC0E 13	0.0	0.336CD-C4	-0.3423E-C3	-C.9186E-06
93	94	0.8681D-03	0.10C0E 13	0.0	0.336CD-C4	C.131CE-C3	C.3516E-C6
94	95	C.8681D-C3	0.1000E 13	0.0	0.336CD-04	-0.5592E-C2	-C.15C1E-C4
95	96	C.8681D-C3	0.10CCE 13	0.0	0.336CD-C4	C.6288E-C2	0.1688E-04
96	97	C.8681D-03	0.1000E 13	0.0	0.336CD-C4	-C.1386E-C1	-0.3720E-04
97	98	C.8681D-C3	0.10C0E 13	0.0	0.336CD-04	-0.2913E-01	-0.7816E-04
98	99	0.8681D-03	0.1000E 13	0.0	0.336CD-C4	-C.2471E C0	-0.6632E-03
99	1CC	0.8681D-03	0.1000E 13	0.0	0.336CD-04	-C.9241E-C1	-C.2480E-C3
101	102	C.8681D-C3	0.10C0E 13	0.0	0.336CD-C4	0.1313E-01	0.3523E-04
102	103	0.8681D-03	0.1000E 13	0.0	0.336CD-C4	-C.4093E-C3	-C.1C99E-05
103	104	C.8681D-C3	0.1000E 13	0.0	0.336CD-04	C.1268E-C3	C.3404E-C6
104	105	C.8681D-C3	0.1000E 13	0.0	0.336CD-C4	-C.5541E-02	-C.1487E-04
105	106	0.8681D-03	0.1000E 13	0.0	0.336CD-C4	C.6242E-C2	C.1675E-04
106	107	C.8681D-C3	0.1000E 13	0.0	0.336CD-C4	-0.1369E-01	-0.3675E-04
107	108	0.8681D-03	0.1000E 13	0.0	0.336CD-C4	-0.2865E-C1	-0.7688E-04
108	109	C.8681D-C3	0.1000E 13	0.0	0.336CD-04	-0.2446E C0	-C.6563E-03
109	110	0.8681D-C3	0.1000E 13	0.0	0.336CD-04	-0.9108E-01	-0.2444E-C3
111	112	0.8681D-03	0.1CC0E 13	0.0	0.336CD-C4	-C.1197E-C1	-C.3212E-04
112	113	C.8681D-C3	0.1CC0E 13	0.0	0.336CD-04	-C.1112E-C2	-C.2983E-05
113	114	0.8681D-C3	0.10C0E 13	0.0	0.336CD-C4	-C.1390E-03	-0.3730E-06
114	115	C.8681D-03	0.1000E 13	0.0	0.336CD-C4	-C.9973E-C4	-C.2676E-06
115	116	0.8681D-C3	0.1000E 13	0.0	0.336CD-C4	0.4821E-04	0.1294E-06
116	117	C.8681D-03	0.1000E 13	0.0	0.336CD-C4	-C.3093E-C3	-C.83C0E-06
117	118	C.8681D-03	0.1000E 13	0.0	0.336CD-04	-0.883CE-C3	-C.2370E-C5
118	119	C.8681D-C3	0.1CC0E 13	0.0	0.336CD-C4	-C.3706E-C2	-0.9945E-C5
119	120	0.8681D-03	0.1000E 13	0.C	0.336CD-C4	C.2338E-C2	C.6276E-C5
131	132	C.6510D-03	0.1000E 13	0.0	0.252CD-04	-0.5938E-C2	-C.1594E-C4
132	133	C.651CD-C3	0.1000E 13	0.0	0.252CD-04	-0.27C1E-C3	-0.7248E-06
133	134	0.651CD-03	0.1000E 13	0.0	0.252CD-C4	-C.8144E-C4	-C.2186E-06
134	135	C.651CD-03	0.1000E 13	0.0	0.252CD-04	-0.5776E-C4	-0.1550E-06
135	136	C.651CD-03	0.1000E 13	0.0	0.252CD-C4	-C.3802E-C4	-C.1020E-06
136	137	C.651CD-03	0.1000E 13	0.0	0.252CD-C4	-C.2309E-C4	-C.6197E-07
137	138	C.651CD-C3	0.1000E 13	0.C	0.252CD-04	-0.9268E-05	-0.2487E-07
138	139	0.651CD-03	0.10C0E 13	0.0	0.252CD-C4	0.515CE-C4	C.1382E-06
139	14C	C.651CD-C3	0.1000E 13	0.0	0.252CD-04	0.2469E-C2	C.6627E-05
151	152	0.1111D-03	0.1CC0E 13	0.0	0.4CCCD-03	-0.5269E-01	-0.1414E-03
152	153	0.1111D-03	0.1000E 13	0.0	0.4CCCD-C3	-C.1752E-C1	-C.47C1E-04
153	154	C.1111D-03	0.1000E 13	0.0	0.4CCCD-C3	C.4915E-02	0.1319E-04
154	155	C.1111D-03	0.1000E 13	0.0	0.4CCCD-C3	-0.8243E-C1	-0.2212E-03
155	156	0.1111D-03	0.1000E 13	0.0	0.4CCCD-C3	C.1005E CC	C.2696E-C3
156	157	C.1111D-C3	0.10CCE 13	0.0	0.4CCCD-03	-0.1792E 00	-0.4810E-03
157	158	0.1111D-03	0.10CCE 13	0.C	0.4CCCD-C3	-C.2559E C0	-0.6868E-03
158	159	0.1111D-03	0.1000E 13	0.0	0.400CD-03	-C.3408E C1	-C.9146E-02
159	16C	0.1111D-C3	0.10CCE 13	0.C	0.4CCCD-C3	-0.1050E 01	-0.2818E-02
181	182	0.1111D-C3	0.1000E 13	0.0	0.4CCCD-C3	-C.3718E-C1	-C.9978E-C4
182	183	C.1111D-03	0.1000E 13	0.0	0.4CCCD-03	-C.6736E-C2	-C.1808E-04
183	184	C.1111D-C3	0.1000E 13	0.0	0.4CCCD-C3	-C.106CE-C2	-C.2845E-05
184	185	C.1111D-03	0.1000E 13	0.0	0.4CCCD-03	-C.5631E-C3	-0.1511E-05
185	186	C.1111D-C3	0.10C0E 13	0.0	0.4CCCD-C3	0.1550E-C3	C.4159E-C6
186	187	0.1111D-03	0.10C0E 13	0.0	0.4CCCD-C3	-C.1742E-02	-0.4675E-05

NCD1	NCD2	AREA	HINT	RINT	TRAN	HEAT FLCW	AVG RATE
187	188	0.1111D-03	0.1000E 13	0.0	0.4000D-03	-0.4984E-02	-0.1337E-04
188	189	0.1111D-03	0.1000E 13	0.0	0.4000D-03	-0.1860E-01	-0.4992E-04
189	190	0.1111D-03	0.1000E 13	0.0	0.4000D-03	0.3482E-02	0.9346E-05
201	202	0.2083D-04	0.1000E 13	0.0	0.7500D-04	-0.3178E-03	-0.8528E-06
202	203	0.2083D-04	0.1000E 13	0.0	0.7500D-04	-0.2479E-03	-0.6654E-06
203	204	0.2083D-04	0.1000E 13	0.0	0.7500D-04	-0.1996E-03	-0.5355E-06
204	205	0.2083D-04	0.1000E 13	0.0	0.7500D-04	-0.1506E-03	-0.4042E-06
205	206	0.2083D-04	0.1000E 13	0.0	0.7500D-04	-0.1011E-03	-0.2712E-06
206	207	0.2083D-04	0.1000E 13	0.0	0.7500D-04	-0.5189E-04	-0.1392E-06
207	208	0.2083D-04	0.1000E 13	0.0	0.7500D-04	-0.3477E-05	-0.9330E-08
208	209	0.2083D-04	0.1000E 13	0.0	0.7500D-04	0.4463E-04	0.1198E-06
209	210	0.2083D-04	0.1000E 13	0.0	0.7500D-04	0.1059E-03	0.2843E-06
211	212	0.6510D-03	0.1000E 13	0.0	0.2474D-01	-0.9629E-01	-0.2584E-03
212	213	0.6510D-03	0.1000E 13	0.0	0.2474D-01	-0.8151E-01	-0.2187E-03
213	214	0.6510D-03	0.1000E 13	0.0	0.2474D-01	-0.6580E-01	-0.1766E-03
214	215	0.6510D-03	0.1000E 13	0.0	0.2474D-01	-0.4967E-01	-0.1333E-03
215	216	0.6510D-03	0.1000E 13	0.0	0.2474D-01	-0.3333E-01	-0.8945E-04
216	217	0.6510D-03	0.1000E 13	0.0	0.2474D-01	-0.1711E-01	-0.4592E-04
217	218	0.6510D-03	0.1000E 13	0.0	0.2474D-01	-0.1133E-02	-0.3040E-05
218	219	0.6510D-03	0.1000E 13	0.0	0.2474D-01	0.1472E-01	0.3950E-04
219	220	0.6510D-03	0.1000E 13	0.0	0.2474D-01	0.3140E-01	0.8426E-04
221	222	0.6510D-03	0.1000E 13	0.0	0.2474D-01	-0.9027E-01	-0.2422E-03
222	223	0.6510D-03	0.1000E 13	0.0	0.2474D-01	-0.8113E-01	-0.2177E-03
223	224	0.6510D-03	0.1000E 13	0.0	0.2474D-01	-0.6576E-01	-0.1765E-03
224	225	0.6510D-03	0.1000E 13	0.0	0.2474D-01	-0.4966E-01	-0.1333E-03
225	226	0.6510D-03	0.1000E 13	0.0	0.2474D-01	-0.3333E-01	-0.8946E-04
226	227	0.6510D-03	0.1000E 13	0.0	0.2474D-01	-0.1712E-01	-0.4593E-04
227	228	0.6510D-03	0.1000E 13	0.0	0.2474D-01	-0.1133E-02	-0.3041E-05
228	229	0.6510D-03	0.1000E 13	0.0	0.2474D-01	0.1463E-01	0.3927E-04
229	230	0.6510D-03	0.1000E 13	0.0	0.2474D-01	0.2889E-01	0.7754E-04
231	232	0.6510D-03	0.1000E 13	0.0	0.2474D-01	-0.1537E 00	-0.4124E-03
232	233	0.6510D-03	0.1000E 13	0.0	0.2474D-01	-0.1317E 00	-0.3534E-03
233	234	0.6510D-03	0.1000E 13	0.0	0.2474D-01	-0.1052E 00	-0.2825E-03
234	235	0.6510D-03	0.1000E 13	0.0	0.2474D-01	-0.7952E-01	-0.2134E-03
235	236	0.6510D-03	0.1000E 13	0.0	0.2474D-01	-0.5443E-01	-0.1461E-03
236	237	0.6510D-03	0.1000E 13	0.0	0.2474D-01	-0.2980E-01	-0.7998E-04
237	238	0.6510D-03	0.1000E 13	0.0	0.2474D-01	-0.5309E-02	-0.1425E-04
238	239	0.6510D-03	0.1000E 13	0.0	0.2474D-01	0.1944E-01	0.5218E-04
239	240	0.6510D-03	0.1000E 13	0.0	0.2474D-01	0.4352E-01	0.1168E-03
1	320	0.8681D-03	0.1000E 13	0.0	0.3734D-04	-0.3323E 00	-0.8918E-03
11	320	0.8681D-03	0.1000E 13	0.0	0.3734D-04	-0.3323E 00	-0.8918E-03
21	320	0.8681D-03	0.1000E 13	0.0	0.3734D-04	-0.3321E 00	-0.8912E-03
31	320	0.8681D-03	0.1000E 13	0.0	0.3734D-04	-0.3206E 00	-0.8603E-03
41	320	0.8681D-03	0.1000E 13	0.0	0.3734D-04	0.1793E 00	0.4811E-03
71	320	0.8681D-03	0.1000E 13	0.0	0.3734D-04	-0.4159E 00	-0.1116E-02
81	320	0.8681D-03	0.1000E 13	0.0	0.3734D-04	-0.4159E 00	-0.1116E-02
91	320	0.8681D-03	0.1000E 13	0.0	0.3734D-04	-0.4158E 00	-0.1116E-02
101	320	0.8681D-03	0.1000E 13	0.0	0.3734D-04	-0.4088E 00	-0.1097E-02
111	320	0.8681D-03	0.1000E 13	0.0	0.3734D-04	0.2329E 00	0.6250E-03
61	320	0.6510D-03	0.1000E 13	0.0	0.2800D-04	0.1888E 00	0.5066E-03
151	320	0.6510D-03	0.1000E 13	0.0	0.2800D-04	0.2018E 00	0.5417E-03
151	320	0.1111D-03	0.1000E 13	0.0	0.1061D-04	-0.1345E 00	-0.3609E-03
181	320	0.2778D-04	0.1000E 13	0.0	0.2652D-05	0.1932E-01	0.5185E-04
201	320	0.2083D-04	0.1000E 13	0.0	0.1989D-05	0.1530E-01	0.4107E-04
10	330	0.8681D-03	0.1000E 13	0.0	0.3734D-04	-0.1614E 00	-0.4331E-03
20	330	0.8681D-03	0.1000E 13	0.0	0.3734D-04	-0.1614E 00	-0.4330E-03
30	330	0.8681D-03	0.1000E 13	0.0	0.3734D-04	-0.1613E 00	-0.4328E-03

NCD1	NCD2	AREA	HINT	RINT	TRAN	HEAT FLCW	AVG RATE
40	330	0.8681D-03	0.1000E 13	0.0	0.3734D-C4	-C.1565E 0C	-0.4200E-03
5C	33C	0.8681D-03	0.1000E 13	0.0	0.3734D-04	0.4573E-C1	C.1227E-03
8C	33C	C.8681D-C3	0.1CC0E 13	0.C	0.3734D-C4	-0.1655E C0	-0.4443E-03
90	330	C.8681D-03	0.1000E 13	0.0	0.3734D-C4	-C.1655E CC	-C.4443E-03
10C	33C	C.8681D-C3	0.1000E 13	0.0	0.3734D-04	-C.1655E CC	-C.4441E-C3
110	33C	0.8681D-C3	0.1000E 13	0.C	0.3734D-04	-C.1627E CO	-0.4365E-03
12C	33C	C.8681D-03	0.1000E 13	0.0	0.3734D-C4	C.9167E-C1	C.2460E-03
7C	33C	C.6510D-03	0.1000E 13	0.0	0.28CCD-04	0.7411E-01	0.1989E-03
140	33C	0.6510D-03	0.1000E 13	0.0	0.28CCD-C4	C.8706E-01	0.2336E-03
16C	33C	C.1111D-03	0.1000E 13	0.0	0.1061D-04	-C.4855E-C1	-C.1303E-03
19C	33C	C.2778D-C4	0.1000E 13	0.0	0.2652D-05	0.8483E-C2	0.2277E-04
21C	33C	0.2083D-04	0.1000E 13	0.0	0.1989D-C5	C.6867E-C2	C.1843E-04

BOUNDARY NODE DATA

NODB	TEMPB	HEAT FLCW	AVG RATE
1001	7.000CCE C1	-2.4323D C1	-6.5274E-02
1003	7.C000E 01	-3.4125D-01	-9.1580E-04
1021	8.C1CCE C1	-2.6462D C1	-7.1015E-02
1022	8.25CCE C1	-1.7866D 01	-4.7945E-02
1023	8.45CCE C1	-1.3863D 01	-3.7204E-02
1024	8.62CCE C1	-1.2492D 01	-3.3524E-02
1025	8.76CCE 01	-1.0914D 01	-2.9290E-02
1026	8.88CCE C1	-1.0200D 01	-2.7373E-02
1027	8.98CCE C1	-8.877CD 00	-2.3823E-02
1028	9.06CCE 01	-7.8905D 00	-2.1175E-02
1029	9.C9CCE C1	-2.C571D CO	-5.52C4E-03
1030	9.09CCE C1	-2.3381D-01	-6.2746E-04
1031	7.CCCCE C1	-1.0107D 01	-2.7122E-02
SYSTEM TCTAL		-1.4563E 02	-3.9081E-C1

EXTERNAL CONNECTICN DATA

NCDS	NCDSB	AREAS	HSURE	POWER	RSURE	TRANS	HEAT FLOW	AVG RATE
3CC	1001	1.7361D-01	1.5000D-02	0.0	0.0	2.6042C-03	-2.1367E 01	-5.7342E-C2
320	1001	1.7361D-02	1.5000D-C2	C.0	0.0	2.6042D-04	-2.C318E 00	-5.4526E-03
33C	1001	1.7361D-02	1.5000D-02	0.0	0.0	2.6042D-04	-9.24CCE-01	-2.4797E-C3
31C	1CC3	5.2083D-02	1.5000D-02	0.0	0.0	7.8125C-04	-3.4125E-01	-9.1580E-C4
151	1021	1.3889D-02	1.1400D-01	0.0	C.0	1.5833D-03	-2.6462E 01	-7.1015E-02
152	1022	1.3889D-02	8.2000D-C2	0.0	0.0	1.1389C-03	-1.7866E 01	-4.7945E-C2
153	1023	1.3889D-02	6.7000D-02	C.0	0.0	9.3055C-04	-1.3863E 01	-3.7204E-02
154	1024	1.3889D-02	6.3000D-02	0.0	0.0	8.75CCD-04	-1.2492E 01	-3.3524E-02
155	1025	1.3889D-02	5.8000D-C2	0.0	0.0	8.0555C-04	-1.0914E 01	-2.9290E-C2
156	1026	1.3889D-02	5.5000D-02	0.0	0.0	7.6389C-04	-1.0200E 01	-2.7373E-02
157	1027	1.3889D-02	5.1000D-02	0.0	C.0	7.C833D-04	-8.877CE 00	-2.3823E-C2
158	1028	1.3889D-02	4.9000D-02	0.0	C.0	6.8055C-04	-7.8905E 0C	-2.1175E-C2
159	1029	1.3889D-02	5.0000D-C2	0.0	C.0	6.9444D-04	-2.C571E CO	-5.52C4E-03
160	1030	1.3889D-02	5.0000D-02	0.0	0.0	6.9444D-04	-2.3381E-01	-6.2746E-C4
181	1031	3.4722D-C2	7.2000D-02	0.0	0.0	2.5000C-03	-1.2945E 00	-3.4740E-03
182	1031	3.4722D-02	7.2000D-02	0.0	0.0	2.5CCCD-03	-1.C621E 00	-2.85C4E-03
183	1031	3.4722D-C2	7.2000D-C2	0.0	0.0	2.50CCC-03	-1.C200E 00	-2.7374E-C3
184	1031	3.4722D-02	7.2000D-02	C.0	C.0	2.50CCC-03	-1.0134E 00	-2.7196E-03
185	1031	3.4722D-02	7.2000D-02	0.0	0.0	2.50CCD-03	-1.CC99E 0C	-2.71C2E-C3
186	1031	3.4722D-02	7.2000D-C2	0.0	0.0	2.5000C-03	-1.0109E 00	-2.7128E-C3
187	1031	3.4722D-02	7.2000D-02	0.0	C.0	2.5CCCD-03	-9.9998E-01	-2.6836E-03
188	1031	3.4722D-02	7.2000D-02	0.0	0.0	2.5000D-03	-9.6883E-01	-2.6CC0E-C3
189	1031	3.4722D-02	7.2000D-C2	C.0	0.0	2.5000C-03	-8.5257E-01	-2.2880E-C3
190	1031	3.4722D-02	7.2000D-02	0.0	0.0	2.5000D-03	-8.7434E-01	-2.3464E-03

TCTAL NUMBER OF ITERATIONS = 433 MAX = 52
ENDED FRCB 1 KCYC = 46 KWIT = 4 S UMTIM = C.37263E 03

```
C
C
C
C     CALCULATION OF OVERALL AND LOCAL HEAT TRANSFER COEF-
C     FICIENTS FROM DATA FOR A WALL HEATER IN A RECTANGULAR
C     CHANNEL.
C     THE DATA REQUIRED INCLUDES THE HEATING STRIP RESIS-
C     TANCE AND VOLTAGE DROPS TO GIVE THE POWER, THE THERMO-
C     COUPLE MILLIVOLT READINGS AND CALCULATION DATA, AND
C     CONSTANT VALUES FOR AREA, FLOW RATE, FLUID PROPERTIES
C     TABLES, AND LOSS FACTOR CALCULATIONS.
C    THE UNITS ARE FEET, MINUTE, BTU, LBM, AND DEGREES F.
C
C
      DIMENSION TRC(14,4),R(18),V(18),TM(40),TD(40),TB(20)
      DIMENSION H(18),U(18),X(18),P(18),GT(18)
      DO 100 I=1,14
      READ(5,10) TRC(I,1),TRC(I,2),TRC(I,3),TRC(I,4)
   10 FORMAT(F10.1,2F10.5,F10.3)
  100 CONTINUE
      DO 200 J=1,18
      READ(5,12) R(J),V(J)
   12 FORMAT(2F10.4)
  200 CONTINUE
      DO 340 K=1,40
      READ(5,14) TM(K)
  340 TD(K)=0.0
   14 FORMAT(F10.3)
      DO 320 L=1,20
  320 TB(L)=0.0
      DO 318 M=1,18
      H(M)=0.0
  318 P(M)=0.0
      DO 322 L=1,18
  322 READ(5,20) U(L),GT(L)
   20 FORMAT(2F8.3)
      READ(5,11) XO,DX,AW,AS
   11 FORMAT(4F10.6)
      READ(5,13) Q,TO,S,A1,A2
   13 FORMAT(3F10.4,2F10.8)
C
C     THE DATA HAS BEEN READ, NOW INTRUPULATE THE TEMPERA-
C     TURES AND WRITE THE LABELS.
C
      DO 400 I=1,40
      IF(TM(I).LT..834) GO TO 990
      L=1
      DO 410 N=2,14
      IF(TM(I).LE.TRC(N,4)) GO TO 412
      L=L+1
  410 CONTINUE
  990 TD(I)=TO+S*TM(I)
      GO TO 400
  412 B=(TM(I)-TRC(L,4))/(TRC(L+1,4)-TRC(L,4))
      TD(I)=TRC(L,1)+B*(TRC(L+1,1)-TRC(L,1))
  400 CONTINUE
      WRITE (6,15) Q
   15 FORMAT('1',////,41X,'HEAT TRANSFER CALCULATIONS FOR A'
     2,/,39X,'WALL HEATER IN A RECTANGULAR CHANNEL',///,35X,
     3'THE FLOW RATE IS ',F5.2,' CUBIC FEET PER MINUTE',///)
      RE=238.7024*Q
      WRITE(6,25) RE
   25 FORMAT(41X,'THE REYNOLDS NUMBER IS',F7.0,/////)
      WRITE(6,17)
   17 FORMAT(47X,'THE WALL TEMPERATURE',//,41X,'STATION',
     111X,'TEMPERATURE',/)
      TSUM=0.0
      DO 420 J=1,32
      WRITE(6,16) J,TD(J)
   16 FORMAT(43X,I2,16X,F6.2)
      TSUM=TSUM+TD(J)
  420 CONTINUE
```

```
      TAVG=TSUM/32.0
      TB(1)=TD(39)
      TB(20)=TD(40)
      WRITE(6,18) TAVG,TB(1),TB(20)
   18 FORMAT(///,33X,'THE AVERAGE WALL TEMPERATURE IS ',
     2F6.2,' DEGREES F',///,35X,'THE ENTERING AND EXITING ',
     4'BULK TEMPERATURES ARE',/,49X,F6.2,' AND ',F6.2,///)
C
C     CALCULATE THE LOG MEAN TEMPERATURE AND THE OVERALL
C     HEAT TRANSFER COEFFICIENT.
C
      D=ALOG((TAVG-TB(1))/(TAVG-TB(20)))
      TLM=(TB(20)-TB(1))/D
      IF(TAVG.LT.70.0) GO TO 999
      N=1
      DO 510 K=2,14
      IF(TAVG.LE.TRC(K,1)) GO TO 520
      N=N+1
  510 CONTINUE
      GO TO 999
  520 E=(TAVG-TRC(N,1))/(TRC(N+1,1)-TRC(N,1))
      RC=TRC(N,2)+E*(TRC(N+1,2)-TRC(N,2))
      C=TRC(N,3)+E*(TRC(N+1,3)-TRC(N,3))
      HAVG=(RC*C*G*(TB(20)-TB(1)))/(AW*TLM)
      WRITE(6,19) TLM,HAVG
   19 FORMAT('1',////,35X,'THE LOG MEAN TEMPERATURE DIFFER',
     3'ENCE IS ',F7.2,//,33X,'THE OVERALL HEAT TRANSFER',
     5' COEFFICIENT IS',F8.4,/,38X,'IN BTU PER MINUTE',
     7' SQUARE FEET DEGREES F',/////)
      TA=(TAVG-TB(1))
      HM=HAVG*(TLM/TA)
      WRITE(6,26) TA,HM
   26 FORMAT(35X,'THE WALL FLUID TEMPERATURE DIFFERENCE IS',
     6F6.2,//,35X,'THE MEAN HEAT TRANSFER COEFFICIENT IS',
     8F8.4,////)
C
C     CALCULATE THE POWER AND LOCAL HEAT TRANSFER COEFFICIENT
C
      TW=TAVG+459.72
      TV=TB(1)+459.72
      TTR=.00C001*(TW**4-TV**4)
      RA=.00001999667*AS*TTR
      DO 600 J=1,16
      W=(.056884*V(J)**2)/R(J)
      UT=U(J)+GT(J)
      F=U(J)/UT
      P(J)=W*(1.0-F)-RA
      R1=(209.1518+1.0/HM)
      R2=175.596852
      CO1=A1*(TB(J)-70.0)/R1
      CO2=A2*(TB(J)-70.0)/R2
      CON=CO1+CO2
      IF(TB(J).LT.70.0) GO TO 999
      M=1
      DO 610 I=2,14
      IF(TB(J).LE.TRC(I,1)) GO TO 620
      M=M+1
  610 CONTINUE
      GO TO 999
  620 G=(TB(J)-TRC(M,1))/(TRC(M+1,1)-TRC(M,1))
      RC=TRC(M,2)+G*(TRC(M+1,2)-TRC(M,2))
      C=TRC(M,3)+G*(TRC(M+1,3)-TRC(M,3))
      TB(J+1)=TB(J)+(P(J)-CON)/(RC*C*G)
      K=2*J
      L=K-1
      TX=(TD(K)+TD(L))/2.0
      H(J)=(RC*C*G*(TB(J+1)-TB(J)))/(AS*(TX-TB(J)))
  600 CONTINUE
      WRITE(6,22)
   22 FORMAT(//,37X,'THE LOCAL HEAT TRANSFER COEFFICIENTS',
     2' AND',//,39X,'THE BULK TEMPERATURES ARE SHOWN BELOW',
     3///,28X,'STATION',5X,'DISTANCE',5X,'POWER',5X,
```

```
   4'TEMPERATURE',5X,'H',/)
    HS=0.0
    DO 630 N=1,16
    HS=HS+H(N)
    SS=FLOAT(N)
    X(N)=-XO+SS*DX
    WRITE(6,23) N,X(N),P(N),TB(N),H(N)
 23 FORMAT(31X,I2,7X,F8.6,4X,F8.6,5X,F6.2,5X,F8.6)
630 CONTINUE
    HA=HS/16.0
    WRITE(6,27) HA
 27 FORMAT(///,31X,'THE AVERAGE LOCAL HEAT TRANSFER',
   2' COEFFICIENT IS',F8.4,///)
    WRITE(6,24) TB(17),TB(20)
 24 FORMAT(///,41X,'THE FINAL BULK TEMPERATURE WAS',//,
   347X,'AS CALCULATED ',F6.2,//,47X,'AS MEASURED   ',
   4F6.2,/////)
    GO TO 900
999 WRITE(6,29)
 29 FORMAT(//,47X,'SOMETHING WENT WRONG',////)
900 STOP
    END
```

HEAT TRANSFER CALCULATIONS FOR A
WALL HEATER IN A RECTANGULAR CHANNEL

THE FLOW RATE IS 2.55 CUBIC FEET PER MINUTE

THE REYNOLDS NUMBER IS 609.

THE WALL TEMPERATURE

STATION	TEMPERATURE
1	124.83
2	125.67
3	125.29
4	124.71
5	125.55
6	125.34
7	125.46
8	124.29
9	125.97
10	124.58
11	125.13
12	124.62
13	125.42
14	125.17
15	125.71
16	124.45
17	125.29
18	125.29
19	125.50
20	124.92
21	125.00
22	125.46
23	124.87
24	125.21
25	125.38
26	124.96
27	125.04
28	124.45
29	125.08
30	124.41
31	124.45
32	125.13

THE AVERAGE WALL TEMPERATURE IS 125.08 DEGREES F

THE ENTERING AND EXITING BULK TEMPERATURES ARE
80.13 AND 90.87

THE LOG MEAN TEMPERATURE DIFFERENCE IS 39.34

THE OVERALL HEAT TRANSFER COEFFICIENT IS 0.0460
IN BTU PER MINUTE SQUARE FEET DEGREES F

THE WALL FLUID TEMPERATURE DIFFERENCE IS 44.95

THE MEAN HEAT TRANSFER COEFFICIENT IS 0.0403

THE LOCAL HEAT TRANSFER COEFFICIENTS AND
THE BULK TEMPERATURES ARE SHOWN BELOW

STATION	DISTANCE	POWER	TEMPERATURE	H
1	0.011416	0.088965	80.13	0.132104
2	0.034249	0.038459	82.08	0.059025
3	0.057082	0.043506	82.92	0.067486
4	0.079915	0.033487	83.86	0.053317
5	0.102748	0.028635	84.58	0.045572
6	0.125581	0.026795	85.20	0.043511
7	0.148414	0.027866	85.77	0.045427
8	0.171247	0.021361	86.36	0.034921
9	0.194080	0.018317	86.81	0.029719
10	0.216913	0.020849	87.19	0.034529
11	0.239746	0.016224	87.62	0.026526
12	0.262579	0.020555	87.95	0.034747
13	0.285412	0.015031	88.38	0.024807
14	0.308245	0.013437	88.69	0.022268
15	0.331078	0.011493	88.95	0.018718
16	0.353911	0.019532	89.18	0.034048

THE AVERAGE LOCAL HEAT TRANSFER COEFFICIENT IS 0.0442

THE FINAL BULK TEMPERATURE WAS

AS CALCULATED 89.58

AS MEASURED 90.87

HEAT TRANSFER CALCULATIONS FOR A
WALL HEATER IN A RECTANGULAR CHANNEL

THE FLOW RATE IS 3.66 CUBIC FEET PER MINUTE

THE REYNOLDS NUMBER IS 874.

THE WALL TEMPERATURE

STATION	TEMPERATURE
1	131.99
2	133.24
3	132.86
4	132.07
5	133.32
6	132.82
7	133.94
8	131.45
9	134.52
10	131.99
11	133.24
12	132.74
13	133.82
14	133.15
15	133.82
16	132.37
17	132.99
18	133.28
19	133.24
20	132.45
21	132.03
22	132.53
23	132.41
24	132.74
25	133.49
26	132.78
27	133.15
28	132.41
29	133.36
30	132.24
31	132.61
32	133.03

THE AVERAGE WALL TEMPERATURE IS 132.88 DEGREES F

THE ENTERING AND EXITING BULK TEMPERATURES ARE
76.99 AND 88.51

THE LOG MEAN TEMPERATURE DIFFERENCE IS 49.91

THE OVERALL HEAT TRANSFER COEFFICIENT IS 0.0551
IN BTU PER MINUTE SQUARE FEET DEGREES F

THE WALL FLUID TEMPERATURE DIFFERENCE IS 55.89

THE MEAN HEAT TRANSFER COEFFICIENT IS 0.0492

THE LOCAL HEAT TRANSFER COEFFICIENTS AND
THE BULK TEMPERATURES ARE SHOWN BELOW

STATION	DISTANCE	POWER	TEMPERATURE	H
1	0.011416	0.123293	76.99	0.149215
2	0.034249	0.063262	78.88	0.078892
3	0.057082	0.064357	79.84	0.080715
4	0.079915	0.056233	80.82	0.072119
5	0.102748	0.045533	81.67	0.058403
6	0.125581	0.046032	82.36	0.060099
7	0.148414	0.046040	83.06	0.060267
8	0.171247	0.036775	83.76	0.048815
9	0.194080	0.031605	84.31	0.042099
10	0.216913	0.036077	84.79	0.049004
11	0.239746	0.025993	85.33	0.035561
12	0.262579	0.036541	85.71	0.050813
13	0.285412	0.028612	86.26	0.039289
14	0.308245	0.027137	86.69	0.037734
15	0.331078	0.022355	87.09	0.030922
16	0.353911	0.029529	87.42	0.041776

THE AVERAGE LOCAL HEAT TRANSFER COEFFICIENT IS 0.0585

THE FINAL BULK TEMPERATURE WAS

AS CALCULATED 87.85

AS MEASURED 88.51

HEAT TRANSFER CALCULATIONS FOR A
WALL HEATER IN A RECTANGULAR CHANNEL

THE FLOW RATE IS 4.88 CUBIC FEET PER MINUTE

THE REYNOLDS NUMBER IS 1166.

THE WALL TEMPERATURE

STATION	TEMPERATURE
1	143.16
2	144.80
3	144.06
4	143.52
5	144.22
6	143.61
7	144.39
8	142.34
9	144.63
10	142.38
11	143.81
12	143.07
13	143.73
14	143.16
15	143.40
16	141.80
17	142.38
18	142.87
19	143.07
20	142.38
21	142.54
22	143.28
23	142.46
24	142.42
25	143.52
26	142.70
27	143.28
28	142.66
29	143.10
30	142.05
31	142.42
32	142.87

THE AVERAGE WALL TEMPERATURE IS 143.13 DEGREES F

THE ENTERING AND EXITING BULK TEMPERATURES ARE
79.82 AND 91.96

THE LOG MEAN TEMPERATURE DIFFERENCE IS 57.02

THE OVERALL HEAT TRANSFER COEFFICIENT IS 0.0666
IN BTU PER MINUTE SQUARE FEET DEGREES F

THE WALL FLUID TEMPERATURE DIFFERENCE IS 63.31

THE MEAN HEAT TRANSFER COEFFICIENT IS 0.0600

THE LOCAL HEAT TRANSFER COEFFICIENTS AND
THE BULK TEMPERATURES ARE SHOWN BELOW

STATION	DISTANCE	POWER	TEMPERATURE	H
1	0.011416	0.147930	79.82	0.155086
2	0.034249	0.081882	81.53	0.087870
3	0.057082	0.080664	82.47	0.087608
4	0.079915	0.070126	83.39	0.077792
5	0.102748	0.054745	84.19	0.061034
6	0.125581	0.059199	84.82	0.066825
7	0.148414	0.055696	85.50	0.063448
8	0.171247	0.044451	86.13	0.051571
9	0.194080	0.037650	86.64	0.043745
10	0.216913	0.044400	87.06	0.052157
11	0.239746	0.040231	87.56	0.047309
12	0.262579	0.045171	88.02	0.054204
13	0.285412	0.034027	88.53	0.040176
14	0.308245	0.038087	88.91	0.045604
15	0.331078	0.026458	89.34	0.031473
16	0.353911	0.035070	89.63	0.042578

THE AVERAGE LOCAL HEAT TRANSFER COEFFICIENT IS 0.0630

THE FINAL BULK TEMPERATURE WAS

AS CALCULATED 90.03

AS MEASURED 91.96

HEAT TRANSFER CALCULATIONS FOR A
WALL HEATER IN A RECTANGULAR CHANNEL

THE FLOW RATE IS 6.10 CUBIC FEET PER MINUTE

THE REYNOLDS NUMBER IS 1457.

THE WALL TEMPERATURE

STATION	TEMPERATURE
1	139.71
2	140.53
3	139.71
4	138.80
5	139.42
6	139.25
7	140.41
8	137.51
9	140.61
10	137.84
11	139.05
12	138.26
13	139.13
14	138.17
15	139.21
16	137.47
17	138.09
18	138.71
19	139.05
20	137.88
21	138.13
22	138.88
23	138.22
24	138.22
25	139.54
26	138.51
27	139.34
28	138.42
29	139.25
30	137.88
31	138.55
32	139.09

THE AVERAGE WALL TEMPERATURE IS 138.84 DEGREES F

THE ENTERING AND EXITING BULK TEMPERATURES ARE
81.23 AND 91.57

THE LOG MEAN TEMPERATURE DIFFERENCE IS 52.27

THE OVERALL HEAT TRANSFER COEFFICIENT IS 0.0779
IN BTU PER MINUTE SQUARE FEET DEGREES F

THE WALL FLUID TEMPERATURE DIFFERENCE IS 57.61

THE MEAN HEAT TRANSFER COEFFICIENT IS 0.0707

THE LOCAL HEAT TRANSFER COEFFICIENTS AND
THE BULK TEMPERATURES ARE SHOWN BELOW

STATION	DISTANCE	POWER	TEMPERATURE	H
1	0.011416	0.148667	81.23	0.169629
2	0.034249	0.082567	82.60	0.097266
3	0.057082	0.082981	83.36	0.098860
4	0.079915	0.073819	84.12	0.089528
5	0.102748	0.059164	84.80	0.071915
6	0.125581	0.060823	85.34	0.075466
7	0.148414	0.058258	85.90	0.072912
8	0.171247	0.049602	86.43	0.062756
9	0.194080	0.042977	86.88	0.054480
10	0.216913	0.049149	87.27	0.062939
11	0.239746	0.043832	87.72	0.056306
12	0.262579	0.049671	88.11	0.064917
13	0.285412	0.039260	88.56	0.050447
14	0.308245	0.044019	88.92	0.057353
15	0.331078	0.031205	89.32	0.040531
16	0.353911	0.039576	89.60	0.052026

THE AVERAGE LOCAL HEAT TRANSFER COEFFICIENT IS 0.0736

THE FINAL BULK TEMPERATURE WAS
AS CALCULATED 89.95
AS MEASURED 91.57

HEAT TRANSFER CALCULATIONS FOR A
WALL HEATER IN A RECTANGULAR CHANNEL

THE FLOW RATE IS 6.10 CUBIC FEET PER MINUTE

THE REYNOLDS NUMBER IS 1457.

THE WALL TEMPERATURE

STATION	TEMPERATURE
1	132.66
2	133.53
3	132.37
4	131.29
5	132.12
6	131.54
7	132.49
8	129.79
9	132.66
10	130.04
11	131.37
12	130.62
13	131.37
14	130.54
15	131.41
16	129.71
17	130.41
18	130.95
19	131.24
20	130.46
21	130.50
22	131.16
23	130.41
24	130.54
25	131.83
26	131.08
27	131.83
28	131.00
29	131.87
30	130.58
31	131.12
32	131.70

THE AVERAGE WALL TEMPERATURE IS 131.25 DEGREES F

THE ENTERING AND EXITING BULK TEMPERATURES ARE
78.32 AND 88.60

THE LOG MEAN TEMPERATURE DIFFERENCE IS 47.61

THE OVERALL HEAT TRANSFER COEFFICIENT IS 0.0861
IN BTU PER MINUTE SQUARE FEET DEGREES F

THE WALL FLUID TEMPERATURE DIFFERENCE IS 52.94

THE MEAN HEAT TRANSFER COEFFICIENT IS 0.0775

THE LOCAL HEAT TRANSFER COEFFICIENTS AND
THE BULK TEMPERATURES ARE SHOWN BELOW

STATION	DISTANCE	POWER	TEMPERATURE	H
1	0.011416	0.148165	78.32	0.182080
2	0.034249	0.081750	79.68	0.104942
3	0.057082	0.082228	80.43	0.107013
4	0.079915	0.073501	81.18	0.098191
5	0.102748	0.060481	81.86	0.081235
6	0.125581	0.061153	82.41	0.083617
7	0.148414	0.058306	82.97	0.080580
8	0.171247	0.050000	83.50	0.070163
9	0.194080	0.044486	83.96	0.062616
10	0.216913	0.051015	84.36	0.072384
11	0.239746	0.044598	84.82	0.063653
12	0.262579	0.050545	85.23	0.073555
13	0.285412	0.040099	85.69	0.057226
14	0.308245	0.045108	86.05	0.065160
15	0.331078	0.034332	86.46	0.049686
16	0.353911	0.035976	86.77	0.052272

THE AVERAGE LOCAL HEAT TRANSFER COEFFICIENT IS 0.0815

THE FINAL BULK TEMPERATURE WAS
AS CALCULATED 87.09
AS MEASURED 88.60

LIST OF REFERENCES

1. Lord Rayleigh, "On the Dynamics of Revolving Fluids," Proceedings of the Royal Society of London, series A v. 93, pp 148-154, 1916. Reprints in Scientific Papers V6, pp. 447-453.

2. Taylor, G. I., "Distribution of Velocity and Temperature Between Rotating Cylinders," Proceedings of the Royal Society of London, series A, v. 135, p. 494-511, 1935.

3. Castle, P., Mobbs, F., and Markho, P. "Visual Observations and Torque Measurements in the Taylor Vortex Regime Between Eccentric Rotating Cylinders," Journal of Lubrication Technology v. 93, pp. 121-129, January 1971.

4. National Advisorary Committee for Aeronautics Technical Memorandum 1375, On the Three Dimensional Instability of Laminar Boundary Layers on Concave Walls, by H. Goertler, p. 32, 1942.

5. National Advisorary Committee for Aeronautics Wartime Report W-87, Investigation of Boundary Layer Transition on Concave Walls, By H. W. Liepmann, p. 22, 1945.

6. Schlichting, H., Boundary-Layer Theory pp. 500-522, McGraw-Hill, 1968.

7. Smith, A.M.O., "On the Growth of Taylor-Goertler Vortices Along Highly Concaved Walls," Quarterly of Applied Mathematics, v. 8, p. 233-362, November 1955.

8. Dean, W. R., "Fluid Motion in a Curved Channel," Proceedings of the Royal Society of London, series A, v. 121, pp. 402-420, 1928.

9. Reid, W. H., "On the Stability of Viscous Flow in a Curved Channel," Proceedings of the Royal Society of London, series A v. 244, pp. 186-198, 1958.

10. Aerospace Research Laboratories Report ARL 65-68, A Simplified Approach to the Influence of Goertler Type Vortices on the Heat Transfer from a Wall, by Lief N. Persen, p. 62, May 1965.

11. McCormack, P. D., Welker, H., and Kelleher, M., "Taylor-Goertler Vortices and Their Effect on Heat Transfer," Journal of Heat Transfer, v. 92, pp. 101-112, February 1970.

12. Cheng. K. C., and Ahiyama, M., "Laminar Forced Convection Heat Transfer in Curved Rectangular Channels," International Journal of Heat and Mass Transfer, v. 13, p. 471-490, 1970.

13. Mori, Y., Uchida, Y., and Ukon, T., "Forced Convection Heat Transfer in a Curved Channel of Square Cross Section," International Journal of Heat and Mass Transfer, v. 14, p. 1786-1805, November 1971.

14. Akiyama, M., Hwang, G. J., and Cheng, K. G., "Experiments on the Onset of Longitudinal Vortices in Laminar Forced Convection Between Horizontal Plates," Journal of Heat Transfer, v. 93, p. 335-341, November 1971.

15. Aerospace Research Laboratories Report ARL-69-0160, Exploratory Experiments in Water on Stream Wise Vortices and Crosshatching of the Surface of Reentry Bodies, by Lief N. Persen, p. 55, September 1969.

16. Beavers, G. S., Sparrow, E. M., and Magnuson, R. A., "Experiements on the Breakdown of Laminar Flow in a Parallel-Plate Channel," International Journal of Heat and Mass Transfer, v. 13, pp. 809-815, May 1970.

17. Nunge, R. J., "Time Dependent Laminar Flow in Curved Channels," Journal of Applied Mechanics, v. 93, pp. 171-176, March 1970.

18. Cohen, M. J. and Ritchie, N., "Low-Speed Three Dimensional Contraction Design," Journal of the Royal Aeronautical Society, v. 66, p. 231-236, April 1962.

19. Office of Naval Research Technical Report Number 75, Laminar Flow Forced Convection Heat Transfer and Flow Friction in Straight and Curved Ducts - A Summary of Analytic Solutions, by R. K. Shah and A. L. London, p. 196, November 1971.

20. Holman, J. P., Heat Transfer, pp. 111-272, McGraw-Hill, 1968.

21. Griffin, O. M., and Votaw, C. W., "The Use of Aerosols for the Visualization of Flow Phenomena," International Journal of Heat and Mass Transfer, v. 16, pp. 217-219, February 1973.

22. United States Naval Research Laboratory NRL Report 5929, Studies of Portable Air-Operated Aerosol Generators, by W. H. Echols and J. A. Young, p. 16, July 1963.

23. Lawrence Radiation Laboratory, University of California, Report UCRL-14754, TRUMP: A Computer Program for Transient and Steady-State Temperature Distributions in Multidimensional Systems, by Arthur L. Edwards, p. 60, July 1969.

24. Erbayram, Coskun, A Computer Program for Solving Transient Heat Conduction Problems, M.S. Thesis, Naval Postgraduate School, Monterey, Dec. 1971.

25. Stuart, J. T. "On the Non-linear Mechanics of Hydrodynamic Stability," Proceedings of the 10th International Congress of Applied Mechanics, pp. 63-97, 1962.

26. Kline, S. J. and McClintock, F. A. "Describing Uncertainties in Single-Sample Experiments," Mechanical Engineering, v. 75, pp. 3-8, January 1953.

INITIAL DISTRIBUTION LIST

		No. Copies
1.	Defense Documentation Center Cameron Station Alexandria, Virginia 22314	2
2.	Library, Code 0212 Naval Postgraduate School Monterey, California 93940	2
3.	Associate Professor M. Kelleher, Code 59kk Department of Mechanical Engineering Naval Postgraduate SChool Monterey, California 93940	1
4.	LT Robert J. McKee, USNR 5118 Angeles Crest Hwy. La Canada, California 91011	1
5.	Mr. George Bixler, Code 59 Department of Mechanical Engineering Naval Postgraduate School Monterey, California 93940	1
6.	Department of Mechanical Engineering Naval Postgraduate School Monterey, California 93940	1

UNCLASSIFIED

Security Classification

DOCUMENT CONTROL DATA - R & D

(Security classification of title, body of abstract and indexing annotation must be entered when the overall report is classified)

RIGINATING ACTIVITY (Corporate author) Naval Postgraduate School Monterey, California 93940	2a. REPORT SECURITY CLASSIFICATION Unclassified 2b. GROUP

EPORT TITLE

AN EXPERIMENTAL STUDY OF TAYLOR-GOERTLER VORTICES IN A CURVED RECTANGULAR CHANNEL

DESCRIPTIVE NOTES (Type of report and inclusive dates)

Master of Science & Mechanical Engineer's Thesis; June 1973

AUTHOR(S) (First name, middle initial, last name)

Robert J. McKee; Lieutenant, United States Naval Reserve

EPORT DATE June 1973	7a. TOTAL NO. OF PAGES 163	7b. NO. OF REFS 26
CONTRACT OR GRANT NO. PROJECT NO.	9a. ORIGINATOR'S REPORT NUMBER(S)	
	9b. OTHER REPORT NO(S) (Any other numbers that may be assigned this report)	

DISTRIBUTION STATEMENT

Approved for public release; distribution unlimited.

SUPPLEMENTARY NOTES	12. SPONSORING MILITARY ACTIVITY Naval Postgraduate School Monterey, California 93940

ABSTRACT

A rectangular cross section channel, with both a straight and a curved portion, was designed and built to create the laminar secondary Taylor-Goertler vortex flow. An aerosol was used to visualize these flow patterns, and photographs of the results are presented. A hot wire anemometer investigation of one location in the curved section was conducted to obtain the mean velocity profiles and turbulence levels. The pressure drop along both the straight and the curved sections was measured and compared. A constant temperature wall heater was also designed and installed in the straight section of the channel. Approximate values of the heating losses were obtained and the overall and local heat transfer coefficients were calculated for the straight portion of the channel. It was concluded that the vortices develop with both velocity increases and distance along the channel, and that the increase in pressure drop due to the vortices varied from near zero to approximately 20% with increasing Reynolds numbers.

DD FORM 1 NOV 65 1473 (PAGE 1)

/N 0101-807-6811

UNCLASSIFIED

Security Classification

A-31408

KEY WORDS	LINK A		LINK B		LINK C	
	ROLE	WT	ROLE	WT	ROLE	WT
TAYLOR-GOERTLER VORTICES						
CURVED CHANNEL FLOW						
SECONDARY LAMINAR FLOW						

Thesis 145054
M2154 McKee
c.1 An experimental study of
Taylor-Goertler vortices
in a curved rectangular
channel.

31 MAR 77 23195

Thesis 145054
M2154 McKee
c.1 An experimental study of
Taylor-Goertler vortices
in a curved rectangular
channel.

thesM2154
An experimental study of Taylor-Goertler
3 2768 001 88211 1
DUDLEY KNOX LIBRARY